Ammonia-Borane and Related Compounds as Dihydrogen Sources

Anne Staubitz,*,† Alasdair P. M. Robertson,‡ and Ian Manners*,‡

Otto Diels-Institut für Organische Chemie, Christian-Albrechts-Universität Kiel, Otto-Hahn-Platz 3, D-24118 Kiel, Germany, and School of Chemistry, University of Bristol, Bristol BS8 1TS, U.K.

Received March 13, 2010

Contents

* To whom correspondence should be addressed. E-mail: astaubitz@oc.uni-kiel.de; ian.manners@bristol.ac.uk.
† Christian-Albrechts-Universität Kiel.
‡ University of Bristol.

1. Introduction

We recently reviewed the latest developments in the chemistry of amine- and phosphine-borane adducts $R_3E{\cdot}BR'_3$ (R, R′ = alkyl, aryl, halogen, or H etc., E = N or P) where we discussed structural features and chemical reactivity of these simple but fascinating compounds as well as their potential applications as, for example reductants and as precursors to inorganic polymers.[1] One amine-borane, ammonia-borane ($H_3N{\cdot}BH_3$) has received disproportionately more attention than any other Lewis acid/base adduct of this type, mainly as a consequence of its potential as a hydrogen storage material. It is also the simplest amine-borane, and this species has been used as an example to study and understand the physical and chemical properties of this class of compound in detail. Some excellent short reviews have appeared that succinctly summarize certain aspects in the field.[2] However, a wealth of new studies have been published in this highly active area and the structural studies of ammonia-borane have not been the focus of a review as yet, so we felt that it was desirable and timely to present a comprehensive, detailed, and critical review of the subject covering developments up to early 2010.

Ammonia-borane is a white crystalline solid that was first prepared by Shore and Parry in 1955.[3] In the second section we will present the various syntheses of ammonia-borane, and in the third we discuss the physical properties of this compound in detail. In section 4 we will then consider ammonia-borane as a hydrogen donor, describing the thermal decomposition in the solid state and in solution, combined with computational studies of these

10.1021/cr100088b
Published on Web 07/14/2010

Anne Staubitz studied biochemistry at the University of Tübingen, Germany, but decided to pursue chemistry after working in Paul Knochel's group (LMU Munich) on novel Grignard reagents for her diploma thesis. She then obtained her Ph.D. in the group of Varinder Aggarwal from the University of Bristol, U.K., before working as a postdoc with Ian Manners, University of Bristol, U.K., in the field of catalytic dehydrocoupling of amine-boranes. After seven enjoyable years in the U.K., she accepted a position as a Juniorprofessorin (Assistant Professor) at the University of Kiel in 2010, where she is working in the field of conducting polymers and switchable polymeric systems.

Alasdair P. M. Robertson studied chemistry at the University of St. Andrews, Scotland, with an integrated year in industry working for a university spin−out company developing a novel geometry solid-oxide fuel cell. He completed his MChem in 2008, with a final year project under Derek Woollins investigating novel complexes of the $S_2N_2^{2-}$ ligand and was awarded the Irvine Jubilee Medal as most distinguished student of that year. He then moved south to the University of Bristol to pursue a Ph.D. under Ian Manners in the field of catalytic dehydrocoupling of group 13/15 adducts, where he is currently in his second year of studies.

Ian Manners was born in London, England, and after receiving his Ph.D. from the University of Bristol in 1985 in the area of transition metal chemistry (with N. G. Connelly), he conducted postdoctoral work in Germany in main group chemistry (RWTH Aachen, with P. Paetzold) and in the USA on polymeric materials (Penn State, with H. R. Allcock). He joined the University of Toronto, Canada, as an Assistant Professor in 1990 and was promoted to Professor in 1995. He was awarded a Canada Research Chair in 2001. In 2006 he returned to his Alma Mater to take up a Chair in Inorganic, Macromolecular and Materials Chemistry, supported by the award of a Marie Curie Chair from the European Union and a Wolfson Research Merit Award from the Royal Society. His research interests focus on the development of new synthetic reactions in inorganic chemistry and their applications in molecular synthesis, polymer and materials science, supramolecular chemistry, and nanoscience and are reflected in over 500 career publications.

processes. This will then lead to a brief discussion of transition metal catalyzed dehydrocoupling reactions of ammonia-borane, where we will discuss the experimental activity of the catalysts, including the mechanistic details. The next section will then deal with a different approach of effecting hydrogen release by incorporating ammonia-borane into scaffolds or using ionic liquids. In the fifth section, the use of main group metal amidoboranes as hydrogen containing materials is described. Another chemically different hydrogen release approach from ammonia-borane (and primary and secondary amine-boranes in general) involves metal catalyzed solvolysis in a protic solvent. We will cover this aspect in section 6. In section 7, *N*-methylated amine-boranes will be reviewed because they provide a useful comparison to ammonia-borane, but catalyzed dehydrogenation or dehydrocoupling aspects will not be dealt with, and we refer the reader to our other review for an in-depth discussion of this topic.[1] In the same section we will discuss the structure and thermal decomposition of alternatives to ammonia-borane, which have received recent interest, such as ammonia-triborane, hydrazine-borane, and guanidinium-borohydride, followed by a section on the recyclability of spent fuel from ammonia-borane, and we then provide a brief conclusion.

2. Syntheses

There are numerous syntheses for ammonia-borane, all of which fall within three types of reaction. They can be classified as salt-metathesis followed by H_2 release, Lewis acid−Lewis base exchange, or isomerization of the diammonate of diborane (DADB). As these routes are well established, we will not discuss them in detail and refer the interested reader to the references given in Table 1.

3. Ammonia-Borane: Physical Properties

Ammonia-borane has been analyzed by almost every possible spectroscopic technique, such as NMR, IR, Raman spectroscopy, and other techniques involving diffraction or scattering, such as X-ray crystallography or inelastic neutron scattering. Its materials properties have been analyzed by anelastic spectroscopy and dipole measurements, thermogravimetric and calorimetric

Table 1. Syntheses of Ammonia-Borane

entry	reaction	solvent	yield/%	ref
1	$NH_4C1 + LiBH_4 \rightarrow NH_3 \cdot BH_3 + LiC1 + H_2$	THF with trace NH_3	45	3
	$(NH_4)_2SO_4 + 2LiBH_4 \rightarrow 2NH_3 \cdot BH_3 + Li_2SO_4 + 2H_2$		45	
2	$NH_4HCO_2 + NaBH_4 \rightarrow NH_3 \cdot BH_3 + NaHCO_2 + 2H_2$	THF or dioxane	95	4
	$(NH_4)_2SO_4 + 2NaBH_4 \rightarrow 2NH_3 \cdot BH_3 + Na_2SO_4 + 2H_2$	Et_2O	96	
3	$NH_4C1 + NaBH_4 \rightarrow NH_4BH_4 + NaC1$	anhydrous NH_3/THF	99	5
	$\rightarrow NH_3BH_3 + NaC1 + H_2$			
	$NH_4F + LiBH_4 \rightarrow NH_3 \cdot BH_3 + LiF + H_2$	NH_3/THF	99	
4	$(NH_4)_2CO_3 + 2NaBH_4 \rightarrow 2NH_3 \cdot BH_3 + Na_2CO_2 + 2H_2$	THF	60−80	6
5	$BH_3 \cdot THF + NH_3 \rightarrow NH_3 \cdot BH_3$	THF, excess of ammonia	50	7
6	$B_2H_6 + 2NH_3 \rightarrow 2NH_3 \cdot BH_3$	Et_2O	45	8
7	$BH_3 \cdot SMe_2 + NH_3 \rightarrow NH_3 \cdot BH_3 + SMe_2$	Et_2O	86	9
8	$[H_2B(NH_3)_2]BH_4 \rightarrow NH_3 \cdot BH_3$	diglyme, small amount of B_2H_6	80−91	10

measurements. Many of those studies were performed long before ammonia-borane became a more prominent potential hydrogen storage material, which attests to the fact that it has always been regarded as an unusual molecule in its own right, from which fundamental insights into inter- and intramolecular bonding and molecular dynamics can be gained. Ammonia-borane exists as a molecular crystal whose somewhat unusual hydrogen bonds (between a proton and a hydride) have been suggested to account for its comparatively high melting point (112−114 °C, depending on the measurement conditions; see section 4.2.1 and compare to the isoelectronic ethane: −181.3 °C[11]). Also note that while this explanation is encountered frequently in the literature, it was contested by Vela and co-workers,[12] who consider electrostatic forces arising from the dipole moment of this polar molecule as the source of this effect (for a detailed discussion of the high melting point, see section 3.6). High pressure analysis of molecular crystals can yield unique insights into intermolecular bonding forces such as hydrogen bonding, because contrary to ionic crystals, molecular crystals tend to be highly compressible. This leads to very large changes in signals associated with translational, vibrational, and torsional movements and unit cell dimensions which is the subject of many papers discussed in detail below.

With such an interest in a single molecule, it is not surprising that contradictory views are held by many researchers and that older hypotheses have to be continually revised as more data accumulates. We aim to highlight development of ideas and controversies in this stimulating field. In the following section we will first consider the analysis of ammonia-borane by X-ray diffraction, neutron powder diffraction, and inelastic neutron scattering, IR, Raman, and microwave spectroscopy, followed by NMR spectroscopy. We will then briefly discuss the mechanical properties of ammonia-borane, followed by a section focusing on its properties as a reagent in terms of solubility, dielectric constant, dipole moment, and other properties. The section following this will deal with the thermal decomposition behavior of ammonia-borane.

3.1. X-ray Powder Diffraction of Ammonia-Borane

Knowledge of the solid state structure of ammonia-borane at different temperatures is vital for the detailed understanding of its thermal behavior. The first detailed study was an X-ray powder diffraction analysis by Hoon and Reynhardt.[13] They found that, at low temperatures, the structure is an orthorhombic $Pmn2_1$ phase that undergoes a transition to a tetragonal $I4mm$ crystal structure at a phase transition temperature of 225 K. However, a single crystal X-ray study of the orthorhombic phase of ammonia-borane by Crabtree and co-workers showed that the nitrogen and boron atom positions were in fact reversed and also located hydrogen atoms for the orthorhombic unit cell.[14] This allowed for the estimation of the H···H distance of the dihydrogen bond (2.02 Å), which is closer than the sum of the van der Waals radii of 2.4 Å. The tetragonal phase as well as the orthorhombic phase have been analyzed by a further single crystal X-ray crystallography study.[15] The orthorhombic structure agreed well with that observed by Crabtree. While the positions of the H atoms could be determined at 90 K, they appeared disordered (or could not be resolved) in the tetragonal phase.

The phase transitions of ammonia-borane have also been studied at increased pressures and at various temperatures by powder X-ray diffraction, combined with a DFT study.[16] At pressures between 1.1 and 1.4 GPa, a new phase formed reversibly, to which the $Cmc2_1$ geometry was assigned (Figure 1). The temperature dependent analysis suggested a slightly lower temperature than in previous work (217 K) for the change of the crystal lattice from $Pmn2_1$ to $I4mm$, but as in those studies, an intermediate phase 10−12 K below that transition could not be confirmed, which had been suggested by the Raman studies of Bowden and Schenter (see section 3.4).[17] The high pressure phase $Cmc2_1$ showed the same number of hydrogen bonds as the $Pmn2_1$ phase, albeit in a differently structured network, and the geometry of the ammonia-borane molecule itself was again barely affected by the crystal phase, confirming its highly covalent character. A further crystallographic phase, $P2_1$, was calculated to link $Cmc2_1$ and $Pmn2_1$, which allowed the completion of a full phase diagram for ammonia-borane.

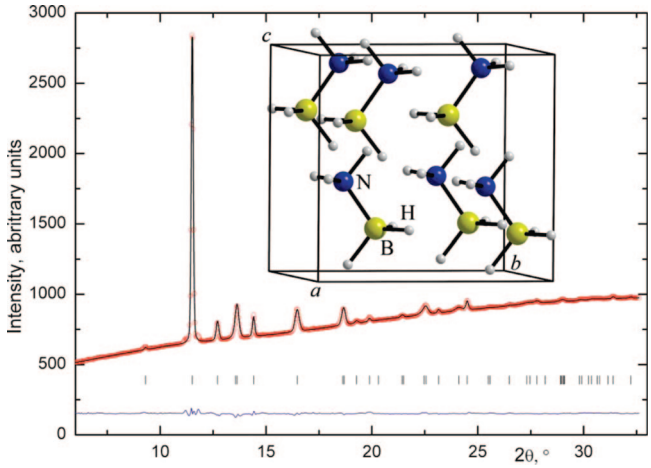

Figure 1. Rietveld refinement profile for the $Cmc2_1$ phase of $NH_3 \cdot BH_3$ at 1.7 GPa, $\lambda = 0.71171$ Å. The structure is shown in the inset. Reprinted with permission from ref 16. Copyright 2009 American Physical Society.

3.2. Neutron Powder Diffraction

The first neutron powder diffraction study used a fully deuterated ammonia-borane, $D_3N \cdot BD_3$.[18] Shortly afterward, this work was complemented in possibly the most detailed study to date by Hess and co-workers.[19] They analyzed the neutron powder diffraction patterns of ^{11}B and deuterium enriched ammonia-borane over a temperature range from 15 to 340 K. As it was no longer possible to employ a Rietveld refinement (a method commonly used for powder diffractograms where a theoretical line shape is refined until it matches the experiment) at the order−disorder transition, the experimental results were supplemented by *ab initio* molecular dynamics simulations. Both low temperature and high temperature phases were found to contain two molecules of ammonia-borane in the unit cell. In the orthorhombic $Pmn2_1$ phase, the B−N bonds formed layers parallel to the *c*-axis, where the B−N bonds were alternately inclined toward the *c*-axis (Figure 2). In the tetragonal $I4mm$ structure, these layers still existed, but the B−N bonds were now aligned parallel to the 4-fold *c*-axis. It was proposed that as temperature increases, the ammonia-borane molecules rotate about the B−N bond parallel to the *c*-axis with N as the pivotal point. Simultaneously, the crystal lattice contracts along the *a*-axis but expands along the *b*-axis, eventually resulting in the tetragonal phase. During this process, the intramolecular geometry is almost unaffected, but the hydrogen bonding is significantly reduced in the tetragonal phase, and it was speculated that further temperature increase would weaken this bonding further and precede hydrogen release.

3.3. Inelastic Neutron Scattering

The inelastic neutron scattering (INS) spectrum of ammonia-borane has also been reported, accompanied by DFT studies in the gas phase and the unit cell.[20] The orthorhombic phase $Pmn2_1$ was analyzed at 30 K. It was found that the B−N bond for the isolated molecule and the B−N bond in the crystal (1.58 Å for this technique, generally for solid state techniques 1.56−1.60 Å; see Table 2) differ substantially in length. For the isolated molecule, a B−N bond length of 1.658 Å was calculated based on a microwave structure,[21] with DFT calculations yielding a value of 1.666 Å. However, while the structural data otherwise compared favorably, the

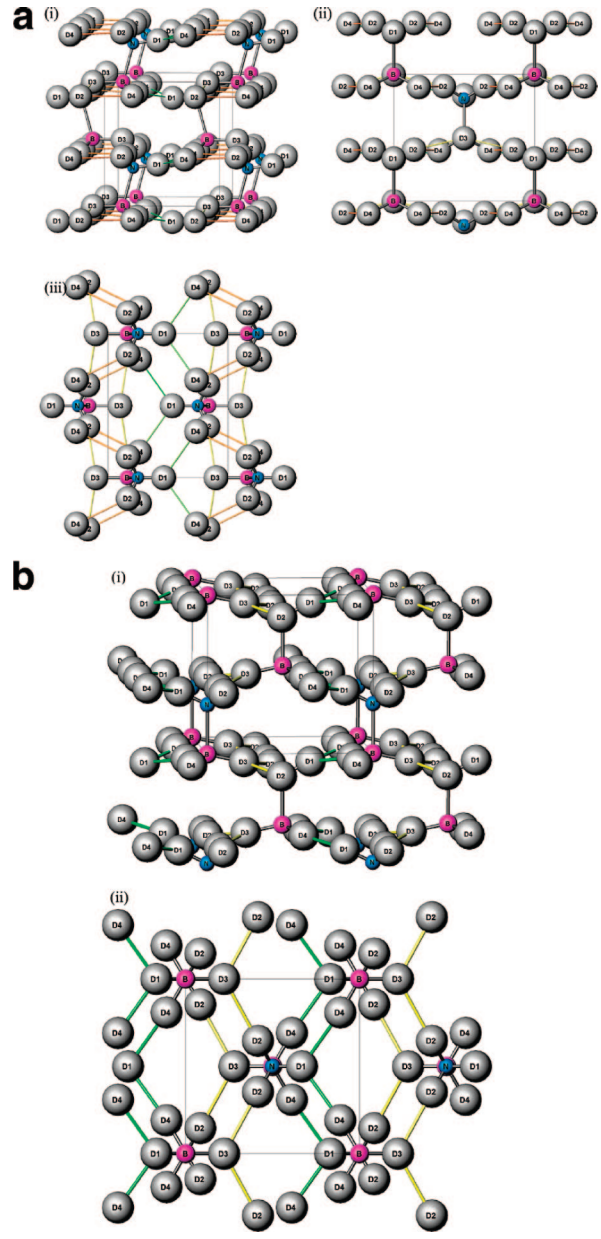

Figure 2. (a) Crystal structure at 15 K (orthorhombic). The dihydrogen bonding network is shown: D2···D3, yellow; D2···D4, orange; D1···D4, green. (i) *b*−*c* plane; (ii) *a*−*c* plane; (iii) *a*−*b* plane. (b) One of four possible orientations of ammonia-borane in the tetragonal phase at 240 K including the dihydrogen bonding network D2···D3 (yellow) and D1···D4 (green). (i) *a*−*c* plane; (ii) *a*−*a* plane. Reprinted with permission from ref 19. Copyright 2009 American Chemical Society.

Ar matrix[22] and gas phase calculated spectrum did show some differences, possibly due to anharmonicity or matrix effects. This reasoning was further supported by the DFT calculations for the solid, which gave an excellent reproduction of the measured INS spectrum (Figure 3). The B−N stretching mode shift (798 cm^{-1} in the INS spectrum; 799/801 cm^{-1} calculated) was also consistent with liquid phase IR in KBr/Nujol (776/790 cm^{-1}) and liquid NH_3 (787 cm^{-1}) and better reproduced than in an earlier *ab initio* computational study (713 cm^{-1}).[23] This shift could be explained by the considerable shortening of the B−N bond in the crystal due to hydrogen bonding between the hydridic and protic hydrogens in the ammonia-borane molecule.

The origin of this shortening of the B−N bond in condensed phases, however, has been the cause of intense

Table 2. B−N Bond Length in Ammonia-Borane

entry	method	medium	*T*/K	B−N/Å	ref
1	IR	Ar matrix	20.28	1.60	22
2	microwave	vapor	301−318	1.6576(16)	21, 25
				1.66(3)	
3	inelastic neutron scattering	crystal $Pmn2_1$	30	1.58 ± 0.02	20
4	single crystal X-ray	crystal $Pmn2_1$	90	1.599(8)	15
		*I*4*mm*	298	1.597(3)	
5	single crystal neutron diffraction	crystal $Pmn2_1$	200	1.58(2)	14
6	powder XRD	powder, $Pmn2_1$	110	1.56	13
7	neutron powder XRD[a]	powder	15	1.593(2)	19
		$Pmn2_1$	100	1.583(3)	
			120	1.582(3)	
			175	1.581(2)	
			220	1.565(4)	
		*I*4*mm*	230	1.571(3)	
			240	1.563(5)	
			275	1.573(2)	
			330	1.585(5)	
			340	1.590(5)	
8	neutron powder XRD	powder $Pmn2_1$	16	1.573	18
		*I*4*mm*	295	1.656	

[a] With a fully deuterated ammonia-borane.

discussion. One DFT study (molecular cluster density functional theory) claimed that strong dipole−dipole interactions were the underlying cause.[12] This theory was lent further support by a previous paper where it was noted that the geometry of ammonia-borane is highly dependent on its surroundings.[24] The B−N bond length for the gas phase was compared with the calculated bond length in hexane and water (SCRF field, Tomasi method; hydrogen bonds from the molecule itself were not included in the calculation), where a contraction of the B−N bond length to 1.62 Å (in hexane) or 1.57 Å (in water) from 1.66 Å was noted. In this study the calculated ^{11}B NMR shifts were also compared with those obtained for ammonia-borane. It was found that if a bond length of 1.66 Å was used, the NMR shift was too far downfield by about 8 ppm but that when a bond distance of 1.5 Å was employed, the shift was predicted almost correctly. When the dissociation energy was computed as a function of the B−N distance, the potential energy surface was relatively flat, which means that different bond lengths are relatively easily accessible and can be easily influenced by the surroundings of the molecule. As a consequence, many different B−N bond lengths for ammonia-borane can be found in the literature (see Table 2 for further details), all of which may be correct, and it is advisible to pay close attention to the experimental conditions under which they were measured.

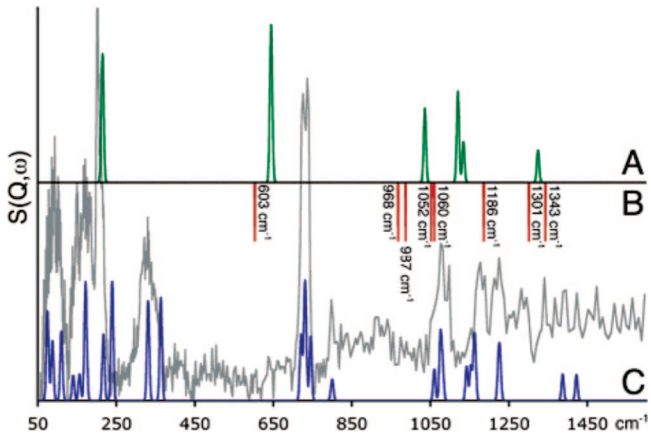

Figure 3. The 50−1600 cm^{-1} INS (gray), DFT (molecular) study (A), Ar matrix IR (B), and DFT (unit cell) (C) of ammonia-borane. Reprinted with permission from ref 20. Copyright 2004 American Chemical Society.

In 2009, the inelastic incoherent neutron scattering (IINS) spectra of ammonia-borane were reinvestigated using ^{11}B-enriched ammonia-borane isotopomers.[26] This enrichment allowed an improved assignment of low frequency torsional motions, which were less well described previously[20] because of the high natural cross section of boron (effective size of a nucleus for capturing a thermal neutron (slow neutron)). The natural cross section for boron is exceptionally large for a second row element, mainly due to the high natural abundance of ^{10}B (19.9%), which has a higher cross section than ^{11}B.[27] This means that the probability of capturing a neutron instead of scattering is large and the IINS signal becomes weaker, so that ^{11}B enrichment increases the signal strength. Qualitatively, this study confirmed the earlier findings. The interpretation of the low frequency translational and torsional modes of NH_3 and BH_3 was only possible in combination with a computational study, because they were not decoupled (independent of each other). Below 210 cm^{-1}, the peaks observed represent a collective motion of the system and cannot intrinsically be assigned. In the region of low frequencies, anharmonicity dominated the dynamics of the molecule and predictions based on harmonic assumptions became less reliable. However, this region is particularly interesting for ammonia-borane, as anharmonicity is concomitant with thermodynamic instability, which is likely to provide a pathway for the phase transition from the orthorhombic to tetragonal crystallographic phase at 225 K.[28]

3.4. Quasielastic Neutron Scattering

A ^{11}B enriched sample of ammonia-borane has also been analyzed by backscattering quasielastic neutron scattering.[29] The difference between inelastic and quasielastic neutron scattering is that the former gives information about vibrations, whereas the latter can be used to analyze reorientations and translations of the molecules.[30,31] Vibrational modes are generally on a time scale of 10^{-13} to 10^{-14} seconds, whereas the modes observed by quasielastic neutron scattering are in the range of 10^{-9} to 10^{-12} seconds. Inelastic neutron scattering can be observed toward the higher neutron energy exchange end of the spectrum, whereas quasielastic neutron

scattering is observed toward the lower end. Both inelastic and quasielastic neutron scattering can be coherent, wherein different scatterers contribute to the spectrum, thus corresponding to collective movements, or incoherent, wherein only one scatterer contributes. Thus, incoherent inelastic neutron scattering arises from the vibrational density of states, whereas, in the quasielastic region, relaxation processes (for example, rotational or translational diffusion) can be observed.

Brown and co-workers employed a time-of-flight neutron spectrometer for temperatures above the phase transition of 225 K and also a high flux backscattering spectrometer (HFBS) for low temperature measurements.[29] From the measurements above the phase transition, an average activation energy for the reorientation of the protons of $E_a = 4.9(5)$ kJ/mol (1.2 kcal/mol) could be derived, which is a little lower than the values obtained by NMR (5.9(5) kJ/mol (1.4 kcal/mol) for BD_3 and 7.3(8) kJ/mol for ND_3 by deuterium NMR) (see below).[32] For the measurements below the phase transition, the calculated activation energy was 7.98 kJ/mol (1.91 kcal/mol), which compared well with 8.37 kJ/mol (2.00 kcal/mol) for the reorientation of the NH_3 moiety during the phase transition measured using solid state NMR techniques (see section 3.5).[31]

3.5. IR and Raman Spectroscopy

The vibrational and rotational modes of ammonia-borane and its deuterated isotopologs have been extensively studied by IR and Raman spectroscopy. The first Raman spectroscopic study enabled determination of the stretching frequencies of these compounds (Table 3).[33] Subsequently, the stretching frequencies for a variety of B−N dative bonds were reported.[34,35]

Table 3. Comparison of the Boron−Nitrogen Stretching Frequencies in Isotopic Derivatives of Ammonia-Borane

compound	ν(B−N) (cm^{-1})	ν^*/ν	$\sqrt{\mu/\mu^*}$
$H_3N{\cdot}BH_3$	785		
$H_3N{\cdot}BD_3$	737	0.94	0.95
$D_3N{\cdot}BH_3$	754	0.96	0.97
$D_3N{\cdot}BD_3$	708	0.90	0.91
$D_3N{\cdot}{}^{10}BD_3$	713	0.91	0.93

The first full IR spectrum of ammonia-borane was reported by Ricker[36] for analytical purposes, followed by the recording of the far IR region.[37] With the advent of matrix isolation techniques,[22,38] it was also possible to obtain and assign IR spectra of isolated ammonia-borane molecules in argon. In this way, well resolved bands for ammonia-borane and its deuterated isotopologs were obtained, which allowed for the complete assignment of the frequencies and calculation of the force constants.[22] This achievement became the basis for computational investigations into this molecule. Due to the presence of hydridic and protic hydrogen atoms, the hydrogen bonding network has received much attention, with respect to high pressure Raman studies (see below) and crystallographic analyses (see previous section).

The recent interest in ammonia-borane prompted a reexamination of the Raman spectra of single crystal ammonia-borane in the temperature range from 88 to 300 K. Particular focus was placed upon the low temperature orthorhombic phase which had not been previously recorded, and a full factor group analysis was performed based on the C_{3v} symmetry of ammonia-borane.[17] From high to low temperatures, a clear phase change became visible at 225 K (tetragonal phase $I4mm$ ($T > 225$ K) to orthorhombic phase $Pmn2_1$ ($T < 225$ K)) by the increase of the numbers of vibrational modes. It was also suggested that there may be a transitional phase just below this temperature, based on the fact that some of the modes for the orthorhombic phase appeared delayed by 10−15 K below the transition temperature. However, X-ray crystallography by this and other groups could not confirm the existence of this phase. Two further studies of Raman spectra of ammonia-borane which focused on high pressure conditions (up to 40 kbar) appeared at almost the same time from Trudel and Gilson[39] and shortly afterward by Custelcean and Dreger.[40] High pressure analysis of molecular crystals can yield unique insights into intermolecular bonding forces such as hydrogen bonding, because, contrary to ionic crystals, molecular crystals tend to be highly compressible. This leads to substantial changes in signals associated with translational, vibrational, and torsional movements and unit cell dimensions. At ambient temperature, Trudel and Gilson found two phase transitions at 5 and 14 kbar. However, this was not confirmed by Custelcean and Dreger, who observed only one disorder−order transition at 8 kbar, which manifested itself in a splitting of the modes with E-symmetry and narrowing of the peak at higher pressure. These authors explained this desrepancy as a result from the experimental conditions. While they ensured hydrostatic conditions using mineral oil as a pressure-transmitting medium, it was not clear from Trudel and Gilson's work whether the possibility of pressure gradients had been taken into account and if measures had been taken to prevent them from occurring. Normally, if the pressure on a material is increased, stretching modes experience a blue shift because of the increased repulsive forces between atoms or groups and the therefore resulting steeper potential wells. For asymmetric hydrogen bonds however, upon increasing pressure, a red shift is generally observed, which can become shifted to higher frequencies again, once symmetry (equal bond distances) has been reached and passed.[39,40] This is generally attributed to an initial lengthening of the A−H bond in A−H···B as A and B move closer to one another. While both, Trudel and Gilson, and Custelcean and Dreger observed a moderate red shift for the N−H stretching mode compared to the free molecule from matrix isolation studies, Trudel and Gilson draw attention to the fact that this is not necessarily proof for hydrogen bonding, because similar shifts were observed in $H_3N{\cdot}BF_3$, where dihydrogen bonding cannot occur.[41,42] Custelcean and Dreger pointed out that no phase transition was observed for $Me_3N{\cdot}BH_3$ and $H_3N{\cdot}BPh_3$, where dihydrogen bonding is absent, which hints at the important role of dihydrogen bonds in pressure induced phase transformations. A third study of the phase transformations was presented by Lin and coworkers, in which they used Raman spectroscopy to pressures up to 22.3 GPa.[43] These workers found three transitions, at 2, 5, and 12 GPa, respectively. An interesting point the authors discussed was the fact that ammonia-borane may "dimerize" at higher pressures, forming DADB ($[(NH_3)_2BH]^+BH_4^-$), which has chemically the same composition. However, DADB is most often thought to be an intermediate in the decomposition of ammonia-borane (see section 4.2), and as higher pressures tend to increase the onset of decomposition, we suggest it to be more likely that the observed phase changes are structural and not chemical in nature. However, it has to be considered that DADB may be more stable at higher pressures and therefore not

decompose as rapidly. Unfortunately, there are insufficient data on the stability and pressure behavior of DADB at the time of writing.

A further Raman spectroscopy study was reported, where extreme pressures up to 60 GPa were used to examine ammonia-borane itself, but also mixtures with molecular hydrogen, to elucidate whether a van der Waals compound $NH_3 \cdot BH_3$-H_2 could exist.[44] For ammonia-borane, phase transitions at 1, 5, and 10 GPa were found. The unusual dihydrogen bonds between the protic N−H and the hydridic B−H persisted up to 50 GPa but weakened at even higher pressures. A closer analysis of the Raman modes showed that, up to this pressure, the H−H dihydrogen bond *increased* in strength with increasing pressure, as did the B−H and the B−N bond, whereas the N−H bonds weakened. The subsequent *weakening* of the H−H dihydrogen bonds at 50 GPa was attributed to a structural rearrangement and breakdown of the crystal lattice, which, however, did not result in hydrogen evolution. For $NH_3 \cdot BH_3$-H_2, two such complexes were found at 6.7 and 10 GPa. Presumably, the hydrogen occupied lattice voids in the corresponding ammonia-borane phases and was stabilized by dihydrogen bonds, but whether such complexes may be useful for hydrogen storage applications will depend on their stability.

3.6. NMR Studies of Ammonia-Borane

The first study of the molecular dynamics of ammonia-borane by solid state NMR spectroscopy was presented by Reynhardt and Hoon,[31] soon after their X-ray study.[13] They analyzed the temperature dependence of T_1, the spin−lattice relaxation time. This parameter is a good indicator of thermal motions in the sample, because spin−lattice relaxation is an enthalpic process, which is caused by time-dependent magnetic and electric fields resulting from these movements. The spin−lattice relaxation time T_1 showed a clear discontinuity at the phase transition temperature. From these data it was possible to extract the activation enthalpy E_a for the rotational motions of ammonia (2.3 kcal/mol) and borane (6.0 kcal/mol) in the low-temperature orthorhombic phase and E_a for the reorientations of borane (1.4 kcal/mol) in the tetragonal phase above 225 K. However, there was significant scattering of the measurements in the ln T_1 vs $1/T$ curve. A similar study was reported for partially deuterated ammonia-boranes, $D_3N \cdot BH_3$ and $H_3N \cdot BD_3$, which enabled separation of the motions of the ammonia and borane moieties in the molecule.[32] In this way, the line shapes were more distinct and facilitated a clear analysis of the ln T_1 vs $1/T$ curve (Figure 4).

From the slopes of these curves, E_a values for the rotation of the deuterated moiety of the adduct could be predicted of 5.9 kJ/mol (1.4 kcal/mol) for $H_3N \cdot BD_3$ and 7.3 kJ/mol (1.7 kcal/mol) for $D_3N \cdot BH_3$, respectively, for temperatures above the phase transition and 26.4 kJ/mol (6.3 kcal/mol) for $H_3N \cdot BD_3$ and 13.7 kJ/mol (3.3 kcal/mol) for $D_3N \cdot BH_3$, respectively, for temperatures below the phase transition. For isolated ammonia-borane, the internal rotational barrier has been estimated to be 8.5 kJ/mol (2.0 kcal/mol) by microwave spectroscopy,[21] which increases in the solid state and is higher than the E_a values for $H_3N \cdot BD_3$ and $D_3N \cdot BH_3$. This indicates that the rotational motions of NH_3 and BH_3 are correlated at $T > 225$ K but are uncorrelated below this temperature.

Almost a decade after Penner's deuterium study, Cho, Autrey, and co-workers initiated another variable temperature solid state ^2H NMR study over a wider range of low temperatures.[45] They could show that it was necessary to simulate the electric field gradient tensor as an ensemble average rather than functions of a single set of averaged Cartesian coordinates. While neutron diffraction studies[20] indicated that, in the solid state, the symmetry of ammonia-borane is no longer C_{3v}, as observed for the free molecule, but C_s instead, the NMR statistical analysis by Cho and Autrey suggested that in the orthorhombic phase the symmetry is fairly close to C_{3v}, which is also the conclusion that Hess and co-workers reached from their neutron powder diffraction study,[19] which could be fitted well to C_{3v} for all phases. It has to be pointed out that, computationally, Hudson and co-workers also found the C_{3v} symmetry to be lowest in energy, but the difference between these structures (C_{3v} and C_s) was relatively small.[20]

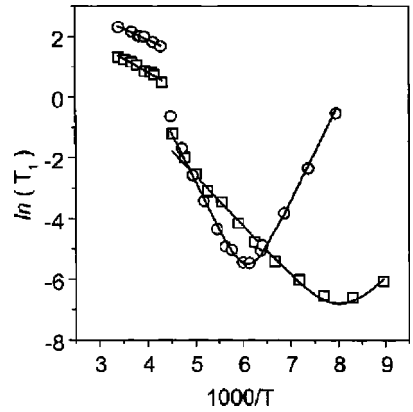

Figure 4. Temperature dependence of the 2D spin−lattice relaxation time T_1 for $NH_3 \cdot BH_3$ (squares) and $NH_3 \cdot BD_3$ (circles) between 115 and 300 K. Reprinted with permission from ref 32. Copyright 1999 American Chemical Society.

The chemical shifts (^{15}N and ^{11}B) and quadrupolar coupling constants (^{11}B) for ammonia-borane and some other amine-borane adducts in the solid state have been measured.[46] Dalal and co-workers investigated the 225 K phase transition of ammonia-borane using high resolution solid state ^{15}N NMR of ^{15}N-enriched ammonia-borane.[47] They measured the ^{15}N-isotropic chemical shift (which is unaffected by rotational and translational changes) using a cross-polarization magic angle spinning (CPMAS) experiment where cross-polarization from a highly sensitive, abundant nucleus (^1H) to ^{15}N allows for good signal-to-noise ratios, coupled with magic angle spinning in order to obtain narrow peak widths through averaging the anisotropy of the chemical shift in solid samples.[48] The chemical shift exhibited a clear temperature dependence, which was almost linear for the tetragonal phase above 225 K, with a dip at the phase transition temperature and leveling out toward lower temperatures (Figure 5). This distinctive dip in the chemical shift against T at the phase transition temperature was interpreted as a clear indication that the NH_3 moieties of ammonia-borane are distorted, which can be seen as displacitive rather than a order−disorder transition, which was the only mechanism implied in earlier studies.

The temperature dependence of the longitudinal (spin-lattice) relaxation time T_1 was also studied (Figure 6).[47] The activation enthalpy (E_a) values for the reorientations of ammonia were extracted, which were 14.5 kJ/mol (3.4 kcal/mol) for the orthorhombic phase ($T < 225$ K) and 6 kJ/mol (1.4 kcal/mol) for the tetragonal phase ($T > 225$ K) and were in good agreement with the values obtained by

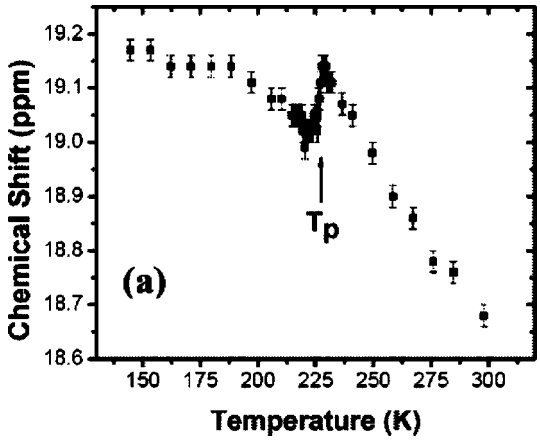

Figure 5. Temperature dependence of the isotropic chemical shift of ^{15}N for ammonia-borane. Reprinted with permission from ref 47. Copyright 2008 American Chemical Society.

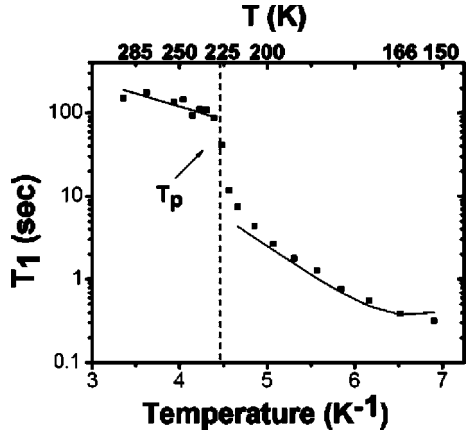

Figure 6. Temperature dependence of the spin−lattice relaxation time T_1 of ^{15}N-ammonia-borane. Reprinted with permission from ref 47. Copyright 2008 American Chemical Society.

Penner (^2D)[32] and Reynhardt and Hoon (^1H).[31] Therefore, it is likely that this change in T_1 is indicative of a motion that affects all these nuclei and hence relates to the phase transformation mechanism (order−disorder mechanism). It also emerged that the correlation time τ_c increased by a factor 10 for BH_3 but by a factor of 100 for NH_3. Since this parameter is directly related to fluctuations in a local magnetic field experienced by a spin, which in turn is caused by molecular motions or reorientations, this was interpreted as evidence that the phase transition is triggered by a slowing down of the NH_3 motion rather than that of BH_3.

3.7. Anelastic Spectroscopy of Ammonia-Borane

Paolone and co-workers have approached the problem of hydrogen dynamics and the tetragonal to orthorhombic phase transition in ammonia-borane by using anelastic spectroscopy.[49] Anelastic spectroscopy can be used to evaluate parameters such as the elastic modulus (a descriptor for the tendency of a substance to be reversibly deformed when a force is applied) and the elastic energy dissipation. The elastic modulus is very sensitive to phase changes and was therefore a useful tool for the study of the tetragonal/orthorhombic phase change in ammonia-borane. The measurements were performed at 3 kbar, which is well below the pressure induced phase transfer(s), which has (have) been observed by Trudel and Gilson[39] and Custelcean and Dreger.[40] The technique was used over a wide range of temperatures (1.3−300 K) and confirmed the phase transfer, which was estimated to occur at 222 K. At this point, a large variation of the elastic modulus was found, concomitant with a spike in the dissipation graph. The advantage anelastic spectroscopy may have over other techniques is its outstanding sensitivity, which made it possible to measure a hysteresis loop to determine the range of coexistence between the orthorhombic and the tetragonal phase. If a first order transition is assumed, this range was found to be very narrow, on the order of 0.4 K.

The phase transition in ammonia-borane was also investigated using calorimetric measurements to analyze the molar heat capacity over a temperature range of 10−289 K.[50] The phase transition entropy, assuming a first-order transition, was determined to be $\Delta S = 6.87$ J mol^{-1} K^{-1} and the phase transition at 224 K.

3.8. Computational Studies of the Structure of Ammonia-Borane

Many of the more recent papers discussed previously employ computational techniques in order to deepen the understanding of the experimentally observed results. However, the first to use a periodic quantum mechanical approach based on the crystallographic unit cell were Morrison and Siddick.[51] They predicted an average interaction energy of 12.7 kJ/mol (3.0 kcal/mol) (although not zero-point corrected) for the dihydrogen bond, which showed that these bonds in ammonia-borane are relatively weak.

The nature of the dihydrogen bond in ammonia-borane has elicited considerable interest from the computational community. A variety of reports investigated which methods were best to use to describe this bond, mostly using the dimeric species (in the gas phase) and also comparisons with ammonia-borane complexes formed with other molecules.[52] While we will not attempt to compare all these studies from a computational point of view, we would like to highlight a few major results. All studies agreed that the head to tail dimer of ammonia-borane does exhibit dihydrogen bonds, but the numbers reported varied. Popelier's estimate of three hydrogen bridges[52e] is closest (in number at least) to the orthorhombic structure found by neutron powder diffraction. While Crabtree suggested that these dihydrogen bonds may be the major contributors toward the relatively high melting point of ammonia-borane, this view was contested by Vela and co-workers.[12] They studied the dimers, trimer, and tetramer of ammonia-borane with DFT and performed a topological analysis of the electron density. They found that the energy of each dihydrogen bond decreased with increasing aggregation, thereby refuting the idea that dihydrogen bond formation is a cooperative process. Alternatively, they proposed that the observed cohesion is a mostly electrostatic effect, as all of the surrounding dipoles of the fragment in question point in opposing directions, thereby inducing an electric field, which pushes electron density from nitrogen to boron and thereby increases the bond strength. Support for this view could be gleaned from Schleyer's analysis of the medium dependence of the bond length,[24] which showed that solvents with different dielectric constants can influence the central B−N bond. However, we would like to highlight that the head-to-tail structures, which were the basis for Vela's work, do not reflect the situation in the crystal in any of the phases which have been discovered for ammonia-borane, because here neighboring ammonia-borane molecules are aligned (compare Figures 2 and 7).

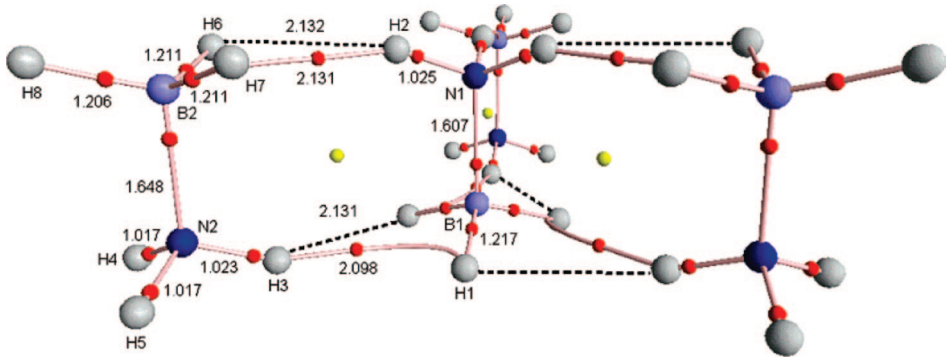

Figure 7. Tetrameric head-to-tail structure of ammonia-borane analyzed by Vela and co-workers.[12] Red and yellow spheres are the bond and ring critical points, respectively. Reprinted with permission from ref 12. Copyright 2008 American Chemical Society.

The nature of the charge transfer in ammonia-borane has also been analyzed.[53] An important result was that the charge-transfer energy at different donor−acceptor distances did not depend on the computation levels or basis sets. However, the degree of electron transfer depended strongly on the population analysis procedures.

4. Hydrogen Release from Ammonia-Borane

4.1. General Requirements for Use of Ammonia-Borane as a Fuel for the Production of H_2 in Fuel Cells

Hydrogen storage for fuel cell applications represents a considerable challenge and is of key importance, especially to the transport sector. The U.S. Department of Energy has set challenging storage targets of 90 g kg^{-1} by weight and 81 g L^{-1} of H_2 by volume by 2015.[54] Hydrogen has a gravimetric energy density of 33.3 kWh/kg at 350 and 700 bar, respectively, which means that one kilogram of H_2 can replace about 3 kg of gasoline. However, its volumetric energy density is 0.8 kWh/L for 350 bar of H_2 and 1.3 kWh/L for 700 bar, which is very low compared to 9.5 kWh/L for automotive gasoline.[55] As a consequence, 3430 L (approximate volume of a midsize car) of H_2 gas are necessary to replace just one gallon (4.5 L) of gasoline at standard pressure and temperature.[56] To further illustrate this point, a 50 L steel cylinder with a pressure of 300 bar only holds a hydrogen mass of 1.36 kg. With an approximate weight of the steel cylinder of about 90 kg, this corresponds to a gravimetric storage density of 1.5 wt %. If hydrogen is stored as a liquid, the gravimetric storage density is approximately 5% but the average daily loss is around 1% due to evaporation.[57] Besides the volumetric and gravimetric energy storage density, there are other requirements, such as practical operational conditions (Table 4) and a possibility to recycle or recharge the spent fuel, which at present only few materials can fulfill.[58]

Ammonia-borane as a potential hydrogen storage material has been the focus of a number of brief reviews or highlight articles[2a−c,59] comparing favorably with many other hydrogen storage materials (Figure 8). It has a high gravimetic storage density of up to 19.6 wt % and is nonflammable and nonexplosive under standard conditions, which makes it a good candidate for hydrogen storage.[56,60] However, despite the theoretical gravimetric hydrogen content of 190 g/kg and volumetric hydrogen content of 100−140 g/L, it has to be borne in mind that if all 3 equivalents of hydrogen were to be released, this would yield boron nitride. This is a chemically very stable compound (with a standard enthalpy of formation of $\Delta H°_{f,298K} = -59.97 \pm 0.37$ kcal/mol[61]), too stable to be regenerated to give ammonia-borane at a reasonable energy expenditure, so that in effect only a maximum of two-thirds of the theoretical hydrogen content of ammonia-borane can be used, 13.06%. A significant effort is being directed toward controlling the kinetics of its decomposition, with respect to onset temperatures, rapid release, and avoidance of side products such as ammonia or borazine, which can damage a fuel cell.

Table 4. U.S. Department of Energy Targets for 2010

variable	value
system gravimetric capacity	2 kWh/kg 0.06 kg H_2/kg system (6 wt %)
system volumetric capacity	1.5 kWh/L 0.045 kg H_2/L system
operating temperature	−30 to 50 °C
min./max. delivery temperature	−40 to 85 °C
cycle life ($^1/_4$ tank fill)	1000 cycles
min. delivery pressure: fuel cell	4 atm
internal combustion engine	35 atm
system fill time	5 kg H_2 in 3 min
min. flow rate	0.02 (g/s)/kW

4.2. Thermal Decomposition of Ammonia-Borane

4.2.1. Thermal Decomposition of Ammonia-Borane in the Solid State

Ammonia-borane is the most widely studied amine-borane adduct in terms of its thermolysis behavior. Its thermal decomposition was observed by many researchers to be a stepwise process, which in its simplified form may be summarized in Scheme 1. The exact temperature (or temperature range) at which a decomposition step occurs and even the shapes of the thermogravimetric and differential scanning calorimetric curves are very much dependent on the heating rate. Therefore, in the following section we will present the data as reported by the various authors without a detailed comparison between different studies. A summary of the conditions used and results is presented in Table 6 at the end of this subsection.

A thermally unstable molecule, ammonia-borane has been found to decompose in three distinct steps, which was studied for the first time in 1978 by thermogravimetric analysis (TGA), differential thermal analysis (DTA), and thermomanometry.[62] At a heating rate of 5 °C/min, the first step commenced at ca. 120 °C and ended at about 133 °C, up to which point a mass loss of 31.6% was reported. Up to 200 °C, a total mass loss of 35% was observed (TGA measurements). The DTA measurements were performed at a faster heating rate (10 °C/min) than TGA, which means

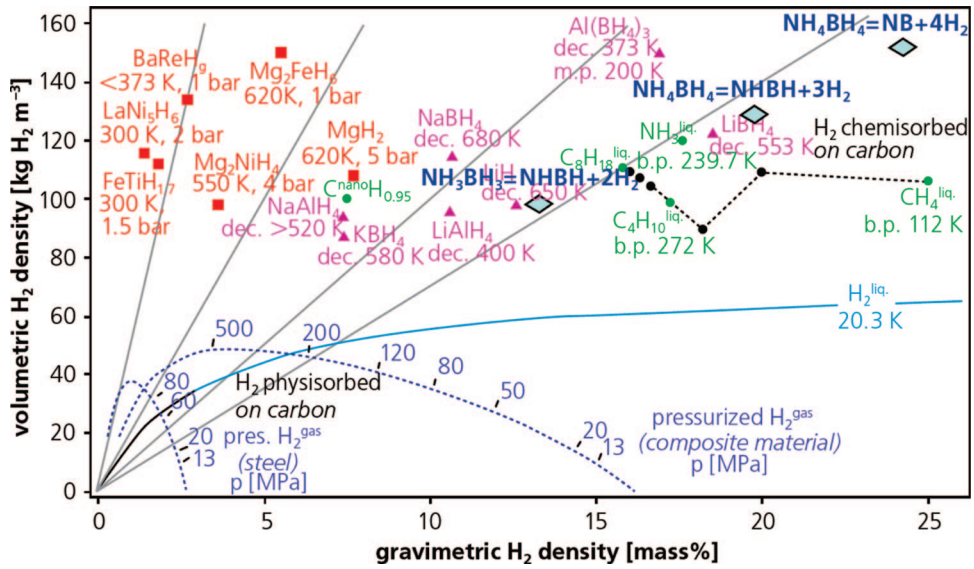

Figure 8. Volumetric and gravimetric hydrogen storage densities in various materials and ammonia-borane and its formal thermal decomposition products. Reprinted with permission from ref 2a. Copyright 2007 Sigma-Aldrich.

that the decomposition events would not have occurred at the same temperatures. By this technique, an endothermic melt transition was observed at 112 °C. At 117 °C a large exotherm commenced with a maximum at 130 °C, which was accompanied by loss of gas. The authors also reported a visible foaming of the mixture (caused by the formation of volatiles), exemplifying a general problem in the thermal decomposition of ammonia-borane. A second broad exothermic peak occurred between 150 and 200 °C. The thermomanometric curve (heating rate 8 °C/min) showed a major pressure increase near 120 °C, with a decrease in slope at 145 °C, indicating a different thermolytic process from the first step. Chemical analysis of the decomposition steps was attempted by pyrolysis/trapping experiments, where the products were analyzed by IR spectroscopy and deduced by the calculation of the mass balance, which did not allow a detailed understanding of the process. A later study of the thermal decomposition of ammonia-borane attempted to resolve the thermogravimetric and DTA signals better by reducing the heating rate to 2 °C/min.[63] The melt endotherm was found at 114 °C, preceded by a slow hydrogen loss, which commenced some 30 °C lower. This endotherm was followed by an exotherm at 125 °C, which the authors ascribed to hydrogen loss to give $[NH_2{=}BH_2]$ and H_2. $[NH_2{=}BH_2]$ had been tentatively identified in the gas phase by mass spectrometry[64] but is highly unstable and forms polyaminoboranes (PAB). At 155 °C, the mixture of polyaminoboranes became unstable and released another equivalent of hydrogen, to give borazine and other related

Scheme 1. Generalized Thermolysis of Ammonia-Borane

$$H_3N{-}BH_3 \longrightarrow 1/x\,(H_2N{-}BH_2)_x + H_2 \quad (1)$$

$$(H_2N{-}BH_2)_x \longrightarrow (HN{-}BH)_x + H_2 \quad (2)$$

$$(HN{-}BH)_x \longrightarrow BN + H_2 \quad (3)$$

$(HN{-}BH)_x$ = polyiminoborane, borazine, polyborazine, cross-linked materials, mostly poorly defined and characterized

products. Wolf and co-workers analyzed the influence of the heating rate on the calorimetrically obtained data (DSC) and also performed detailed isothermal studies.[65] The results revealed that, at 1 °C/min, an exotherm at 95 °C *preceded* the melt endotherm, which occurred at a few degrees higher, which in turn was followed by a large exothermic peak with a maximum at 113 °C, overlapped by a further peak starting at 125 °C. When the heating rate was reduced to 0.05 °C, the first exotherm could be completely separated beginning at 82 °C with no melt endotherm apparent. This meant that, given enough time at lower temperatures, the decomposition process is complete *before* the melt. Melt endotherms at higher rates only exist because there may be still some residual ammonia-borane. Melting points tend to be strongly influenced by the impurities present, and therefore, the observed melting temperature may be highly variable with the heating rate. A somewhat more detailed study, which confirmed these findings and included also FT-IR and mass spectrometric analyses, was published two years later.[66] In this context a study of the thermal stability of ammonia-borane at constant 50−60 °C is of interest, as this represents the extreme temperatures that may be found in a fuel cell.[67] The estimated half-life of the at these temperatures metastable ammonia-borane was found to be on the order of months at 50 °C, but only weeks at 60 °C.

For the complete release of the third molecule of dihydrogen, much higher temperatures are required (above 1200 °C).[68] Analysis of the volatile pyrolysis products for the first step suggested, besides hydrogen, traces of B_2H_6 (matrix isolation)[69] (mass spectrometry),[66] $[H_2N{=}BH_2]$ (matrix isolation)[69] and borazine (IR analysis and MS).[70,71]

The nonvolatile white residue of the first decomposition step of ammonia-borane is often described as polyaminoborane (PAB) of the composition BNH_4 but is likely to contain borazinyl residues, cyclic and cross-linked structures. This intermediate product from the thermolysis of ammonia-borane was also investigated by TGA and DSC (Figure 9).[72] The three decomposition steps have been assigned to the loss of 1 equivalent of dihydrogen to give polyiminoboranes and related compounds (eq 4)[68d,73] and gradual loss of formally half an equivalent to give a material of the composition NBH (eq 5) and finally boron nitride (eq 6). However, this analysis

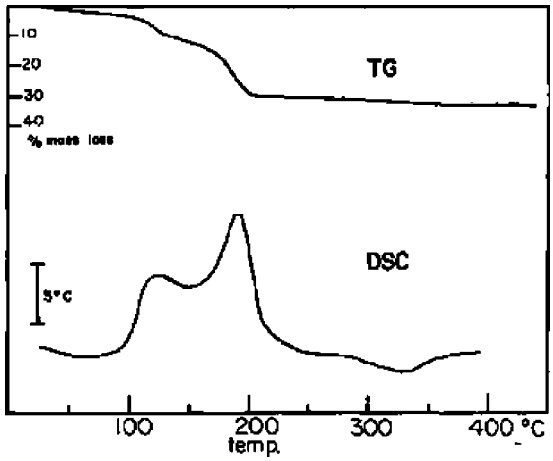

Figure 9. TG-DSC curves of $(NH_2\text{-}BH_2)_x$ in nitrogen at a heating rate of 10 °C min^{-1}. Reprinted with permission from ref 72. Copyright 1985 Elsevier.

was not attempted to verify by IR studies, which would have been able to reveal residual hydrogen.

$$NBH_4 \rightarrow NBH_2 + H_2 \quad (4)$$

$$NBH_2 \rightarrow NBH + {}^1/_2H_2 \quad (5)$$

$$NBH \rightarrow NB + {}^1/_2H_2 \quad (6)$$

The white solid product of the first decomposition step of ammonia-borane, which is often simplified as "polyaminoborane", has also been analyzed by photoelectron X-ray spectroscopy (XPS), from which it was concluded that boron and nitrogen are present in equal amounts in similar chemical environments, which is not inconsistent with the assignment as polyaminoborane.[64] Since this raised issues as to whether the sample analyzed by Geanangel and Wendlandt was chemically uniform, Baumann and co-workers repeated the analysis of polyaminoborane and prepared their samples by the isothermal decomposition of ammonia-borane at 90 °C.[74] They found that the first mass loss peak of samples prepared in this way started at 122 °C but that the extent of the mass loss was highly dependent on the heating rate (7.1 wt % for 1 °C/min to 20.3 wt % for 10 °C/min). However, these authors also analyzed the mass loss volumetrically (gaseous components only) and found that, independent of the heating rate, the volumetric mass loss was 7.6 wt % only, which corresponds well to the release of about 1 equivalent of dihydrogen. The remainder is probably comprised of smaller fragments and cyclic oligomers of polyaminoborane.

A much more detailed picture of the mechanism of the decomposition of ammonia-borane was provided by Shaw and Autrey and co-workers, who used solid state ^{11}B and $^{11}B\{^1H\}$ MAS NMR spectroscopy to follow the reaction *in situ* under isothermal conditions of 88 °C.[75] The peak shape in solid state NMR is highly dependent on the external magnetic field and while spectra at 7.1 T showed a broad peak with second order quadrupolar interactions, this effect was much reduced at 18.8 T, where only a single peak was visible for ammonia-borane at $\delta = -24.0$ ppm (Figure 10). Shortly after heating, a new species containing a BH_3 group formed, which showed quartet splitting in the proton coupled ^{11}B NMR spectrum. It was proposed that this represented a new, "mobile" phase of ammonia-borane, because there was no visible melting at this temperature, which is below the reported melting point of 112−114 °C (however, the estimation of a melting point in ammonia-borane is problematic; see discussion in previous section). After this induction period, hydrogen started to evolve, and three further species were observed: the diammoniate of diborane (DADB), $[(NH_3)_2BH_2]^+[BH_4]^-$, and two BH_2N_2 species which were possibly the linear $(NH_3BH_2NH_2BH_3)$ and the cyclic dimer $(NH_2BH_2)_2$ of aminoborane. After longer decomposition times, broad and relatively poorly defined peaks of thermally produced polyaminoborane started to emerge (for the chemical shifts of the features discussed, see Table 5).

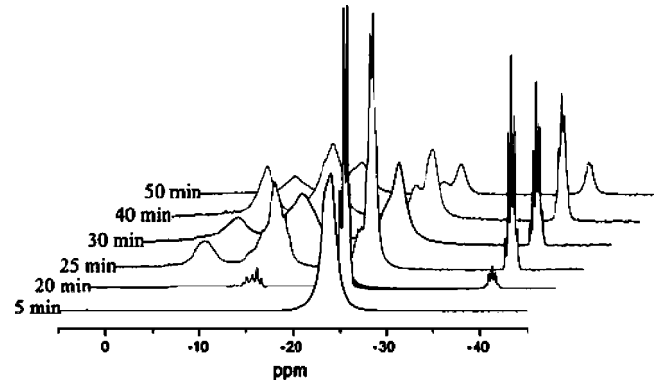

Figure 10. Evolution of signals in ^{11}B MAS NMR at an external field strength of 18.8 T. Reprinted with permission from ref 75. Copyright 2007 RSC Publishing.

Table 5. Chemical Shifts and Coupling Constants of Products Observed at Low Conversion during the *in situ* Heating of Ammonia-Borane at 18.8 T

^{11}B NMR chemical shift (ppm)	identity	$^{11}B-^1H$ *J*-coupling/Hz
−38.2	BH_4 (DADB)	77
−24.0	AB	−
−22.5	new phase AB	94
−21.1	BH_3 (linear dimer)	84
−13.2	BH_2 (DADB)	116
−12.1	BH_2 (linear dimer)	104
−10.9	BH_2 (??)	103
−10.7	BH_2 (??)	102

Based on these observations, a mechanistic model was presented which was comprised of three distinct steps: induction, nucleation, and growth (Scheme 2). In the induction period, a mobile phase of ammonia-borane is generated, in which the dihydrogen bonding network is perturbed. In the subsequent nucleation process, the diammoniate of diborane, DADB, is generated, which can then react with ammonia-borane to form dimeric, oligomeric, and eventually polymeric products or isomerize to form the cyclic dimer.

Further evidence to support this mechanism was provided by a study which used TGA/DSC, optical microscopy, and high temperature X-ray powder diffraction to examine this process.[76] In the initial stage, where very little hydrogen was released, an exotherm was observed, where the sample loses its crystallinity and birefringence, which was interpreted as a sign for the formation of the new more mobile form of $NH_3 \cdot BH_3$ and the diammoniate of diborane, $[NH_3BH_2\text{-}NH_3]^+[BH_4]^-$. The phase change could even be observed visually, when a crystal of ammonia-borane was heated to 90 °C (Figure 11).[77] From these images, a phase front can clearly be seen traveling through the crystal. When a heated crystal was quench cooled, it was possible to arrest these phases and analyze them by Raman spectroscopy to identify

Scheme 2. Proposed Thermal Dehydrogenation Mechanism of Ammonia-Borane Showing Discrete Induction, Nucleation, and Growth Steps Leading to Hydrogen Release

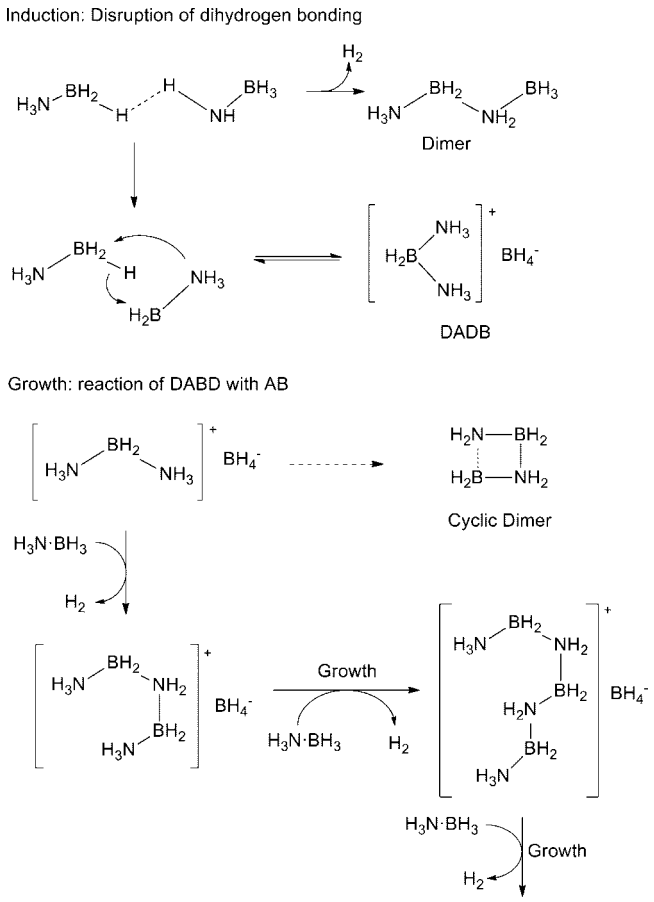

their composition. Before the phase front, the Raman spectrum showed crystalline ammonia-borane, but closer to the phase front, the peaks broaden significantly, and beyond the phase front, a frequency corresponding to a B−H stretching mode was observed which compared well to an authentic sample of DADB.

A brief report focused on another analytical technique, emission thermophotometry (ETP), which was employed for the analysis of the thermal decomposition of ammonia-borane.[78] It was observed that when ammonia-borane was heated in the presence of oxygen at a heating rate of 20 °C/min, there was a light emission starting at 180 °C and continuing up to 350 °C (the highest temperature at which measurements were obtained). The high onset temperature suggested that it was not ammonia-borane itself that ignited (light emission) but rather a decomposition product. Since pentaborane was known to ignite with a white luminescence in oxygen mixtures below the explosion limit,[79] it was surmised that a similar B−H oxidation may have occurred, although this phenomenon was never further investigated.

The thermal decomposition of ammonia-borane was also analyzed at high pressures up to 600 bar up to 450 K.[80] Dihydrogen was used as a pressurizing gas (using mercury as a pressure transmitter) because there was a particular interest in the question of whether any reversibility of the dehydrogenation could be observed. However, no evidence for a reversible process was found. The DSC trace at 600 bar with a heating rate of 0.15 K/min showed a first exothermic mass loss at 360 K (87 °C) and a second at approximately 132 °C, which were not fully resolved. Both events led to a loss of approximately 1 equivalent of volatiles each (Figure 12). With this low heating rate, no melting transition was observed, as ammonia-borane would have fully decomposed before the melting temperature of 114 °C would have been reached. Lowering the pressure to 250 bar did not significantly alter the results. It could be argued that all the observed effects were simply due to a low heating rate, with the pressure effect almost negligible, because the crystallographic form of ammonia-borane is reported to change from tetragonal to orthorhombic only at higher pressures than the 600 bar used for this study (8 kbar;[40] possibly 5 kbar;[39] for a discussion see section 3.4).

The thermal decomposition of ammonia-borane in the solid state at high pressures of up to 9 GPa was also investigated by Raman spectroscopy.[81] Contrary to the dehydrogenation at ambient pressure, only two distinct decomposition steps were found, with the first producing polyaminoborane and the second giving a precursor to hexagonal boron nitride, speculated to contain layers of planar hexagons, terminated by H bonds. At higher pressures, the decomposition steps occurred at higher temperatures. For example, at 1 GPa (10 kbar), the first equivalent of hydrogen was released at 127 °C, whereas the second step commenced at 200 °C with an average heating rate of 1 °C/min (temerature increased in 10 K increments), which was clearly visible due to the disappearance of the N−H and B−H stretching bands. At 5.5 GPa, a change in the spectrum occurred at 140 °C but did not coincide with hydrogen release and was therefore interpreted as a phase change. At 192−200 °C the first hydrogen releasing step commenced, and the second took place between 230 and 237 °C. Another study focused on the interaction of ammonia-borane and hydrogen under extreme conditions (temperature and pressure) by Raman spectroscopy.[82] Ammonia-borane became amorphous when heated at 120−127 °C at 0.7 GPa (7 kbar), with decomposition commencing at 140 °C. It was particularly insightful that decomposed ammonia-borane could not be converted back to ammonia-borane even under pressures up to 3 GPa, further highlighting the difficulties in recycling this material. A detailed analysis of the Raman spectra indicated that the decomposition process was mechanistically similar to the processes at ambient pressures, where amorphization of

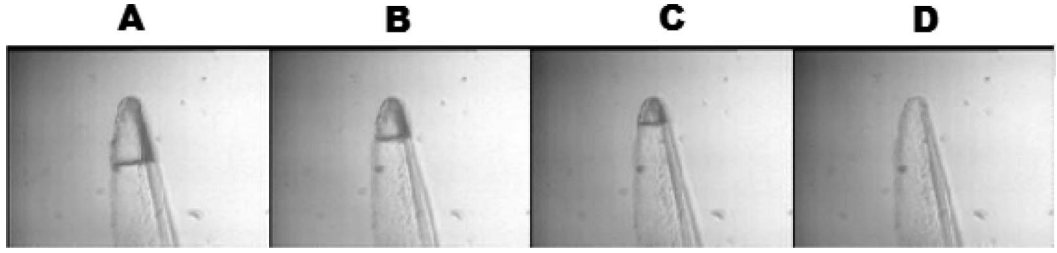

Figure 11. Optical micrograph images of a single crystal of $NH_3 \cdot BH_3$ heated to 90 °C. Reprinted with permission from ref 77. Copyright 2008 American Chemical Society.

Table 6. Thermal Decomposition of Ammonia-Borane

entry	heating rate/(°C/min)	decomposition range, weight loss, interpretation if known	ref
1	5	TGA 120−133 °C: 31.6% (reaction 1) up to 200 °C: 35% (total) (reaction 2)	62
2	10	DTA 112 °C: endotherm (melt) from 117 °C; maximum 130 °C: large exotherm (reaction 1) 150−200 °C: broad exotherm (reaction 2)	62
3	8	thermomanometry 120 °C: decrease in slope at 145 °C	62
4	2	TGA, DTA 84−114 °C: slow hydrogen loss 114 °C: endotherm (melt) 125 °C: exotherm (reaction 1) 155 °C: release of another equiv of H_2 (reaction 2)	63
5	1	95 °C, exotherm (beginning of reaction 1) "a few degrees higher", endotherm (melt) 113 °C: large exotherm (reaction 1) starting at 125 °C exotherm (reaction 2)	65
6	0.5	82 °C: exotherm (reaction 2) no melt	65

ammonia-borane is followed by isomerization to DADB, which precedes decomposition.

Lowering the pressure below ambient pressure was also shown to have a dramatic effect on the thermal decomposition of ammonia-borane, using TGA, DTA, and mass spectrometry.[83] The samples were held at 90 °C under various pressures between 50 and 1040 mbar, where at ambient pressure, hydrogen was released after approximately 6 h, dropping to around 3.5 h at 50 mbar. Other impurities such as diborane, aminoborane (NH_2═BH_2), or borazine were also observed with higher intensity at lower pressures.

4.2.2. Thermal Decomposition of Ammonia-Borane in Solution

The first studies on the thermal decomposition process of ammonia-borane in solution aimed to spectroscopically identify the elusive, postulated [H_2N═BH_2] species.[84] For this purpose, thermal reactions (reflux conditions) of 0.15 M ammonia-borane in acetonitrile, diglyme, glyme, 2-methyl tetrahydrofuran, pyridine, and tetrahydrofuran were analyzed by *ex situ* ^{11}B NMR spectroscopy. While acetonitrile and pyridine showed a reaction with the substrate, the etheral solvents showed mainly products associated with hydrogen loss. In all of the above reactions, a peak at around δ = −11 ppm occurred in varying amounts, which was assigned to cyclotriborazane by comparison with an authentic sample, but it was conceded that small cyclic oligomers of different ring sizes were not distinguishable. Borazine (δ = 30.2 ppm) and μ-aminodiborane (δ = −28.9 ppm) were also identified, and a simple hypothesis for the main decomposition pathway was presented (eqs 7 and 8).

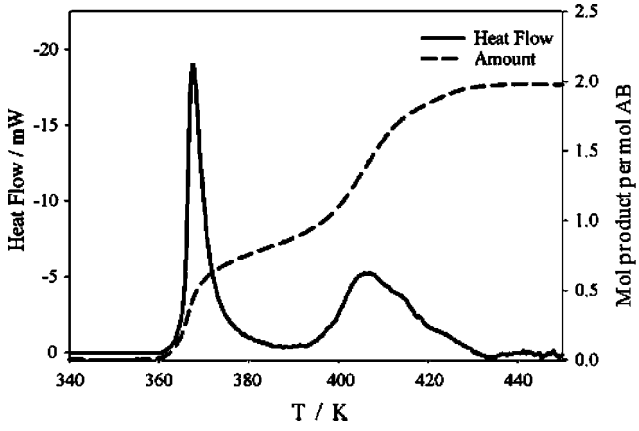

Figure 12. Temperature depedence of the heat flow (−) and the amount of released volatile products (- -) at the thermal decomposition of ammonia-borane $H_3N{\cdot}BH_3$ (transitometer ST6-VI, 600 bar, mercury as pressure transmitter, heating rate 0.15 K min^{-1}). Reprinted with permission from ref 80. Copyright 2006 Elsevier.

$$H_3N{-}BH_3 \rightarrow 1/x(H_2N{-}BH_2)_x + H_2 \quad (7)$$

$$3/x(H_2N{-}BH_2)_x \rightarrow (HN{-}BH)_3 + H_2 \quad (8)$$

Two decades later, the solution decomposition of ammonia-borane was reinvestigated, fueled by renewed interest in this molecule as a hydrogen storage material.[85] A 500 MHz spectrometer with a high pressure spinning NMR cell (produced from polyether ether ketone (PEEK)) made it possible to follow the reaction of ammonia-borane in glyme (1 M) at various temperatures *in situ* with a much higher resolution of the peaks. The first significant finding was that the reaction followed second order kinetics in ammonia-borane, as a consequence of which the stability of an ammonia-borane solution is extremely concentration dependent. Because of this observation, the authors also ruled out the unimolecular formation of [H_2N═BH_2], followed by a [2 + 2] cycloaddition, similar to earlier findings concerning the decomposition of *N*,*N*-dimethylamineborane by Beachly and Ryschkewitsch (see section 6.1): For the latter process to conform to second order kinetics, the [2 + 2] cyclization would need to be rate determining, leading to a buildup of [H_2N═BH_2], which was not observed experimentally. By ^{11}B NMR spectroscopy performed at 80 °C, the initial products appeared between δ = −10.8 and −15 ppm (Figure 13).

The initial peak at δ = −10.8 ppm was tentatively assigned to be cyclodiborazane (CDB), followed by three peaks growing at the same rate (δ = −10.9 ppm (BH_2), δ = −5.0 ppm (BH), and δ = −23.4 ppm (BH_3), possibly *B*-(cyclodiborazanyl)aminoborohydride (BCDB)). Cyclotriborazane, δ = −10.6 ppm, (CTB) assigned by comparison to an authentic sample, was the last peak to grow in. In order to further corroborate these results, the authors also measured ^{15}N NMR spectra (Table 7).

Based on these results, a novel mechanism for dehydrogenation of ammonia-borane in solution was postulated

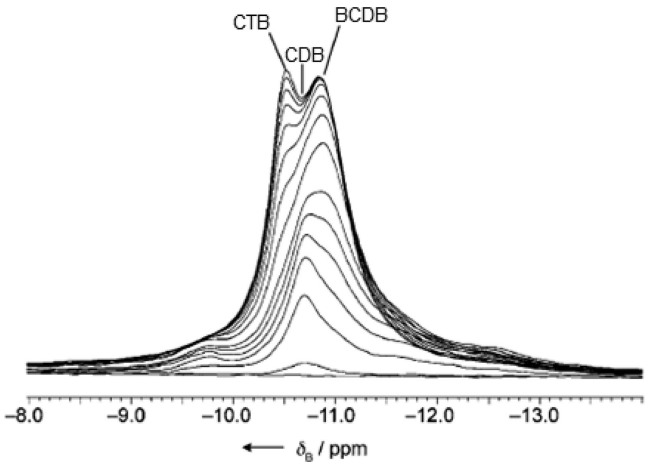

Figure 13. Time-dependent $^{11}B\{^1H\}$ NMR spectra for the first 3.5 h (0, 10, 20, 30, 40, 50, 60, 80, 120, 140, 160, 180, 200, 220 min, from bottom to top) of the thermolysis of $H_3N{\cdot}BH_3$ (1 M) at 80 °C. Cyclodiborazane was the first species to appear. Reprinted with permission from ref 85. Copyright 2008 Wiley VCH.

Table 7. ^{11}B and ^{15}N NMR Data for Decomposition Products of Ammonia-Borane, in Order of Appearance

species	^{11}B (ppm)[a] (80 °C)	$^1J_{BH}$ (Hz)	^{15}N (ppm)[b] (20 °C)	$^1J_{NH}$ (Hz)
$H_3N{\cdot}BH_3$	−21.6 (BH_3)	96 (q)	−384.5 (NH_3)	70 (q)
CDB	−10.8 (BH_2)	104 (t)	−376.7 (NH_2)	65 (t)
BCDB	−23.4 (BH_3)	93 (q)	−375.9 (NH_2)	65 (t)
	−10.9 (BH_2)	104 (t)	−370.9 (NH_2)[c]	66 (t)
	−5.0 (BH)	114 (d)		
CTB	−10.6 (BH_2)	102 (t)	−370.0 (NH_2)	66 (t)
borazine	31.1 (BH)	133 (d)	−281.7 (NH)	102 (d)
polyborazylene	27.2 (B)		−324.4 (NH)	75 (d)

[a] ^{11}B NMR chemical shifts relative to the IUPAC standard $BF_3{\cdot}OEt_2$ ($\delta = 0$ ppm) at 20 °C ($\Xi = 32.083974$). [b] ^{15}N NMR chemical shift references to NH_4Cl ($\delta = -360.2$ ppm) relative to the IUPAC standard CH_3NO_2 ($\delta = 0$ ppm; $\Xi = 10.136767$). [c] Signal for the NH_2 group outside of the ring.

(Scheme 3). It is proposed that ammonia-borane reacts initially in a bimolecular reaction to give the instable diammoniate of diborane (DADB). This may then undergo hydrogen loss with concomitant ring closure to give cyclodiborazane (CDB), which may react with another equivalent of ammonia-borane under hydrogen loss to give BCDB. Both CDB and BCDB may convert into cyclotriborazane (CTB), although there was no direct evidence for this. This reaction mechanism is largely based on the NMR data but seems slightly at odds with a second order fit for the kinetics, since firstly the initial step was assumed to be reversible (which is not an assumption for the simple second order fit used), and secondly, ammonia-borane is also postulated to be consumed in a subsequent step. Depending on the actual rate constants for the steps involved, it may be difficult to differentiate between different kinetic models, and additional studies such as kinetic isotope effects may be required.

Interestingly, the formation of borazine ($\delta = 31.1$ ppm) was also observed, concurring with the formation of CTB, which seemed inconsistent with borazine formation by simple dehydrogenation of CTB. This result seemed also not to be in accordance with an earlier report that substantial borazine formation from CTB required temperatures above 100 °C.[86] However, it has to be considered that an isothermal experiment and a temperature gradient experiment cannot be directly compared, as the onset of decomposition is highly heating rate dependent. The earlier work[86] also described an

Scheme 3. Initial Decomposition Pathways of Ammonia-Borane Based on the Results of *in situ* NMR Spectroscopy[a]

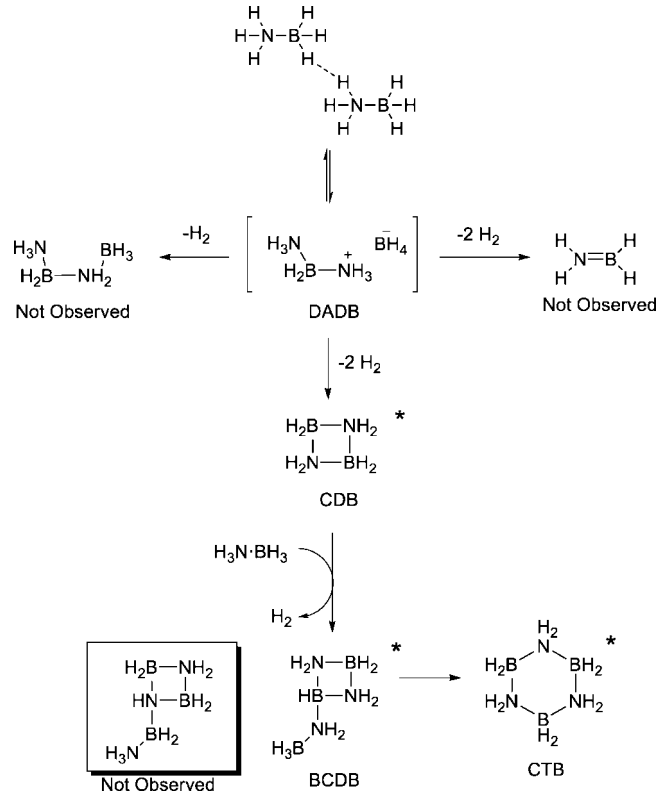

[a] Asterisks denote species observed by ^{15}N and ^{11}B NMR spectroscopy. DADB was only observed at very low concentrations in the thermolysis study at 50 °C. Adapted from ref 85.

intermediate species at ($\delta = -22.0$ ppm, -BH_3), which similarly is evidence against a simple dehydrogenation process from CTB to borazine. A catalytic effect of BH_3 as a Lewis acid derived from dissociated ammonia-borane, as theoretically predicted for the gas phase (see section 4.2.3), was not considered.

4.2.3. Thermal Decomposition of Ammonia-Borane: Computational Studies

The solid- and solution-state decomposition of ammonia-borane are highly complex processes, and it is unlikely that experiments alone will be able to reveal the full picture. This topic elicited considerable interest in the computational community, and a large body of information has accumulated over the past few years. However, the actual findings can be method (DFT or *ab initio*), functional, or even basis set dependent, so that a quantitative comparison or a detailed comparison of the computational approach between different papers is impossible and will not be attempted here.

Himmel and Schnöckel estimated the standard reaction enthalpies at 25 °C with H_2 for a range of main group compounds, for which they suspected that multiple bonding between the elements would be possible, among them ammonia-borane and its dehydrogenation products.[87] The hydrogenation of iminoborane to aminoborane was predicted to be exothermic (B3LYP, −133.3 kJ/mol (−31.8 kcal/mol); MP2, −123.3 kJ/mol (−29.4 kcal/mol), whereas the hydrogenation of aminoborane to ammonia-borane was found to be endothermic (B3LYP, 26.6 kJ/mol (6.4 kcal/mol); MP2, 28.8 kJ/mol (6.9 kcal/mol).

The thermodynamics of the dehydrogenation of ammonia-borane were then reinvestigated (in the gas phase), as the interest in its use as a potential hydrogen storage compound increased.[88] In this case, a high accuracy coupled cluster approach was used, which also predicted the hydrogenation of iminoborane to aminoborane to be exothermic (−31.4 kcal/mol at 25 °C) and the hydrogenation of aminoborane to ammonia-borane to be endothermic (5.1 kcal/mol at 25 °C). In addition to the higher accuracy of the predicted values, the dehydrogenation of iminoborane was also analyzed (134.3 kcal/mol at 25 °C).

The first mechanistic computational analysis of the thermal decomposition of ammonia-borane in the gas phase predicted an asymmetric transition state for the loss of the first equivalent of dihydrogen with a very high activation energy of 40 kcal/mol.[89] This was followed by two more detailed studies where the reaction was analyzed by DFT and *ab initio* methods.[90] The kinetic barrier proved to be rather high (32−33 kcal/mol), and in order to reconcile this with the experimentally observed values, it was suggested that an increase of the effective rate constant could be achieved by tunneling processes. The same reaction was re-examined two years later,[91] where it was found that the dissociation energy of ammonia-borane is *lower* than the energy of the transition state postulated earlier. This led to the hypothesis that BH_3 freed by this dissociation could act as a Lewis acidic catalyst for the reaction by interacting with the ammonia-borane. Indeed, three possible TSs were found for the abstraction of a protic hydrogen from nitrogen (Figure 14), where this abstraction led to a drastically lowered TS (**TSba-BN**) of about 20.9 kcal/mol (with complex **ba-com1** as a point of reference). The effect of tunneling was also tested, but here it was found that, at temperatures relevant for thermal dehydrogenation, the rate enhancing effect was small. While the basic results found in this work were corroborated, van Duin and co-workers, who used a different computational approach (reactive force field method) concluded that the BH_3 molecules formed tended to recombine with ammonia rather than react with ammonia-borane.[92] They found that, at higher temperatures, unimolecular hydrogen elimination is faster than BH_3 catalysis.

While the dehydrogenation of ammonia-borane (or indeed other primary and secondary amine-borane adducts) to yield initially $R_2N{=}BH_2$ is widely favored by most, although not all, reports, it is significantly less clear by which mechanism this species then oligomerizes. Whether it reacts with another equivalent of $R_2N{=}BH_2$ or the amine-borane adduct itself and whether a catalyst is needed for these reactions has been investigated in great detail.[93] This work is less concerned with the initial formation of $[H_2N{=}BH_2]$, which is conceded could be either formed catalytically, by the influence of a transition metal or of a Lewis acid such as BH_3, or formed by dissociation of the complex. However, it was argued that this species could either react with a molecule of ammonia-borane to give **sp3dimer** or dimerize to give **CDB** (Scheme 4). **sp3dimer** could dehydrogenate to give 2 equivalent of $[H_2N{=}BH_2]$, which renders this species an autocatalyst for its formation. Besides dimerizing, it could also react to give a highly reactive intermediate **bh3int**, which proved to be a key species. Either by [2 + 2] cycloadditions or hydroboration reactions, which were energetically close, **bh3int** could react with $[H_2N{=}BH_2]$ to give oligomeric species or the cyclic species **BCDB**, which has also been experimentally identified by Baker and co-workers.[94] The exact ratio of the observed products was concluded to be likely a kinetic distribution because similar configurational isomers proved to have similar energies.[93] In general, removal of H_2 was exothermic by 6.4 kcal/mol.

Upon publication of experimental studies pointing toward the involvement of DADB as a crucial intermediate in the decomposition of ammonia-borane in the solid state, this reaction was rapidly analyzed computationally.[95] Using a CCSD(T) approach, it was demonstrated that while there are a number of head-to-tail ammonia-borane dimers, the ionic

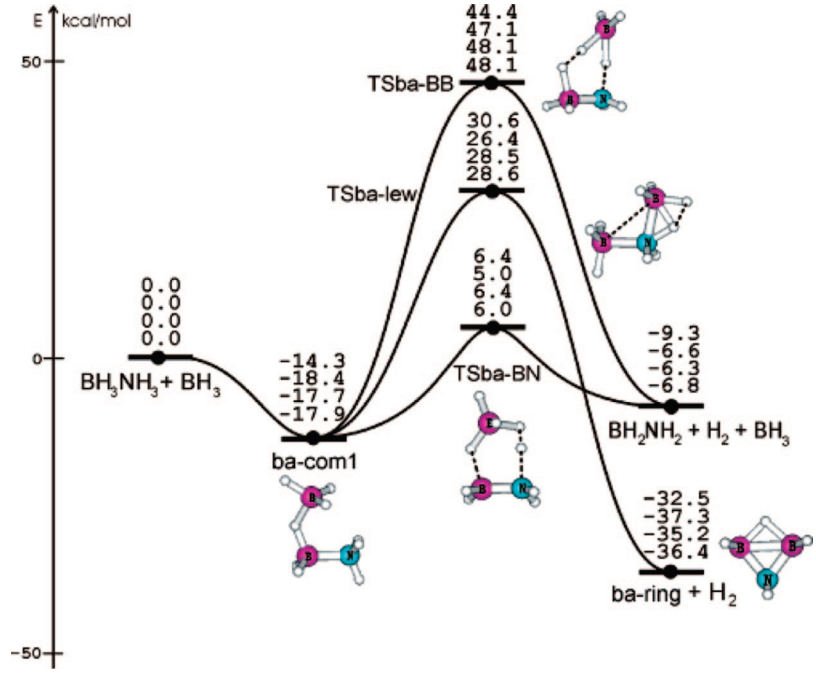

Figure 14. Computational prediction of BH_3 catalyzed dehydrogenation of ammonia-borane. Relative energies in kcal/mol are given in order from top to bottom: B3LYP/aVTZ, MP2/aVTZ, CCSD(T)/aVTZ, and CSD(T)/CBS, respectively. Zero point energies were derived from B3LYP for the first entry and from MP2 for the others. Reprinted with permission from ref 91. Copyright 2007 American Chemical Society.

Scheme 4. Possible Pathways for the Reaction of $[H_2N{=}BH_2]$ with Itself or Ammonia-Borane, Leading to Oligomers in an Autocatalytic Pathway[a]

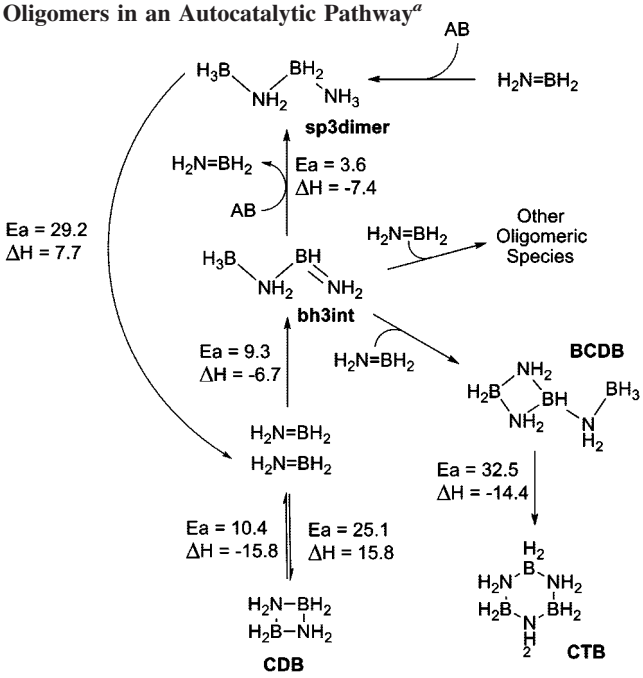

[a] All energies are in kcal/mol.

DADB was 10.6 kcal/mol higher in energy than the most stable of them (in the gas phase, which may overestimate the effect somewhat). DADB could be generated in three different ways: (i) from two monomers with a barrier of approximately 26 kcal/mol, (ii) from two NH_3 molecules, successively adding to diborane, and (iii) from ammonia-borane with successive addition of the borane and the amine, all via a different initial pathway but eventually the same rate limiting barrier. The crucial step is the loss of dihydrogen from DADB (Figure 15), which was predicted to proceed via a low barrier of about 20 kcal/mol to give the linear dimer.

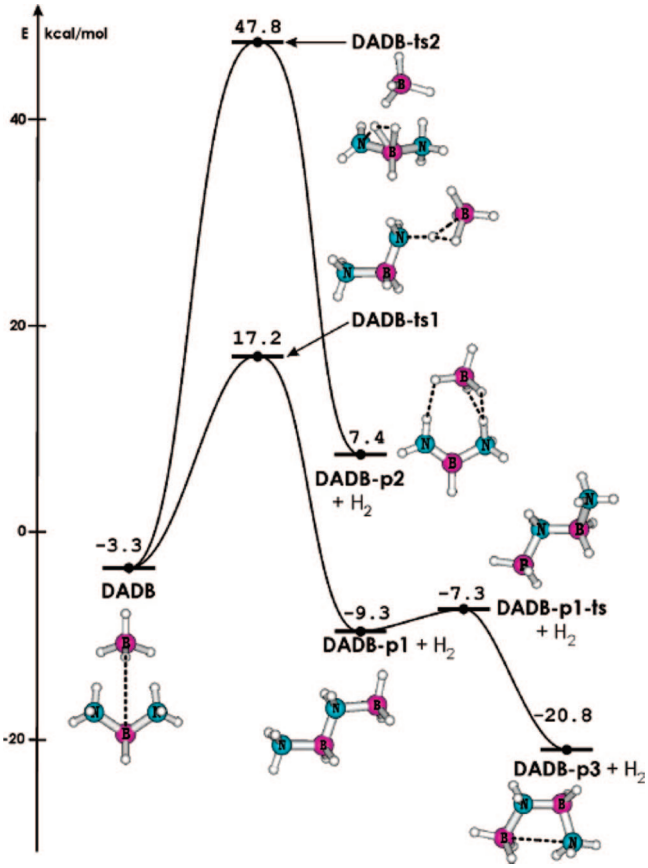

Figure 15. Postulated mechanism for H_2 release from **DADB**. Relative energies in kcal/mol were obtained from CCSD(T)/aVTZ + ZPE calculations. Reprinted with permission from ref 95. Copyright 2007 American Chemical Society.

Most computational studies deal with ammonia-borane and its various (proposed) decomposition products in the gas phase or at least as discrete molecules onto which a solvent effect is sometimes superimposed. Only one paper to date used a periodic quantum mechanical approach, taking into account a full crystallographic cell.[96]

As described earlier, ammonia-borane behaves differently in solution and in the solid state so that both methods are important to gain a complete understanding of the thermolytical processes involved. Miranda and Ceder defined the reactions that may occur during the thermal decomposition based on experimental thermogravimetic and DSC measurements (earlier section) as follows:[96]

Formation of polyaminoborane

$$x\mathrm{NH_3 \cdot BH_3(s)} \rightarrow [\mathrm{NH_2{-}BH_2}]_x + x\mathrm{H_2(g)} \quad (9)$$

Formation of cyclotriborazane

$$3\mathrm{NH_3 \cdot BH_3(s)} \rightarrow (\mathrm{NH_2{-}BH_2})_3 + 3\mathrm{H_2(g)} \quad (10)$$

Formation of polyiminoborane

$$[\mathrm{NH_2{-}BH_2}]_x \rightarrow [\mathrm{NH{-}BH}]_x + x\mathrm{H_2(g)} \quad (11)$$

Formation of boron nitride

$$[\mathrm{NH{-}BH}]_x \rightarrow x\mathrm{BN} + x\mathrm{H_2(g)} \quad (12)$$

Formation of borazine

$$3\mathrm{NH_3 \cdot BH_3(s)} \rightarrow \mathrm{B_3N_3H_6(g)} + 6\mathrm{H_2(g)} \quad (13)$$

Dehydropolymerization of borazine

$$\mathrm{B_3N_3H_6(g)} \rightarrow [\mathrm{B_3N_3H_6}]_x + \mathrm{H_2(g)} \quad (14)$$

They also analyzed potential rehydrogenation steps as follows:

Rehydrogenation of borazine

$$\mathrm{B_3N_3H_6(g)} + 3\mathrm{H_2(g)} \rightarrow (\mathrm{NH_2{-}BH_2})_3 \quad (15)$$

Their DFT study used the crystallographically determined structure by Crabtree and co-workers for ammonia-borane and polyethylene as a model for PAB. This would have introduced its own errors, as evidence mounts that polyaminoboranes and polyolefins are very different polymers, but the possible conformations were taken into account.

This study showed that the formation of PAB and PIB was exergonic at all temperatures and increasingly so with increasing temperature (Figure 16). The formation of polyborazylene PB was exergonic in all cases but relatively constant over a wide temperature range (between −8 and −12 kcal/mol). The rehydrogenation free energy of borazine to form cyclotriborazane was positive at all temperatures and increased with increasing temperatures.

Perhaps the most important finding in this paper was the indication of the importance of analyzing the reactions in the solid state. While the reaction enthalpies for the first reaction (eq 9) are similar in the solid state and for isolated

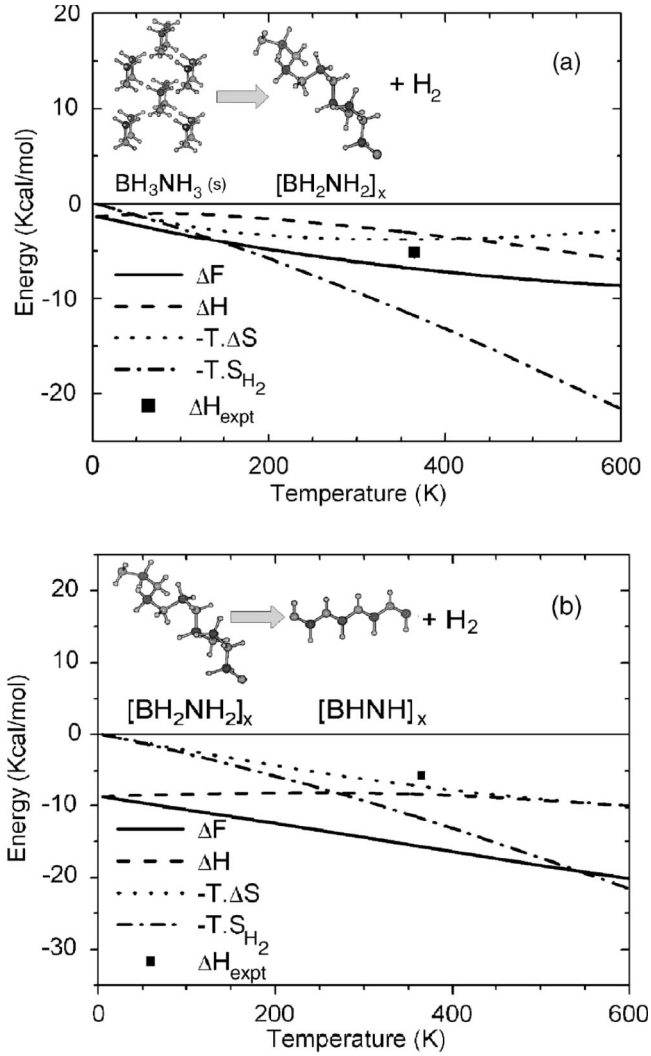

Figure 16. Thermodynamic properties for the thermal decomposition reactions of ammonia-borane. Helmholtz free energy difference, full line; reaction enthalpy, dashed line; reaction entropy, dotted line; entropic term of the H_2 molecule, dotted-dashed line. The square represents the experimental data available for the reaction enthalpy. (a) Polyaminoborane formation; (b) polyiminoborane formation. Reprinted with permission from ref 96. Copyright 2008 American Institute of Physics.

molecules, this is no longer true for the formation of iminoborane. Here the reaction $NH_3 \cdot BH_3 \rightarrow 2H_2 + HNBH$ was predicted to be strongly endothermic *in the gas phase* ($\Delta H = +30.99$ kcal/mol[96] or $\Delta H = 29.5$ kcal/mol[88]) at 0 K; the corresponding reaction to form polyiminoborane was an exothermic reaction *in the solid state* ($\Delta H = -9.57$ kcal/mol).[96] It was concluded from this that a direct reversibility of the reaction was unlikely.

4.3. Metal-Catalyzed Reactions

The first report in the open literature by Manners and coworkers detailing a clear catalytic dehydrocoupling of amine-boranes in 2001 focused on the use of Rh(I)- or Rh(III)-based precatalysts at, or close to, ambient temperature.[97] The initial and subsequent report included a description of the effective first use of ammonia-borane itself as a substrate to give borazine and an insoluble material with a complex and presumably oligomeric structure.[9,97] In 2006, an extremely effective catalyst was reported by Goldberg and Heinekey.[98] They demonstrated that Brookhart's iridium pincer complex,

Scheme 5. Two Independent Routes for the Formation of the Dormant Borohydride Complex

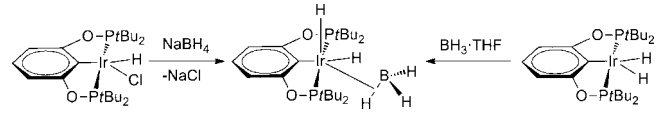

$(POCOP)Ir(H)_2$ (POCOP = $[\mu^3$-1,3-$(OPtBu_2C_6H_3)]$)[99] was able to dehydrogenate ammonia-borane in a dilute THF solution with a catalyst loading of 0.5 mol % within 14 minutes. The product of the reaction was poorly soluble and was characterized by IR, powder X-ray diffraction, and solid state ^{11}B MAS NMR spectroscopy. The authors proposed that this product is cyclopentaborazane $[NH_2\text{-}BH_2]_5$, based on the PXRD pattern, which is close to the data set reported by Shore.[100] However, it cannot be concluded that the product was not linear and oligomeric or polymeric in nature. It is significant that only 1 equivalent of hydrogen was released. There is too little evidence at present to fully understand this selectivity, but it is possible that the main reason may be the sterically crowded catalytic center, which hinders the reaction of secondary amine-boranes. Initial recycling studies showed that the catalyst was converted over time to a resting state; addition of hydrogen was then shown to regenerate the active catalyst. The dormant species was initially assumed to be $(POCOP)IrH_2(BH_3)$. It was possible to prepare this complex by two other independent routes and to characterize its structure by neutron diffraction.[101] The first route involved the treatment of the precursor of $(POCOP)IrH_2$ with sodium borohydride, whereas in the second route Brookhart's catalyst was employed directly and $BH_3 \cdot THF$ added (Scheme 5). Although the signal to parameter ratio was not high, it was possible to determine that in the dormant borohydride complex two H atoms on Ir are bound like hydrides, whereas BH_3 assumes the role of a B−H-σ-donating ligand.

A possible mechanism for the dehydrogenation by $(POCOP)IrH_2$ was described by Paul and Musgrave, who used a slightly simplified model.[102] They analyzed two different pathways, one via a 14-electron iridium species, which they concluded could not take place at room temperature, and another via a 16-electron species. Here, the catalyst was initially electrostatically stabilized by binding the substrate via the hydridic B−H hydrogen. In a concerted transition state (TS), the protic hydrogen N−H was transferred to the iridium, followed by dissociation of the dehydrogenated amine-borane. In the second TS, the dihydrogen was formed and left the complex. Both barriers for the TSs were similar, so it is possible that there are two rate limiting steps in this reaction. Experimentally, the tetrahydride appeared as the major detectable intermediate, which is in accordance with the mechanism presented.

When proposing suitable catalytic systems for a hydrogen storage application, the chemical and physicochemical properties are just one aspect to consider. It is also important to ascertain that the catalyst is economically viable, which is why systems based on nonprecious metals are of considerable interest. One class of such systems is based on nickel carbene complexes (Figure 17).[103] On mixing a $Ni(cod)_2$ solution in C_6D_6 with various *N*-heterocyclic carbene ligands, and adding this mixture to a solution of ammonia-borane in diglyme in a 1:10 ratio at 60 °C, immediate hydrogen evolution was observed. After 4 h, up to 2.8 equivalents of hydrogen had evolved, which makes this one of the most effective (presumably) homogeneous systems for the dehydrogenation of ammonia-borane to date. The major products

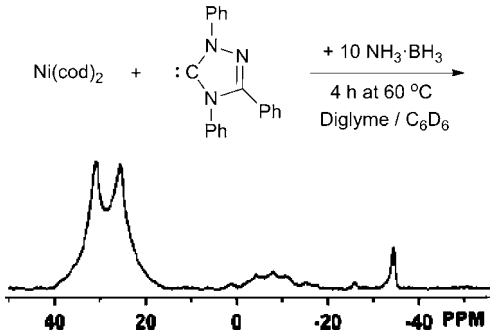

Figure 17. $^{11}B\{^1H\}$ NMR spectrum in C_6D_6/diglyme from the reaction of 10 equiv of $NH_3 \cdot BH_3$ with 1 and 2 equiv, respectively, of $Ni(cod)_2$ and Enders' NHC after 4 h at 60 °C. The signal at −36 ppm is attributable to the NHC-BH_3 adduct (ca. 2% of total B). Reprinted with permission from ref 103. Copyright 2007 American Chemical Society.

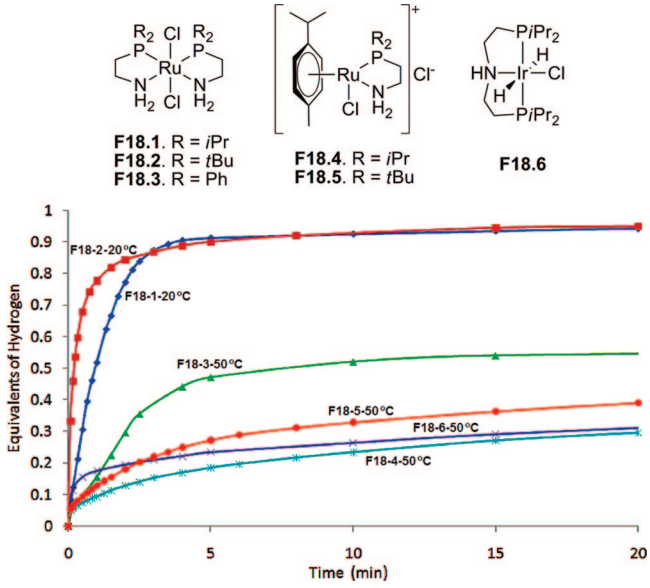

Figure 18. Fagnou's results on $MeNH_2 \cdot BH_3$ dehydrogenation with ruthenium catalysts. Reprinted with permission from ref 105. Copyright 2008 American Chemical Society.

showed peaks from 40 to 18 ppm by ^{11}B NMR spectroscopy and were attributed to cross-linked borazine-type species. Importantly, this was one of the first studies to report kinetic isotope effects for $NH_3 \cdot BD_3$ (1.7), $ND_3 \cdot BH_3$ (2.3), and $ND_3 \cdot BD_3$ (3.0), which combined with computational studies[104] provided useful mechanistic insights. The reactions were fitted using a first-order rate law for a time frame up to 120 min, but more detailed kinetic studies may be needed to confirm the applicability of this rate law, since diversions from it often only become evident when the reaction is observed in full.

The mechanism for this reaction elicited a debate in the literature, where several computational studies appeared.[104] All agree that the carbene ligand on nickel participated in a proton abstraction from nitrogen, but for the subsequent steps, a large number of pathways are conceivable, the majority of which are comprised of interlinked catalytic cycles. A detailed description and discussion of these proposals is beyond the scope of this review and is presented elsewhere by us.[1]

In 2008, two highly active ruthenium catalysts were reported independently at nearly the same time.[105,106] While ammonia-borane is formally isoelectronic to ethane, its polarity and electronic structure is more closely related to methanol. Therefore, *t*BuOK activated Ru-catalysts were screened for the dehydrogenation of ammonia-borane,[105] which had already been successfully used for alcohol redox processes.[107] Thereby, this report introduced a further concept for the hypothesis driven catalyst discovery besides the isoelectronic relationship with ethane (Goldberg and Heinekey) and the similarity of the process to other E-H/E-H dehydrocoupling processes (Manners). Those catalysts released up to 1 equivalent of hydrogen within 5 minutes, with catalyst loadings as low as 0.03 mol %. Interestingly, up to 2 equivalents of dihydrogen were released from *N*-methylamine-borane and the overall hydrogen yield from ammonia-borane could be increased via codehydrogenation it with *N*-methylamine-borane.

Fagnou and co-workers briefly investigated a possible mechanism for this transformation in analogy to alcohol redox processes (Figures 18 and 19). They suggest a Ru-dihydride as the catalytically active species, which would be formed *in situ*. This could then be protonated at the amido group of the ligand by the protic hydrogens of ammonia-borane, which would then lead to the dehydrogenated ammonia-borane intermediate and a *trans*-Ru-dihydride. The latter could then be protonated by the ligand to give a dihydrogen complex, which would then be able to evolve dihydrogen and release the active catalytic species.

The second catalyst was a new Ru(II) complex bearing a PNP amido chelate ligand, which could undergo reversible hydrogenation reactions at both the amine functionality and the ethylene backbone (Scheme 6).[106]

This complex proved to be a very active catalyst for the dehydrogenation of ammonia-borane. Catalyst loadings of 0.1 mol % led to the evolution of slightly more than 1 equivalent of hydrogen within 10 min (pseudo-first-order rate constant = 0.0013 s^{-1}). Even catalyst loadings as low as 0.01 mol % were effective (0.83 equivalent of hydrogen,

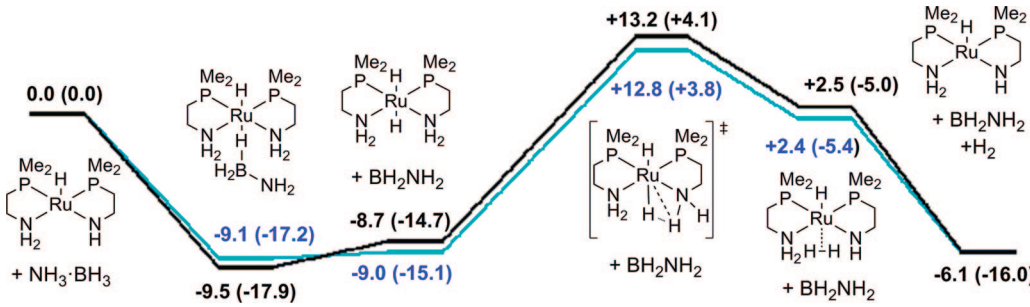

Figure 19. Possible mechanism for the dehydrogenation of ammonia-borane with Ru catalysts. Black and blue lines indicate different conformers of the P,N ligands of the Ru species. Reported values are in kcal/mol. ΔG_{298K} in THF (ΔG_{298K} gas phase). Reprinted with permission from ref 105. Copyright 2008 American Chemical Society.

Scheme 6. Hydrogenation/Dehydrogenation Equilibria between the Amino (S6-2), Amido (S6-3), and Enamido (S6-1) Complexes

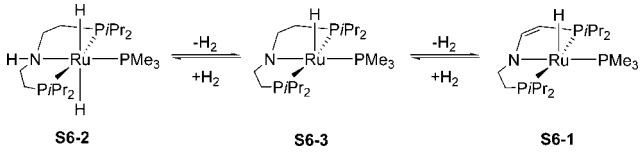

Table 8. Reactivity of Ammonia-Borane with Acids at 60 °C

acid	loading (mol %)	conc. of AB (M)	time (h)	H_2 (equiv)
$B(C_6F_5)_3$	25	0.14[a]	24	0.6
$B(C_6F_5)_3$	0.5	2.6[b]	20	1.1
$HOSO_2CF_3$	25	0.13[a]	18	0.8
$HOSO_2CF_3$	0.5	6.2[c]	18	1.3
HCl	0.5	2.9[c]	20	1.2

[a] Reaction in glyme. [b] Reaction in tetraglyme. [c] Reaction in diglyme.

Scheme 7. Postulated Mechanism for the Initial Reaction of Ammonia-Borane with Acids[a]

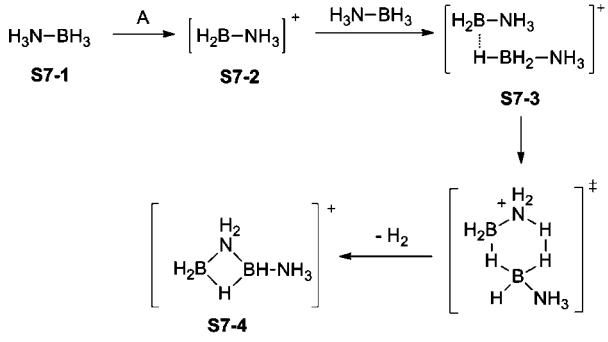

[a] The counter anion was either $HB(C_6F_5)_3$ or OTf.

pseudo-first-order rate constant = 0.0021 s^{-1}). At the time of writing, the mechanism for this reaction has not been fully studied. Kinetic isotope effects (KIEs) suggest a concerted mechanism, with KIEs of 2.1 ($D_3B{\cdot}NH_3$), 5.2 ($H_3B{\cdot}ND_3$), and 8.1 ($D_3B{\cdot}ND_3$) found relative to $H_3B{\cdot}NH_3$ dehydrogenation.

Perhaps unsurprisingly, the mechanisms are very different depending on the metal and/or the ligands used. However, a common denominator is that all require an initial interaction between the boron or the hydridic hydrogen on the boron and the metal, either via an electrostatic interaction or, in the case of the nickel carbene, a H−B σ-complex-like structure.

4.4. Lewis- and Brønsted Acid-Catalyzed Dehydrocoupling

The successful use of Lewis and Brønsted acids to release hydrogen from ammonia-borane under nonhydrolytic conditions at 60 °C was reported by Baker and Dixon (Table 8).[108]

They postulated that the acid initially abstracts a hydride from ammonia-borane to form an amine-borenium ion (**S7-2**), which then reacts with another ammonia-borane molecule with loss of dihydrogen to eventually form **S7-4** (Scheme 7).

S7-4 itself could then abstract a hydride from ammonia-borane or other neutral oligomers to give a linear dimer, which would consume a borenium cation to give **S8-7** and the cationic part of DADB without release of dihydrogen (Scheme 8).

It was reasoned that, therefore, if the amount of acid was reduced, the formation of **S8-7** should be repressed and more ammonia-borane (or its oligomers) present for actual loss of dihydrogen. Indeed, when less acid was used, the overall yield of dihydrogen increased, although it has to be pointed out that the concentration of ammonia-borane was also increased at the same time, so that a concentration effect seems equally likely. The proposed mechanism was further reinforced by computational studies and ^{11}B NMR measurements and similarities to the dehydrogenation of ammonia-borane in ionic liquids and in glyme without additional reagents.

In this context, it is necessary to mention that the dehydrocoupling of amine-boranes, including ammonia-borane, has been achieved using a frustrated Lewis acid Lewis base pair.[109] The reactivity of Lewis acids and bases which are too sterically hindered to react directly, or may only form metastable complexes, has been used extensively to activate small molecules and recently been reviewed.[110] In addition, a computational study has appeared explaining the molecular mechanism of the reaction.[111]

4.5. Hydrogen Release from Ammonia-Borane Facilitated by Scaffolds

In the area of hydrogen storage, the concept of using additives to destabilize a hydrogen containing compound to lower the onset temperature of hydrogen release is fairly well established.[112–114] This approach has also been utilized for ammonia-borane, which will be discussed in the following section.

In 2005, a related approach to reduce the dehydrogenation temperature of ammonia-borane in the solid state was to form nanocomposites of a matrix with intercalated ammonia-borane. It was recently demonstrated that such a nanocomposite of mesoporous silica and ammonia-borane in a 1:1 mixture allowed the thermal decomposition of ammonia-borane at 50 °C with a half-reaction time of 85 min compared to a half-reaction time of 290 min at 80 °C for neat ammonia-borane.[115] This corresponded to peak dehydrogenation temperatures of approximately 110 °C for ammonia-borane and approximately 98 °C for the nanocomposite by DTA, when a heating rate of 1 °C/min was used. An even more spectacular decrease in the decomposition temperature could be achieved with a 24 wt % carbon cryogel/ammonia-borane nanocomposite (Figure 20).[116] In this case, the dehydrogenation started at <80 °C, with a decomposition peak at approximately 90 °C, with no further decomposition peak at higher temperatures. Volumetric measurements indicated

Scheme 8. Chain Termination without Hydrogen Release

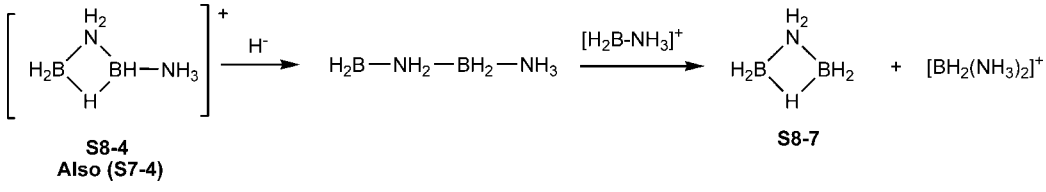

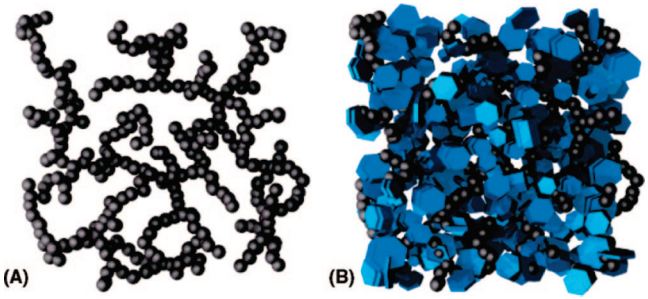

Figure 20. Schematic of an unmodified carbon cryogel (A) and a carbon cryogel/ammonia-borane nanocomposite. Reprinted with permission from ref 116. Copyright 2007 American Chemical Society.

a 9 wt % loss of dihydrogen, and no borazine formation was observed by mass spectrometry.

The mechanism(s) by which the catalysis occurs may be similar for both cases. It is possible that the observed effect may be primarily a function of the considerably increased surface area for the ammonia-borane, due to being forced into nanoscale pores, which is known to lower the phase transition temperature and thereby presumably the dehydrogenation temperature. Another possibility is that, on the surface of the cavities, there are exposed functional groups, such as SiOH in the first case and carboxylic acids in the second case. It is known (see section 4.4) that acids can accelerate the dehydrogenation of amine-boranes. In agreement with both explanations is the fact that smaller pore sizes reduce the decompostion temperature.

In order to deepen the understanding of the dynamic behavior of ammonia-borane in mesoporous silica, quasielastic neutron scattering experiments were used.[29] It was speculated that the incorporation of ammonia-borane in mesoporous silica led to reduced barriers of activation for proton movements, which may contribute to the faster hydrogen release kinetics of ammonia-borane in this environment.

A much more detailed analysis of the deposition of ammonia-borane in mesoporous silica was made possible by using hyperpolarized ^{129}Xe NMR spectroscopy.[117] This highly sensitive technique utilizes the fact that the chemical shift of ^{129}Xe shows a strong dependence on the size, shape and connectivity of the pores in porous materials and also chemical environments such as the adsorbent itself. For these studies, commercially available mesoporous silica was used, which was infiltrated with THF solutions of ammonia-borane in various quantities before drying. In a sample without ammonia-borane (0:1 AB:MCM, Figure 21), there were two signals evident: one at 0 ppm for free ^{129}Xe gas and a downfield shift (green arrows) for ^{129}Xe adsorbed into the pristine cavities. When the inside of the pores was coated with about 33 wt % of ammonia-borane, a new signal, slightly upfield from the peak for the pristine pores, emerged, which was assigned to ^{129}Xe interacting with adsorbed ammonia-borane in the pores. At higher ammonia-borane loadings, a peak only slightly downfield from free ^{129}Xe appeared, which was interpreted to be due to interparticle spacing as a result of the deposition of excessive ammonia-borane. The saturation loading appeared to be around 33 wt %, which was higher than the 22 wt % calculated from the known surface area for this batch of mesoporous silica, suggesting that ammonia-borane was present in quantities beyond that of a monolayer. While this technique cannot provide any further insight into the hydrogen dynamics of ammonia-borane in confined spaces, it was speculated that

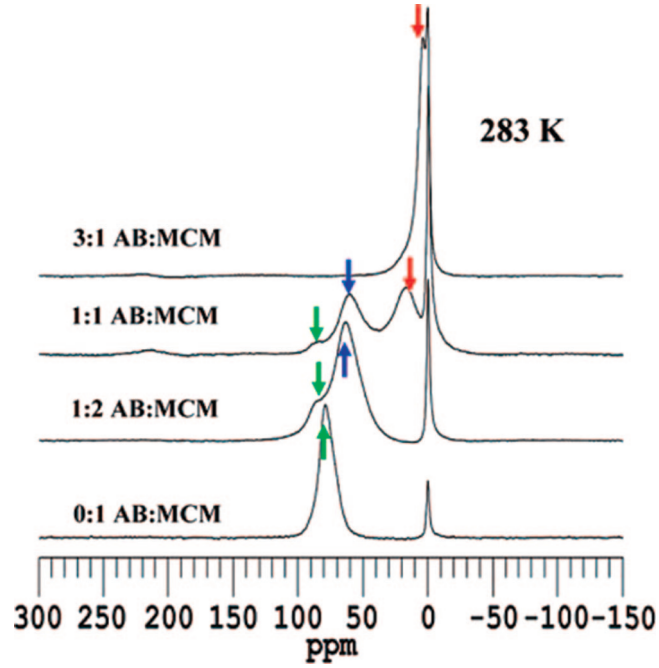

Figure 21. Hyperpolarized ^{129}Xe NMR spectra for 0:1, 1:2, 1:1, and 3:1 AB-MCM (ammonia-borane-mesoporous silica) materials at 283 K. Peak labels correspond to pristine mesoporous channels in MCM (green arrows), mesoporous channels coated with AB (blue arrows), and interparticle spacing due to the excessive AB aggregated outside the MCM mesochannels (red arrows). Reprinted with permission from ref 117. Copyright 2009 American Chemical Society.

the dihydrogen bonding network of ammonia-borane was disturbed at the surface of the mesoporous silica, which might facilitate the formation of diammoniate of diborane, as suggested by *in situ* NMR spectroscopic studies,[85] and thus lower the decomposition temperature of ammonia-borane.

The nature of the ammonia-borane/mesoporous silica nanocomposite was further analyzed by the highly sensitive anelastic spectroscopy technique and by differential scanning calorimetry.[118] As described in detail in section 2, ammonia-borane is known to undergo a crystallographic phase transition at approximately 225 K from a low temperature orthorhombic phase to a higher temperature tetragonal phase. In anelastic spectroscopy (performed below 5 kbar so as not to measure in the region of the known pressure induced phase transition), this can be seen as a clear change in the Young's modulus with a change in temperature. However, mesoporous silica that had been infused with 1 weight equivalent of ammonia-borane showed a much reduced change, whereas mesoporous silica that had been infused with 0.5 weight equivalent of ammonia-borane showed none (Figure 22). A similar effect was seen in the DSC measurements, where the 225 K phase transition of ammonia-borane was detected as a clear strong peak, whereas the 1:1 mixture showed only a very small peak that was completely absent in the 1:2 mixture (Figure 23). This in itself was insufficient to prove the absence of a phase transition, as it was considered that the order of the transition may have changed from first to higher order, which would proceed without heat exchange and hence be invisible by DSC. However, combined with the anelastic spectroscopy data, where there was no change in the Young's modulus in the 1:2 mixture, the absence of a phase transition of ammonia-borane in mesoporous silica was proven conclusively. It is worthwhile to note that the hyperpolarized ^{129}Xe NMR spectroscopy study found that,

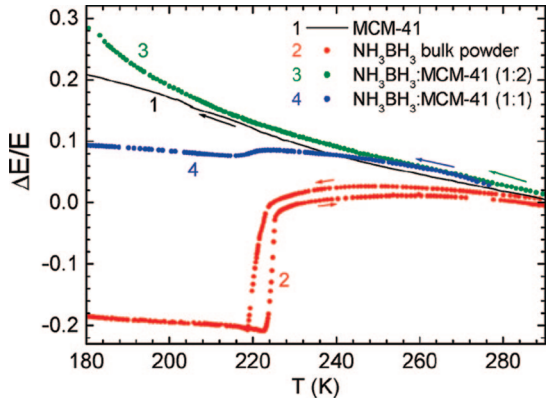

Figure 22. Temperature dependence of the variation of the Young's modulus relative to its room temperature value. Ammonia-borane (red dots), pure mesoporous silica (black line), and ammonia-borane infused in mesoporous silica MCM-41 (green and blue dots). Reprinted with permission from ref 118. Copyright 2009 American Chemical Society.

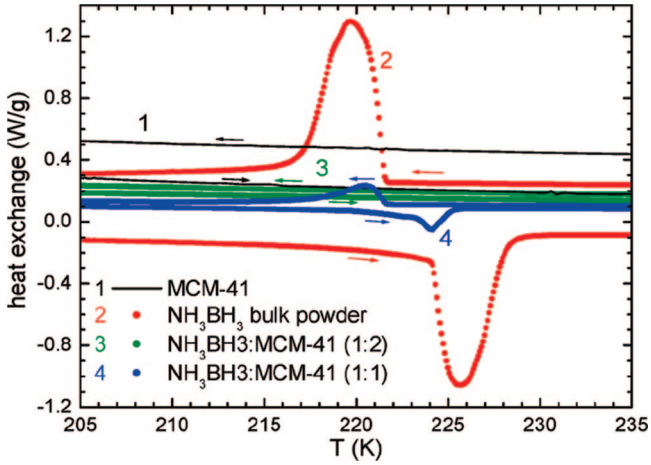

Figure 23. DSC curves of ammonia-borane (red dots), pure (black line), and infused in mesoporous silica MCM-41 (green and blue dots), measured both on cooling and on heating (5 K/min). Reprinted with permission from ref 118. Copyright 2009 American Chemical Society.

at the 1:2 loading, the ammonia-borane layer in the cavities is already beyond monolayer thickness,[117] which could be interpreted as the structural change of ammonia-borane in mesoporous silica being translated from the direct surface/ammonia-borane interaction to layers which are slightly further away. It is to be expected that this change in dynamic behavior of ammonia-borane upon infusion into mesoporous silica has a strong influence on the decomposition kinetics of this compound.

Synchrotron X-ray powder diffraction data of ammonia-borane infused in mesoporous silica allowed structural changes to be followed in the temperature range 80−300 K.[119] Contrary to the case of free ammonia-borane, where the phase change from low temperature orthorhombic to the higher temperature tetragonal phase occurred at 225 K, in the nanoscaffold, the tetragonal phase was visible between 110 and 240 K and became disordered at higher temperatures. These studies further underpin the drastic effects that a porous support for ammonia-borane can have and may in time lead to an improved mechanistic understanding of the facilitated hydrogen release in these systems.

In a further study of the decomposition of ammonia-borane in carbon cryogel, these processes were analyzed using a combination of *in situ* ^{11}B NMR spectroscopy and IR spectroscopy.[120] In particular, the fact that in mesoporous silica the exothermicity of the reaction was decreased to −1 kJ/mol (−0.2 kcal/mol), whereas in carbon cryogel it is was increased to −120 kJ/mol (−28.7 kcal/mol), was puzzling and indicated that fundamentally different processes must be taking place. By ^{11}B NMR spectroscopy at 85 °C, a low intensity peak at $\delta = -22.1$ ppm started to form adjacent to the peak for ammonia-borane at $\delta = -23.6$ ppm, possibly due to a new phase of ammonia-borane.[75] The intensity of this peak increased over time, while peaks from reaction products started to appear (BH_2 peaks at −12 ppm and BH_4 peaks at −38 ppm). A peak at $\delta = 28$ ppm could indicate the formation of a polyborazylene-like species, which was interpreted as an indication that polymerization of borazine is favored over release, thereby accounting for the clean formation of dihydrogen by this process. Interestingly, a new peak at $\delta = 16$ ppm was also observed which was not evident either in neat ammonia-borane decomposition or in decomposition in mesoporous silica, since borates have characteristic shifts in this region of the ^{11}B NMR spectrum, and this resonance could be interpreted as surface-O-BX_2 (Figure 24).

The ammonia-borane/carbon cryogel composite was also studied by Fourier transform infrared spectroscopy (FTIR). The carbon cryogel component reduced the effective signals for ammonia-borane and its decomposition products, which made the interpretation of the spectra difficult. However, weak bands in the region diagnostic of B−O and OBO stretching and bending frequencies were observed[121] which, if correct, would be further evidence for a chemical participation by the scaffold for dihydrogen release from ammonia-borane. This contribution was termed "catalysis", but there was no evidence that this is in fact not a stoichiometric process. Indeed, given the stability of B−O bonds, this seems unlikely and it is possible that the process

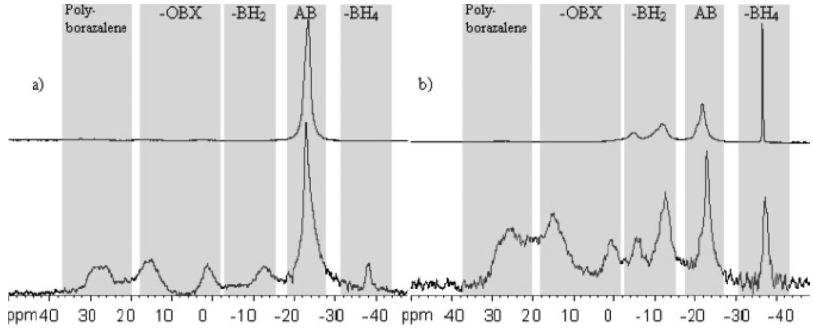

Figure 24. ^{11}B NMR of neat AB (top) and CC-AB (bottom): (a) before heating; (b) after heating CC-AB for 10 min at 85 °C and AB for 50 min at 85 °C. No reaction of AB at 10 min; data not shown. Reprinted with permission from ref 120. Copyright 2007 American Chemical Society.

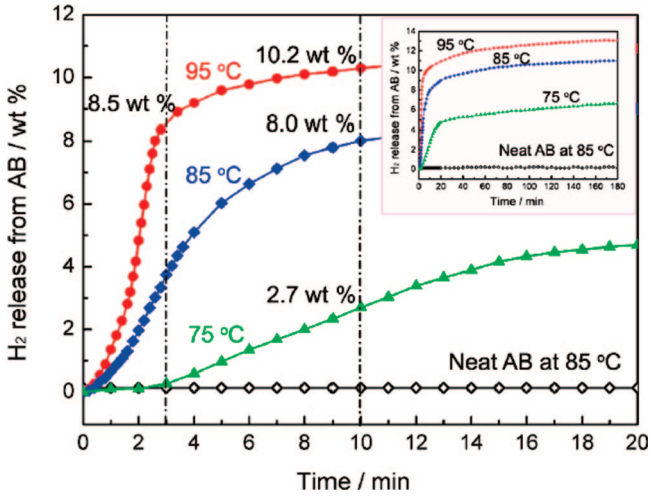

Figure 25. Time dependences of hydrogen release from AB/JUC-32-Y at 95 °C (red circle), 85 °C (blue diamond), and 75 °C (green triangle) and from neat AB at 85 °C (black diamond). Reproduced with permission from ref 124. Copyright 2010 American Chemical Society.

resembles the (uncatalyzed or acid catalyzed) hydrolysis of ammonia-borane at higher temperatures. Further hypotheses are that defects sited in the carbon cryogel mesoporous scaffold and limited diffusion of ammonia-borane in the scaffold led to faster kinetics, in addition to the surface interactions, which would destabilize the hydrogen bonding network in neat ammonia-borane, as mentioned earlier.

The addition of ammonia-borane during the process of formation of carbon cryogels was also investigated.[122] The pyrolyzed carbon cryogel which was modified with ammonia-borane displayed an increased surface area and larger mesopore volume than the untreated precursor. The pores of the structure were relatively monodisperse and did not change significantly upon pyrolysis. However, since this work made use of ammonia-borane mostly as a ceramic precursor, we will not discuss it in further detail. Nevertheless, it was demonstrated that such modified structures can be useful scaffolds to facilitate the dehydrogenation of ammonia-borane, which was infused after fabrication (cryogel/ammonia-borane = 1:1, modified cryogel/ammonia-borane = 1:1.2).[123] The suppression of borazine formation in the modified carbon cryogels was similar to that measured from unmodified structures: in both cases lower than that for ammonia-borane without additives. DSC showed that while the pure carbon cyrogel could suppress the onset of decomposition to 109 °C, the modified carbon cryogel suppressed it to 103 °C: a modest improvement.

The thermolysis of ammonia-borane could also be improved by incorporating it into a metal−organic framework (MOF).[124] One such material, JUC-32-Y, consisted of the transition metal yittrium as Y^{3+} and the rigid organic ligand 1,3,5-benzenetricarboxylate, into which ammonia-borane was infused in a molar ratio of 1:1. At 85 °C, up to 8 wt % of H_2 (with respect to ammonia-borane, not the whole system) could be released within 10 min; at 95 °C even 10.2 wt % could be removed (Figure 25). From the viewpoint of hydrogen storage for fuel cells, another important finding was that the typical catalyst poisons, such as borazine, ammonia, or diborane, which are observed during the thermolysis of neat ammonia-borane, were completely absent (by MS).

A further approach to the confinement of ammonia-borane within a matrix that enhances hydrogen release is illustrated by the behavior of poly(methylacrylate)/ammonia-borane blends with 17 and 45 wt % of ammonia-borane.[125] At a heating rate of 2 °C/min, a one step decomposition process was observed by TPD/MS with a peak centered at 96 °C for the 45 wt % sample (with some hydrogen release between 120 and 150 °C due to residual crystallized ammonia-borane) and for the 17 wt % sample at 95 °C (for neat ammonia borane, this study reported 106 and 154 °C). While no borazine or diborane was evolved, ammonia was observed above 90 °C, which would necessitate efficient temperature control of such a process if it were to be used in conjunction with a fuel cell. Mechanistically, it was postulated that the ester groups on the surface of the polymer matrix may act as Lewis bases, weakening both B−H and B−N bonds, thus accounting for the faster hydrogen release kinetics as well as free ammonia. This speculation was further strengthened by the observation of B−O bonds by X-ray photoelectron spectroscopy and Fourier transform infrared spectra.

4.6. Hydrogen Release from Ammonia-Borane Facilitated by Additives

Hydrogen can be produced from ammonia-borane with an oxidizing agent such as ammonium nitrate. This was first claimed in the patent literature[126] and was subsequently examined in the open literature.[127] However, as the decomposition kinetics were not dramatically altered and there were numerous side products identified in the gas stream from the TGA measurements, this does appear to be a useful method for hydrogen generation for fuel cells.

A much more detailed report on the effect of additives on the decomposition kinetics of ammonia-borane identified three different general stages for the process of hydrogen release:[77] an induction, where the dihydrogen network of ammonia-borane is broken, a nucleation process for the formation of the diammoniate of diborane, followed by hydrogen release through dehydrocoupling. The decomposition reactions with ammonium chloride, sodium borohydride, or DADB were followed under isothermal conditions between 75 and 90 °C by solid state ^{11}B NMR and Raman microscopy (to identify the transition from crystalline to amorphous); the released gas was measured volumetrically and analyzed using gas chromatography. Addition of DADB or ammonium chloride to neat ammonia-borane led to a significantly reduced induction time for hydrogen release (Figure 26), whereas the addition of $NaBH_4$ showed no marked effect. Based on earlier work on the mechanism of solid state decomposition of ammonia-borane (as discussed in section 4.2.1), it was not surprising that the ionic DADB,

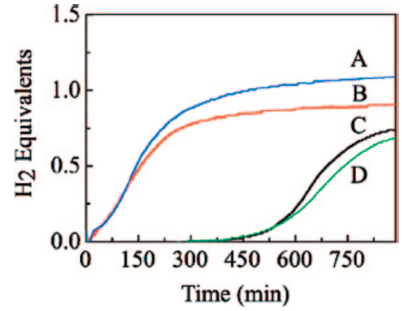

Figure 26. Effect of additives on the induction period for H_2 release from solid ammonia-borane at 80 °C. (A, blue) $NH_3 \cdot BH_3$/NH_4Cl (5 wt %); (B, red) $NH_3 \cdot BH_3$/DADB (5 wt %); (C, black) $NH_3 \cdot BH_3$; (D, green) $NH_3 \cdot BH_3$/$NaBH_4$ (5 wt %). Reprinted with permission from ref 77. Copyright 2009 RSC Publishing.

which has been identified as one of the first decomposition products of ammonia-borane, which is also a solid acid, may interrupt the dihydrogen network, lowering the onset of decomposition.

A similar approach was reported, where $CoCl_2$, $NiCl_2$, and $CuCl_2$ were mechanically stirred with ammonia-borane to affect hydrogen release.[128] $CuCl_2$ proved to be the most effective additive (2 equivalents of hydrogen were released in ca. 6 hours with 15 mol % of metal catalyst) and facilitated hydrogen release at ambient temperature. The solid state nature of the process puts the gravimetric hydrogen content at about 8 wt %, and crucially, no borazine or ammonia impurities were detected in the gas flow, making this a very interesting process with regard to fuel cell applications.

Lithium imide (Li_2NH) and lithium nitride (Li_3N) were introduced as two further additives for the release of hydrogen from ammonia-borane in solution.[129] When these additives were mixed in THF (one Li atom per ammonia-borane), no hydrogen was evolved at ambient temperature (although H_2 evolution was vigorous in the solid state). At 45 °C, a two step decomposition process was observed by MS and manometric measurements, whereby NH_3 was released initially, followed by around 10 wt % of hydrogen. Analysis by ^{11}B NMR spectroscopy and XRD of the dried sample led to the conclusion that the first step was a reaction between the respective additive and ammonia-borane to form the corresponding lithium amidoborane, with concomitant release of ammonia. The subsequent decomposition was then proposed to proceed analogously to the thermal decomposition of lithium amidoboranes, as described in section 5. However, the situation appeared to be different if $LiNH_2$ and ammonia-borane were mixed in the solid state.[130] When these two solids were mixed, an exotherm and the formation of a liquid phase were observed, which was postulated to be a hybrid material of the composition $LiNH_2BH_3 \cdot NH_3$, which was shown to differ from its individual components by solid state ^{11}B NMR and PXRD. This liquid proved to be unstable at ambient temperature, slowly evolving hydrogen and transforming into an amorphous solid. When the liquid phase was heated, rapid hydrogen loss was observed by MS at temperatures as low as 60 °C, with a total loss of 3.2 equiv of hydrogen with heating to 250 °C. In order to analyze the molecular process leading to this hydrogen loss, partially deuterated samples of ammonia-borane, $NH_3 \cdot BD_3$ and $ND_3 \cdot BH_3$, were used and the relative amount of HD and H_2 release measured (Scheme 9). In the first instance, the released gas was predominantly HD, whereas, in the second case, a ratio of 2:1 for H_2/HD was found. Based on these results, the mechanism was postulated to comprise a rate limiting step, where an H from the lithium amide moiety combines with a hydride from boron, followed by a rapid step in which a second equivalent is released from Li and B. In the last step, the dihydrogen may then be comprised of one hydride from boron and another from the amine moiety, originally from ammonia-borane. The high gravimetric hydrogen content of this system (11.9% equal to 3.2 equivalents of hydrogen) makes this an attractive target, although more effort needs to be invested to render this a stable system at ambient temperatures and to reduce the level of impurities found in the gas stream, specifically NH_3, which were quite considerable (1.5 vol %).

Scheme 9. Postulated Mechanism for the Release of Hydrogen from a Lithium Amide/Amine-Borane Hybrid Material as Evidenced by Isotope Studies[a]

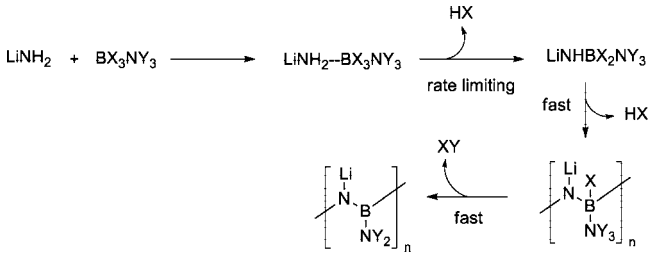

[a] In the case of X = D and Y = H, 3 equivalents of HD are being released. In the reverse case, X = H and Y = D, twice as much H_2 as HD is being released.

4.7. Thermal Decomposition in Ionic Liquids

A different approach to lowering the temperature of the thermal decomposition of ammonia-borane was attempted by Sneddon and co-workers, who carried out the thermolysis in an ionic liquid (bmim Cl = 1-butyl-3-methylimidazolium chloride).[131] While heating pure ammonia-borane at 85 °C gave a negligible amount of dihydrogen after 3 h, heating in bmim Cl showed immediate release of dihydrogen and gave 0.95 equivalent after 3 h at 85 °C and even 1.5 equivalents after 3 h at 95 °C (0.8 equivalent at 95 °C after 3 h for ammonia-borane). The nonvolatile products were analyzed by ^{11}B NMR spectroscopy, and the chemical shifts compared to calculated shifts. It was inferred from this that primarily acylic linear and branched products had been obtained. Initially, considerable amounts of the ions BH_4^- and BH_2^+ were formed, likely to be stabilized by the ionic liquid, which then disappeared over time. This observation is similar to Autrey's and Shaw's when they followed the thermal decomposition of ammonia-borane by *in situ* ^{11}B NMR spectroscopy, where DADB was observed as an initial product (see section 4.2.2).[85] The mechanistic role of the ionic liquid has not been determined, but the authors speculated that it may help reduce the energy of polar transition states during the dehydrogenation process.

The use of a hexagonal boron nitride (h-BN) framework was also attempted for the facilitated dehydrogenation of ammonia-borane.[132] It was argued that the potential advantage of such an approach is the fact that no other elements are being introduced into the system, thus potentially facilitating a regeneration process. Mixtures of these materials were prepared in different ratios via ball milling, which increased the surface area of the h-BN particles from 12 m^2/g to 251 m^2/g and the thermolysis was analyzed by TGA, DSC, MS, PXRD, and MAS-^{11}B-NMR spectroscopy. Indeed, with increased h-BN content, the onset of the decomposition decreased substantially to approximately 70 °C for a ratio of 4/1 h-BN/AB, probably due to the disruption of hydrogen bonding of AB by h-BN. However, the concomitant formation of borazine increased dramatically, rendering this system unsuitable for fuel cell applications.

5. Main Group Metal-Amidoboranes as Hydrogen Containing Materials

Metal amidoboranes are a subclass of amine-boranes, where one of the acidic protons on nitrogen has been replaced by a metal. At present, these compounds are mainly being evaluated for their hydrogen storage properties. Generally, the amidoboranes were prepared and then analyzed, but in some cases, a metal hydride was simply added to ammonia-borane and it is not always clear whether the metal

Scheme 10. Synthesis of $Ca(NH_2 \cdot BH_3)_2$ from Calcium Hydride and Ammonia-Borane

$$CaH_2 + 2\,NH_3 \cdot BH_3 \xrightarrow[25\ ^\circ C]{THF} Ca(THF)_2(NH_2 \cdot BH_3)_2 + 2\,H_2$$

$$Ca(THF)_2(NH_2 \cdot BH_3)_2 \xrightarrow{Vacuum} Ca(NH_2 \cdot BH_3)_2 + 2\,THF$$

amidoborane actually formed. These reports were also included in this section, as were reports in which there was an intention to form the amidoborane but the metal hydride acted merely as an additive.

The uncatalyzed and many of the catalyzed dehydrogenation reactions of ammonia-borane are relatively high yielding in hydrogen gas but are often not applicable to hydrogen production for fuel cells, as they may produce borazine, diborane, ammonia, or related side products, which are known catalyst poisons. Moreover, the ceramic yields of these processes are often low, which suggests mass loss due to volatile molecules other than hydrogen and implies that the materials loss in such a fuel would be substantial.

One strategy to overcome this problem is to mix various additives with ammonia borane or to mechanically mill the sample (see previous section).[133] It has been shown experimentally that pyrolyzing a ground mixture of aluminum powder with ammonia-borane in a ratio of 1:10 led to a reduced weight loss of about 25% (compared to about 33% for ammonia-borane) at the same temperature, suggesting reduced levels of volatile side products.[71] However, neither were these side products analyzed nor the extent of hydrogen release quantified. It was also not examined whether an aluminum amidoborane or other species had formed.

The first suggestion that a main group metal amidoborane, $LiNH_2BH_3$, may be a promising hydrogen storage material was published in 2006 at a conference,[134] but the concept was only explored in detail in 2007.[135] Therefore, $Ca(NH_2 \cdot BH_3)_2$ can be seen as the first main group amidoborane which was systematically evaluated for its hydrogen storage properties. It was synthesized by mixing stoichiometric amounts of CaH_2 and ammonia-borane at ambient temperature and then removing most of the remaining THF ligands from the initial product, $Ca(THF)_2(NH_2 \cdot BH_3)_2$, under vacuum (Scheme 10). $Ca(NH_2 \cdot BH_3)_2$ was air and moisture stable in both the solid state and solution. The chemical shifts in the ^{11}B NMR spectrum were almost identical to those of ammonia-borane, but the coupling constants were different, $^1J_{BH} = 93.0$ Hz for ammonia-borane and $^1J_{BH} = 86.0$ Hz for $Ca(NH_2 \cdot BH_3)_2$, which allowed identification of the different species.

In order to evaluate the suitability of this material for hydrogen storage purposes, the thermal decomposition behavior of $Ca(NH_2 \cdot BH_3)_2$ was analyzed by TGA (0.5−1 °C/min, MS and GC (gas chromatography for quantification)). The initial weight loss starting at 70 °C was attributed to remaining THF. The major weight loss occurred between 120 and 245 °C with an inflection point at 170 °C and contributed about 8 out of 12 wt % to this point. The released volatiles from this step were predominantly hydrogen, but small quantities of borazine and ammonia (below 0.1%) were detected. DSC measurements showed that the loss of the first equivalent of hydrogen was endothermic by 3.5 kJ/mol (0.8 kcal/mol), which is in contrast to the exothermic hydrogen loss in ammonia-borane, $NH_3 \cdot BH_3$. It was postulated that this fact may also explain why the overall volume

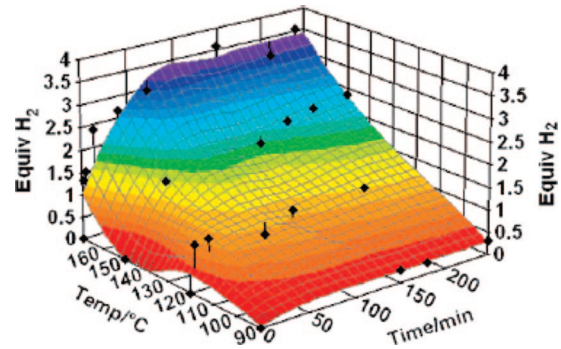

Figure 27. Thermal hydrogen-release profile for $Ca(NH_2 \cdot BH_3)_2$. The colored surface is fitted to the black data points. Reprinted with permission from ref 135. Copyright 2007 Wiley VCH.

loss of hydrogen varied with temperature (Figure 27), which is not observed for ammonia-borane.

Since then, the interest in main group metal amidoboranes as potential hydrogen storage materials has increased substantially. Alkali metal amidoboranes were first described in 1938, with the first reported synthesis of sodium amidoborane via the reaction of ammonia, borane-etherate sodium (eq 16).[136] Other, more convenient routes include the reaction of ammonia-borane in THF with sodium hydride at low temperatures or a disk/ball mill solid state reaction of ammonia-borane with sodium hydride (eq 17).[137] Additionally, the reaction of sodium amide[138] with ammonia-borane in THF also yields sodium amidoborane at ambient temperature (eq 18), which results in a slightly cleaner reaction.[139]

$$Et_2O \cdot BH_3 + NH_3 + Na \rightarrow NaNH_2BH_3 + {}^1/_2H_2 \quad (16)$$

$$NH_3 \cdot BH_3 + NaH \rightarrow NaNH_2BH_3 + H_2\ (\text{THF or mill}) \quad (17)$$

$$NH_3 \cdot BH_3 + NaNH_2 \rightarrow NaNH_2BH_3 + NH_3\ (\text{THF, RT}) \quad (18)$$

The first report suggesting that $NaNH_2 \cdot BH_3$ or $LiNH_2 \cdot BH_3$ could be useful hydrogen storage materials was published by Chen and co-workers.[137] They utilized the same concept of adding an electropositive lightweight main group metal additive, in this case lithium hydride or sodium hydride, which were milled with ammonia-borane in ratios of 1:1.[137] During this process, 1 equivalent of hydrogen gas was released (identified by MS), and a product was obtained, which the authors identified as the corresponding alkali-metal amidoborane by solid state ^{11}B MAS NMR spectroscopy (Figure 28) and high resolution PXRD.

The thermal decomposition of these materials was monitored using temperature-programmed desorption (TPD), coupled with an MS analyzer (Figure 29).[137,139] While ammonia-borane was found to release hydrogen at 108 °C, $LiNH_2 \cdot BH_3$ and $NaNH_2 \cdot BH_3$ released hydrogen cleanly at considerably lower temperatures, 92 and 89 °C, respectively.[137] Formation of borazine was observed at 154 °C for ammonia-borane but could be reduced to levels below the detection threshold of mass spectrometry in the case of the alkali-metal amidoboranes. It was proposed that the replacement of hydrogen by a more electron donating substituent such as an alkali metal would affect the bonding situation for the rest of the complex. It was further suggested that a

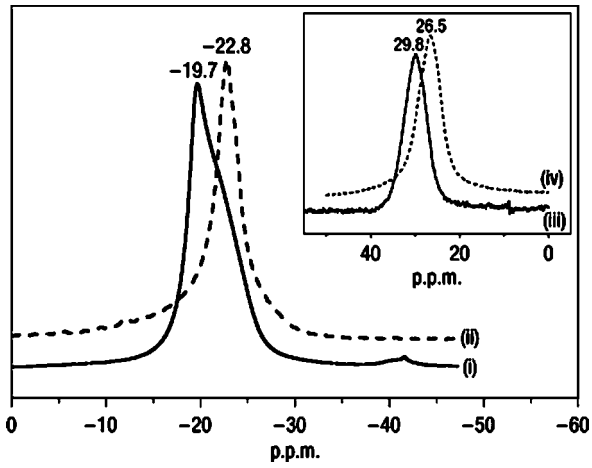

Figure 28. High-field 289.2 MHz (21.2 T) ^{11}B NMR of $LiNH_2 \cdot BH_3$ and $NH_3 \cdot BH_3$ samples: (i) as-prepared $LiNH_2 \cdot BH_3$ sample (−19.7 ppm); (ii) untreated $NH_3 \cdot BH_3$ (−22.8 ppm); (iii) $LiNH_2 \cdot BH_3$ sample after dehydrogenation to 140 °C (+29.8 ppm); (iv) polyborazylene (+26.5 ppm). Reprinted with permission from ref 137. Copyright 2008 Nature Publishing Group.

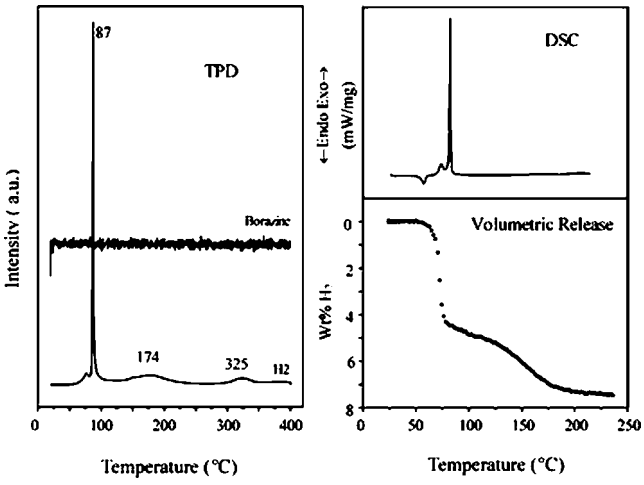

Figure 29. TPD, DSC, and columetric release measurements on synthesized $NaNH_2 \cdot BH_3$ solid. Reprinted with permission from ref 139. Copyright 2008 RSC Publishing.

stronger dative bond is being formed, as evidenced by a shorter N−B bond distance.[137]

The unit cell for both systems determined by PXRD was the orthorhombic space group *Pbca*, which was also found computationally to be the most stable crystal lattice (Figure 30).[140] The latter report also described the N−M bond to be predominantly ionic, which would corroborate the suggestion by Chen that the B−N bond is stronger in the metal amidoboranes than in ammonia-borane. However, there is no proposal as to how this change would affect the kinetic profile of the reaction. Furthermore, the grade of purity of the alkali-metal amidoboranes is not clear, since the lithium hydride used was only 95% pure and the ^{11}B NMR showed a shoulder in the region of the starting material. Therefore, the possibility remains that impurities may contribute to the catalytic process.

However, a year later, Grochala and Fijalkowski reported a reinvestigation of this process, which contradicted some of the initial findings.[141] They employed the same ball milling

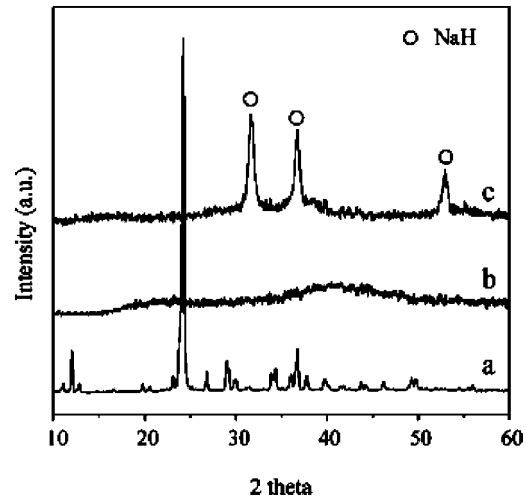

Figure 30. XRD patterns of (a) synthesized $NaNH_2 \cdot BH_3$ and its dehydrogenation product collected at (b) 90 °C and (c) 200 °C. Reprinted with permission from ref 140. Copyright 2008 RSC Publishing.

technique as reported by Chen, with similar purities of the starting materials, after having established that increased purity did not change the results. From their TGA data they calculated an average mass loss of 6.6 wt %, which is lower than the reported 7.5 wt % and was subject to considerable variability, which the authors attribute to the fact that the product from various parts of the mill was not homogeneous. We believe that this finding should prompt the reader to some caution with respect to the results obtained from ball-milled samples, especially when quantifications are attempted.

Like Chen and co-workers, Grochala and Fijalkowski observed a major exothermic mass loss at around 90 °C, noting that the actual value of the exotherm is heating rate dependent. Analysis by both IR and MS revealed, however, that there was substantial contamination of the gas released with ammonia although borazine was not observed. This feature, besides the air and moisture sensitivity of sodium amidoborane, would present a serious problem to its application in fuel cells, as it can react with proton exchange membranes and affect the reduction of O_2 at the electrodes. When a lower heating rate (1 °C/min) was used, the evolution temperature of H_2 was lowered by approximately 10 °C, but the evolution of NH_3 occurred much earlier and over a broader temperature range (30−70 °C).

The DSC data presented by both groups are rather different, presumably due in part to different heating rates. Chen's data show an endotherm at 57 °C and a small exotherm followed by a large exotherm at about 80 °C (Figure 29).[139] Grochala's data revealed a broad endotherm between 45 and 80 °C followed by a large exotherm. While it seems clear that the latter can be attributed to the exothermic loss of hydrogen, the interpretation of the endotherms is under discussion. Chen proposed that the first endotherm is a melt transition, but as no melting is visible to the eye at this temperature, Grochala disputed this interpretation and suggests the melting occurs during the small endotherm just before the exothermic reaction. Grochala suggested that the first endotherm is a head to tail dimerization (eq 19), similar to a suggestion by Harder for the related calcium amidoboranes (see below).

$$2NaNH_2{-}BH_3 \xrightarrow{(55-80\ ^\circ C)} [NH_3Na]^+[BH_3(NHNa)BH_3]^- \quad (19)$$

They further propose that this ionic salt could decompose to give the observed ammonia (eq 20) and the corresponding sodium salt, which itself is proposed to decompose to yield sodium hydride and a sodium amido bisborane (eq 21).

$$[NH_3Na]^+[BH_3(NHNa)BH_3]^- \xrightarrow{(90-110\ ^\circ C)} Na^+[BH_3(NHNa)BH_3]^- + NH_3 \quad (20)$$

$$Na^+[BH_3(NHNa)BH_3]^- \xrightarrow{(90-110\ ^\circ C)} NaH + BH_3(NHNa)BH_2 \quad (21)$$

XRD gave some corroborating evidence for this hypothesis: samples which had been heated to 110 or 250 °C, respectively, showed a NaH phase in an otherwise amorphous sample (Figure 31). Although there was already some NaH present in the starting material, this result is in part comparable to Chen's, who also reported a residual NaH phase from a sample heated to 200 °C, but who found a completely amorphous phase in a sample which had been degenerated at 90 °C (Figure 30). However, Chen attributed this to a simpler reaction pathway (eq 22), where amorphous boron nitride is being formed, although there was no experimental proof of the existence of boron nitride in the sample.

$$NaNH_2BH_3 \rightarrow NaH + BN + 2H_2 \quad 7.55\ wt\ \%\ H_2 \quad (22)$$

At virtually the same time that Chen and co-workers presented their results regarding ball milled sodium hydride or lithium hydride with ammonia-borane, Wang and co-workers made the same discovery concerning a ball milled 1:1 mixture of lithium hydride and ammonia-borane.[142] They report an onset hydrogen release temperature of 80 °C (Chen: 92 °C) with a concomitant mass loss of 7 wt %. They also report a high hydrogen purity with no borazine or diborane contaminants, although it is not reported whether detection of NH_3 was attempted, which would be interesting in view of Grochala's results concerning $NaNH_2 \cdot BH_3$. At isothermal heating at 120 °C, hydrogen release corresponding to a storage capacity of 10 wt % was achieved (Chen: 10 wt % at 90 °C). Wang and co-workers noted that the dehydrogenation rate for $LiNH_2 \cdot BH_3$ at 100 °C was 5 to 6 times faster than that for ammonia-borane, which would be a considerable advancement for fuel cell applications.[60d] Based on elemental analysis and ^{11}B MAS NMR spectroscopy of the residue after pyrolysis, the authors tentatively concluded that the final decomposition product is of the composition $[LiBNH_{1.4}]$ (eq 23).

$$NH_3 \cdot BH_3 + LiH \xrightarrow[-H_2]{\text{milling}} LiNH_2BH_3 \xrightarrow[-1.8H_2]{\text{heating}} \text{“LiNBH”}_{\sim 1.4} \quad (23)$$

In order to promote understanding of the reaction of ammonia-borane with lithium hydride, this reaction was investigated in suspension (THF).[143] The gas evolution of 0.27 M suspensions of a 1:1 LiH/ammonia-borane mixture was measured at temperatures from 40 to 55 °C. The kinetics were considerably faster in suspension as compared to the solid state presumably due to increased mass transport. Hydrogen was the only gas observed, although it is not reported by which method. The reaction occurred in two steps. In the first, approximately 1 equivalent of H_2 was released, following a first-order rate law in the substrates consistent with the formation of $LiNH_2 \cdot BH_3$. The second step released approximately 1.8 equivalents of H_2, following a zero-order rate law in the reactant ($LiNH_2 \cdot BH_3$). The product of the second step was an insoluble amorphous white solid, which was further analyzed by ^{11}B MAS NMR spectroscopy. The major species was assigned to be -$B(N_2H)$ with some BH_3 and BH_4. The overall reaction was postulated to be as shown below in eq 24:

$$LiNH_2 \cdot BH_3 \rightarrow [LiNBH] + 2H_2 \quad (24)$$

However, it was concluded that further insight into the nature of the product may be hampered due to the fact that the starting materials had purities ≤95%. The solid state reaction of lithium hydride and ammonia-borane by ball milling was re-examined by monitoring the reaction process together with XRD analysis.[144] It was found that a lithium amidoborane/ammonia-borane complex ($LiNH_2BH_3 \cdot NH_3BH_3$) and two allotropes of lithium amidoborane (α- and β-$LiNH_2BH_3$, both with orthorhombic symmetry) were synthesized in this process. The β-$LiNH_2BH_3$ allotrope required energetic ball milling and reverted to α-$LiNH_2BH_3$ after prolonged milling. Both modifications of $LiNH_2BH_3$ were able to release 10.8 wt % of H_2 at 180 °C, whereas the $LiNH_2BH_3 \cdot NH_3BH_3$ complex released up to 14.3 wt %. Yao and Lu combined the approach of kinetically facilitating the dehydrogenation of ammonia-borane in nano confinement with the destabilizing effect of LiH on ammonia-borane.[145] They impregnated an ordered mesoporous carbon framework, with a large surface area and interconnected pores, CMK-3, with ammonia-borane on its own (50 wt %) (ammonia-borane/CMK-3) and 5 wt % Li doped ammonia-borane (50 wt %) (ammonia-borane/Li-CMK-3). Their TGA analysis/MS (heat-

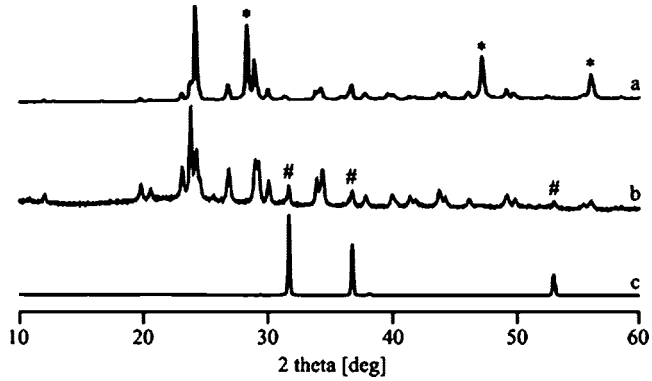

Figure 31. Powder X-ray diffratograms of Na-Ab samples with small amounts of residual NaH (#): (a) as-synthesized sample (25 °C); (b) sample heated *in situ* to 55 °C; and samples heated ex-situ to: (c) 110 °C or (d) 250 °C. An unidentified broad peak at 27.6° seen exclusively at 55 °C is marked (∗). Reprinted with permission from ref 141. Copyright 2008 RSC Publishing.

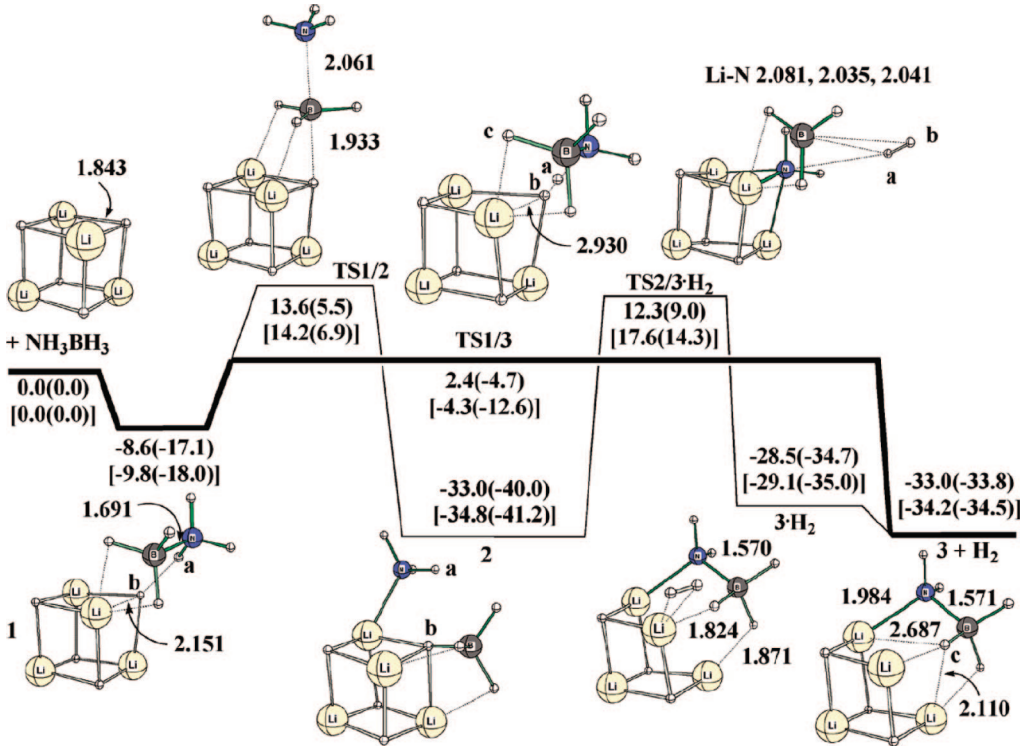

Figure 32. Free energy surface for the reaction of $(LiH)_4 + NH_3 \cdot BH_3$. Free energies (kcal/mol) are relative to $(LiH)_4 + NH_3 \cdot BH_3$ at 298 K. The values in parentheses are relative enthalpy (kcal/mol) to $(LiH)_4 + NH_3 \cdot BH_3$ at 298 K. The values in brackets are free energies and enthalpies for the $(NaH)_4 + NH_3 \cdot BH_3$ reaction pathway. Distances are in units of angstroms. Reprinted with permission from ref 146. Copyright 2009 American Chemical Society.

ing rate 1 °C/min) demonstrated that both ammonia-borane on its own and ammonia-borane/CMK-3 showed a substantial mass loss beyond the release of merely H_2 below 150 °C with two distinct steps at 110 and 145 °C for ammonia-borane and only one gradual loss starting at 40 °C and with an inflection point at 140 °C for ammonia-borane/CMK-3. Indeed, analysis by mass spectrometry showed considerable contributions from both NH_3 and, in the case of ammonia-borane only, borazine in the gas stream. Ammonia-borane/Li-CMK-3, on the other hand, released pure hydrogen very gradually with an overall weight loss of 7 wt % over the range 75−150 °C in the TGA experiment. The same weight loss was observed at isothermal heating 60 °C over the course of 2 hours. As an explanation for the improved kinetics in CMK-3, the authors cite size confinement and the acidic properties of the surface (pH = 3.7). The beneficial effect of LiH with respect to the increased purity of the released hydrogen gas is attributed to an immobilization of N-containing species during thermal decomposition. The LiH loading of 5% is much smaller than the loss of N-containing volatiles in the case of ammonia-borane/CMK-3, and with a pH that low, the CMK itself is likely to react with at least some of the lithium hydride. The authors speculated that ammonia-borane may complex with the surface to give surface−OH···H-BH_2−NH_3···Li−O-surface complexes, weakening the E−H bonds and thus catalyzing the release of hydrogen and presumably preventing the release of NH_3.

The mechanism of the formation of $LiNH_2 \cdot BH_3$ has been investigated by Lee and McKee by computational methods[146] and also at the same time by Kim and co-workers.[147] Assuming that neither compound is likely to sublime to a great extent under the experimental conditions employed, the reaction was presumably a solid state surface/surface reaction. In order to simulate the crystal surface of LiH, Lee and McKee employed the $(LiH)_4$ cluster as a model, which is the smallest LiH cluster known to exist. The reaction was predicted to initiate with an adsorption of $NH_3 \cdot BH_3$ on the $(LiH)_4$ cluster followed by formation of a $(LiH)_3 \cdot LiNH_2 \cdot BH_3$ complex and H_2, proceeding via a low activation barrier (Figure 32; also presented are the corresponding values for the NaH case). This is in contrast to Kim's results, which showed a barrierless process,[147] but because Kim considered only LiH, it is likely that Lee and McKee's results are more reliable in that respect. Another mechanism involving bond cleavage was discounted because of higher activation barriers (also presented in Figure 32). The authors speculated that the relatively low activation barrier for this process may be key to the avoidance of borazine formation. This is because, for pure ammonia-borane, the activation barrier (as discussed earlier), to form the intermediate aminoborane, $[NH_2{=}BH_2]$, a potential precursor for borazine, is higher.

The $(LiH)_3 \cdot LiNH_2 \cdot BH_3$ cluster was then predicted to react with ammonia-borane in an even more facile manner. The hydrides on boron on ammonia-borane were predicted to interact with the electropositive Li in the cluster whereas the protic H on nitrogen in ammonia-borane is set up to form an electrostatic bond with a hydride in the cluster, thereby forming more $LiNH_2 \cdot BH_3$ and thus gradually disintegrating the original cluster. The lowering of activation barriers of further steps is then in accordance with the results of Kim and co-workers and may be an indication of a cooperative H_2-loss mechanism. For the subsequent reaction, where H_2 is lost from $(LiNH_2 \cdot BH_3)_2$, the first 2 equivalents were predicted to be lost reversibly (Figure 33). In this mechanism, the dimer forms a TS with a Li−H−Li bridge, with the $[H_2N{=}BH_2]$ fragment bound to one Li atom via the N atom. From the following intermediate, H_2 is eliminated, where one H is from the Li−H−Li bridge, whereas the other one is from the protic Li···$NH_2{=}BH_2$. Further dehydrogenation was shown to be less favored, but the authors speculated

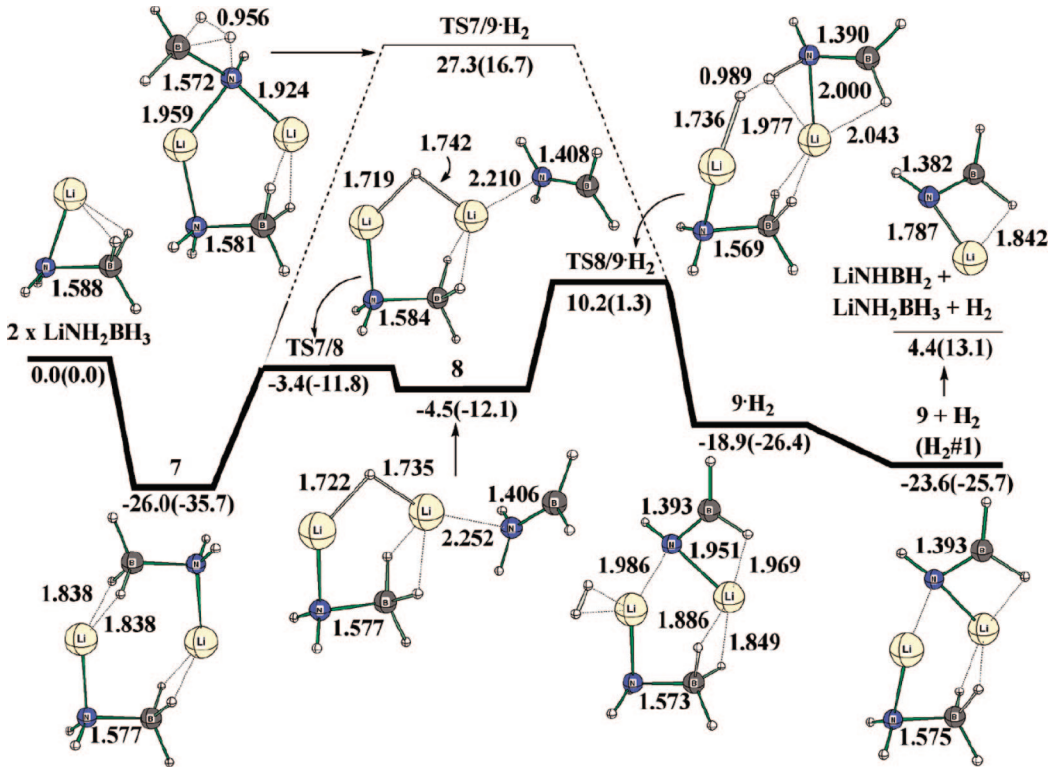

Figure 33. Dehydrogenation from a complex of two $LiNH_2 \cdot BH_3$ molecules. Reprinted with permission from ref 146. Copyright 2009 American Chemical Society.

that this reaction may still occur if the lattice energy stabilization accompanying H_2 loss is sufficiently large.

The mechanisms for the second step, presented by Kim, suggested a slightly different interpretation. While he discounted an N−B bond breaking mechanism or a direct mechanism, he identified a mechanism related to McKee's but with N−B intermolecular bond formation, which was found to be lower in energy. Here, the Li cation also plays a role in decreasing the energy barrier for intermolecular N−B bond formation, which would give rise to the formation of N−B oligomers (eq 25) as products.

$$Li^+[NH_2BH_3]^- + n\,NH_2BH_2 \longrightarrow Li^+[NH_2BH_2NH_2BH_3]^- \xrightarrow{(n-1)\,NH_2BH_2} Li^+[(NH_2BH_2)_nNH_2BH_3]^- \quad (25)$$

However, McKee stressed that in their mechanism $[NH_2BH_2]$ is not formed. It would appear that Kim based the formation of $[NH_2BH_2]$ on the same TS (**TS7/8**), and as neither study reports an intrinsic reaction coordinate (IRC), it is not possible to conclude if this pathway is viable. Both groups agree that the mechanism is completely different from that proposed for ammonia-borane itself, which is thought to occur via the formation of DADB.

Wang and co-workers turned their attention to alkaline-earth metal amidoboranes, mechanically milling magnesium hydride with ammonia-borane (1:0.5), and studying the thermal decomposition using TGA/DSC/MS (heating rate 2 °C/min), XRPD, Raman spectroscopy, and ^{11}B MAS NMR spectroscopy.[148] TGA/DSC/MS showed two decomposition steps, the first between 60 and 100 °C, with an inflection weight loss curve at approximately 80 °C, and a second inflection point at about 110 °C, both associated with loss of hydrogen (MS) but not borazine or diborane. Any NH_3 release was not reported. If the reaction was performed at a 100 °C isotherm, 8 wt % of H_2 could be released within 4 hours. The reaction was also less exothermic (−7 kJ/mol (1.7 kcal/mol)) than that of neat ammonia-borane (−21 kJ/mol (−5.0 kcal/mol)), $LiNH_2 \cdot BH_3$, and $NaNH_2 \cdot BH_3$ (−3 to −5 kJ/mol (−0.7 to −1.2 kcal/mol)).[145] Elemental analysis and PXRD of the samples at various stages of the process revealed fundamental differences between the MgH_2/ammonia-borane and the LiH or NaH/ammonia-borane systems. First, the milling process did not alter the chemical composition of the sample, so no reaction to form $Mg(NH_2{-}BH_3)_2$ was observed. Surprisingly, during heating to 200 °C, the MgH_2 phase could be observed by *in situ* PXRD in unchanged intensity and angle, which suggested that hydrogen release from ammonia-borane is promoted by the solid phase interaction between ammonia-borane and MgH_2, probably due to the Coulombic attraction between the hydridic H atom in MgH_2 and the protic H in the NH_3 moiety of ammonia-borane. This hypothesis was further underlined by analysis with Raman spectroscopy, where the milled ammonia-borane/MgH_2 mixture and the neat ammonia-borane showed marked differences in intensity and shifts, thus suggesting a different lattice structure. Differences between the samples could also be seen in the ^{11}B MAS NMR spectroscopy, where the peak for ammonia-borane, normally at −22.8 ppm, was shifted to −26.7 ppm. This latter resonance disappeared quickly. The resonance at −22.8 ppm did form *in situ*, which was then followed by the appearance of two additional peaks at −12.9 and −38.3 ppm, which were assigned to BH_2 and BH_4 in $[(NH_3)_2BH_2^+][BH_4^-]$ (Figure 34). The less exothermic reaction of the ammonia-borane/MgH_2 system as compared to ammonia-borane may thus arise from the fact that MgH_2 treated ammonia-borane is already in a energetically more favorable phase than pure

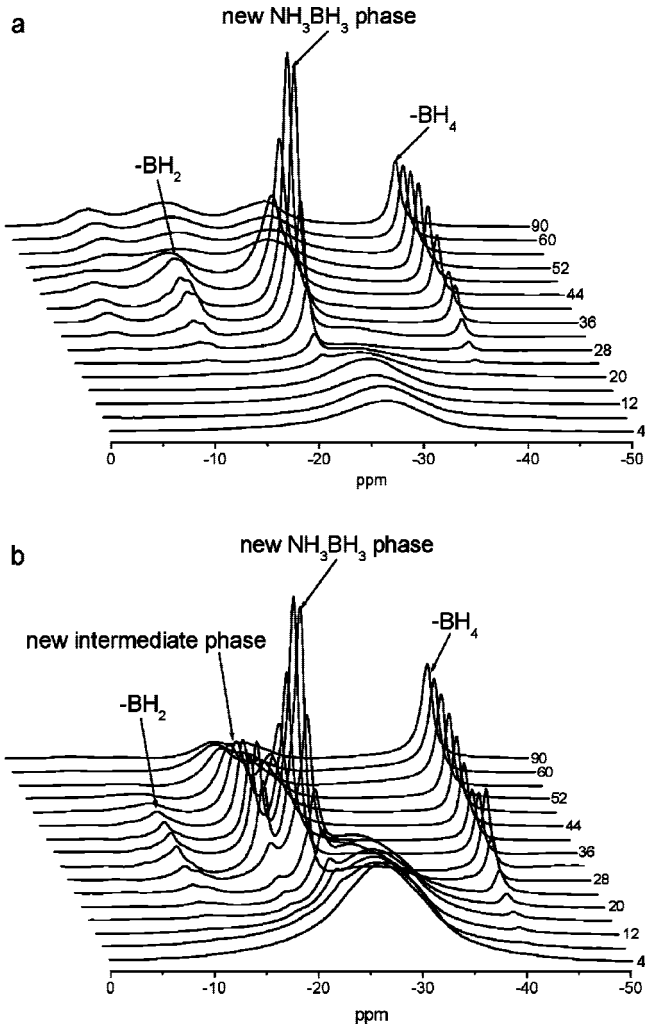

Figure 34. Time resolved $^{11}B\{^1H\}$ MAS NMR spectra for the thermal decomposition of (a) neat AB at 85 °C; (b) the AB/0.5 MgH_2 material at 75 °C. For both samples NMR spectra were recorded at 2 min intervals, with the first spectrum taken 4 min after heating started. For simplicity only selected spectra are presented. Reprinted with permission from ref 148. Copyright 2008 RSC Publishing.

ammonia-borane. It is therefore not surprising that the regeneration of MgH_2 treated dehydrogenated ammonia-borane samples was unsuccessful even at pressures up to 10 MPa H_2.

The reasons for the differing thermal hydrogen release properties of the alkaline and alkaline earth amidoboranes were investigated by Wu and co-workers.[149] They reproduced and refined the powder X-ray diffractograms for $LiNH_2 \cdot BH_3$ first reported by Chen and Li and also determined the powder X-ray diffractogram of $Ca(NH_2 \cdot BH_3)_2$. In order to improve the understanding of the bonding situation in these compounds, DFT studies were also performed (crystal lattice). These complexes had been previously calculated (gas phase), but these earlier calculations predicted a bending of the M−N bond toward the central B−N bond,[150] which was not observed crystallographically. The samples for their study were prepared by the ball milling technique, using stoichiometric amounts of the metal hydride and ammonia-borane. It was pointed out that the generation of $Ca(NH_2 \cdot BH_3)_2$ required much more prolonged ball milling, which is consistent with the report by Wang and co-workers on the attempted formation of $Mg(NH_2 \cdot BH_3)_2$,[148] which could not be achieved by ball milling and points to a general trend of lower reactivity of alkaline earth metal hydrides as opposed by alkaline metal hydrides and may be attributable to their lower basicity.

The B−N bond lengths in $LiNH_2 \cdot BH_3$ and $Ca(NH_2 \cdot BH_3)_2$ were determined as 1.547 Å and 1.546 Å, respectively, both of which were shorter than the B−N bond of ammonia-borane in the solid state (∼1.58 Å); for details, see Table 2. Like Chen and Li, the authors interpreted this as a stronger bond in the metal amidoboranes. Based on Mulliken charges, Wu and co-workers assigned the N−metal bond an ionic character. As a consequence of the substitution of a proton with a metal, the remaining hydrogens on nitrogen became less protic, but the hydrogens on borane became more hydridic. Wu and co-workers also analyzed the thermogravimetric properties of their samples (TGA 1 °C/min). $Ca(NH_2 \cdot BH_3)_2$ began to evolve hydrogen at 80 °C with a sharp weight loss between 100 and 140 °C with an inflection point at 100 °C, which is somewhat different from the observations of Burrell and co-workers[135] (see before) and may be a result of an absence of THF contamination in Wu's samples of $Ca(NH_2 \cdot BH_3)_2$. However, gas contamination by diborane, borazine, or ammonia was not investigated. At 250 °C, the samples had released up to 4 equivalents of hydrogen, but the reaction was not reversible under a hydrogen pressure of up to 50 bar. $Ca(NH_2 \cdot BH_3)_2$ could be a useful starting point for the development of a new hydrogen storage material, due to its high hydrogen content, and endothermic loss of hydrogen, which would potentially allow for a reversible process. The differences observed by Burrell and Wu highlight again how critically important the purity of the sample is in these solid state thermal reactions.

Well-defined, soluble calcium amidoborane complexes have also been prepared (Scheme 10),[151–153] but as they play only a peripheral role within the theme of hydrogen storage and are more of a mechanistic interest, they will not be discussed in this review and we refer the reader to our other review on group 13/group 15 adducts for a detailed account.[1]

Ball milling, which was an efficient method for the synthesis of most alkaline and earth alkaline amidoboranes (except $Mg(NH_2 \cdot BH_3)_2$), also proved to be a feasible technique for the synthesis of strontium amidoborane ($Sr(NH_2 \cdot BH_3)_2$), which crystallized in a monoclinic structure with the *C*2 space group.[154] While hydrogen release initiated at as low as 60 °C with a heating rate of 2 °C/min and became violent at 93 °C, this compound does not hold much promise as a practical hydrogen storage compound due to the detection of considerable amounts of NH_3 and some diborane in the emitted gas stream and also because the gravimetric hydrogen content is rather low due to the high atomic mass of strontium (87.6 g/mol).

Finally, in this section of main group metal amidoboranes, we would also briefly like to mention the utility of this approach for the generation of preceramic materials. Shore and co-workers reacted ammonia-borane with $Me_3N \cdot AlH_3$, which produced 1.32 equivalents of dihydrogen.[155] From this they isolated an insoluble white solid, which they analyzed by IR. They reasonably assumed, though did not in fact prove, that in this reaction an Al−N bond between the adducts had been formed, similarly to the formation of Li, Na, or Ca amidoborane, as shown some years later (see above). Treatment with liquid nitrogen enabled them to remove residual NMe_3, while pyrolysis under a flow of NH_3

at 1000 °C produced an AlN/BN material without any loss of the heavier elements.

A very similar approach for the release of hydrogen from ammonia-borane has been pursued by Sneddon and co-workers, who used a strong non-nucleophilic base in the solid state, ionic liquids, or tetraglyme solutions to lower the onset of the decomposition.[156] They found that the addition of bis(dimethylamino)naphthalene, also known as a proton sponge, in catalytic amounts to a solution of ammonia-borane in an ionic liquid almost doubled the dehydrogenation rate at 85 °C for the release of 2 equivalents of hydrogen and the formation of borazine was suppressed. Similarly to the NMR results presented by Shaw and Autrey on the decomposition of ammonia-borane in the solid state and solution, DADB was observed as an intermediate. The mechanism of this anionic polymerization remains unclear, especially since the mechanism suggested by the authors does not include the formation of this salt.

6. Metal-Catalyzed Solvolysis in Protic Solvents

6.1. For the Release of Hydrogen

A chemically different approach to catalytic dehydrocoupling reactions for the utilization of B−N materials for hydrogen production/storage is metal-assisted solvolysis. Since tertiary amine-boranes may be used as hydrogen source,[157] it is the borane moiety of the complex which reacts, providing hydridic hydrogen atoms, whereas the protons to form hydrogen are obtained from the protic solvent. The concept of using transition metals for the solvolytic catalyzed dehydrogenation has been used extensively in the field of electroless plating, where *N*,*N*-dimethylamine-borane in particular is often used as a reductant, which is briefly discussed in our other review.[1] Ammonia-borane, on the other hand, has only been described in patents for this particular use, even though the mechanism for catalytic solvolysis may be similar. However, the idea of using such a process with the explicit aim of generation of hydrogen was only introduced in 2006.[158] In this report, it was shown that while ammonia-borane is stable in water, addition of catalytic amounts of Pt black, Pd black, or a Rh precatalyst ($\{Rh(1,5\text{-cod})(\mu\text{-Cl})\}_2$) led to the rapid release of up to 2 equivalents of dihydrogen. In terms of weight, this is equivalent to 8.9 wt % of the system $NH_3 \cdot BH_3/H_2O$. At the time, a number of different metal catalysts were evaluated, with the Pt black catalyst shown to be the most efficient—the reaction was complete within 10 min using 1.8 mol % of Pt black. This report initiated substantial efforts to find improved catalysts for this system, as it was immediately recognized as a promising way of generating hydrogen for use in fuel cells.

Because of the large volume of subsequent publications in this area (Table A8, Appendix), it is beyond the scope of this review to discuss them all in detail. We refer the reader to the already published reviews in this area,[159] and we will merely give a brief overview of the basic concepts used to improve catalysts for this transformation.

One of the most important characteristics of a good catalyst is the accessibility of the catalytic sites, and high internal surface area, which has already been reviewed.[160] For example, this was shown by using a templated synthesis to produce catalytically active Ni−Pt hollow nanospheres as catalysts (Figure 35).[161]

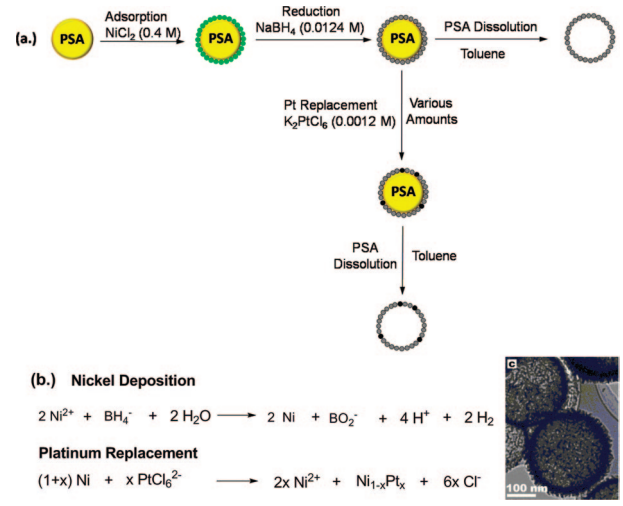

Figure 35. (a) Preparation of the hollow spheres; (b) overall equations for nickel deposition and platinum replacement; (c) TEM image of a hollow sphere. Adapted and partially reproduced with permission from ref 161. Copyright 2007 American Chemical Society.

Nickel(II) chloride was adsorbed onto a PSA (poly(styrene-*co*-methacrylic acid)) template, reduced by $NaBH_4$, and reductively doped with varying amounts of platinum, before dissolving the polymeric core to form a hollow sphere. Commercial nickel powders showed essentially no catalytic activity, but pure nickel hollow spheres showed already substantial catalysis. By increasing the amount of Pt doping, the catalytic activity could be increased to release of approximately 3 equivalents of dihydrogen (2 equivalents from ammonia-borane, 1 equivalent from water) within 20−30 min for a Ni/Pt ratio of 88/12. This structural catalyst design of the hollow spheres led to a very high surface area with concomitant low density and avoided aggregation. Most importantly, only small amounts of precious metal had to be used. If the results are compared to those using pure Pt black,[158] the use of the nanospheres allows the reduction of the Pt loading to 0.2 mol % instead of 2 mol %, despite the concentrations (0.5 wt % and 0.33 wt %, respectively) and reaction times (20−30 and 10 min, respectively) being similar.

The importance of the physical structure of the catalyst was even more elegantly demonstrated when it was shown that even a nonprecious metal such as iron can show remarkable reaction kinetics, provided the suitable morphology of the catalyst is ensured.[162] In an attempt to utilize iron nanoparticles, $FeSO_4$ was reduced with $NaBH_4$ and ammonia-borane was added immediately afterward (ammonia-borane/$FeSO_4$/$NaBH_4$ = 1/0.12/0.16), recording the reaction progress by MS and volumetrically. The reaction took more than 160 min to complete. However, when the nanoparticles were formed *in situ*, i.e. the ammonia-borane was added immediately, the reaction proceeded to completion within 8 min (Figure 36).

Careful analysis by PXRD, TEM, and SAED (selective area electron diffration) revealed that while, in the first case, α-Fe crystallites had formed, the *in situ* reduction led to amorphous nanoparticles. These formed suspensions in water, which the crystalline nanoparticles did not and, astonishingly were also similarly effective in air. Furthermore, these amorphous nanoparticles could be recycled without loss of

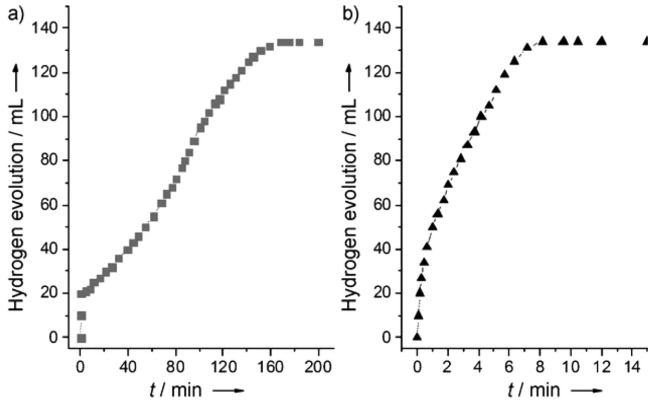

Figure 36. Comparison between (a) presynthesized Fe-nanoparticles and (b) *in situ* reduced Fe-nanoparticles. Reprinted with permission from ref 162. Copyright 2007 Wiley VCH.

activity. This was the first time that a nonprecious metal catalyst achieved similar efficiencies to platinum based materials for ammonia-borane hydrolysis.

The advantage of these processes is their high efficiency, their chemical robustness, and the fact that inexpensive metal catalysts have been developed, which make this process economically interesting.

6.2. Noncatalytic Hydrothermolysis

In a contribution from 2008, it was shown that noncatalytic hydrothermolysis may be a viable option for a process that releases dihydrogen from ammonia-borane and water.[163] A mixture of ammonia-borane in gelled water with nanoscale aluminum powder in a ratio of $AB/Al/H_2O = 2:3:3$ was prepared, which was subsequently ignited. The fuel burnt in a self-sustained combustion, because the release of hydrogen is exothermic, to release 7.7 wt % of dihydrogen, which is significantly more than the theoretical yield for Al/H_2O mixtures alone: 5.6 wt %. Another way to realize catalyst free hydrothermolysis was to use Ar pressure to increase the boiling point of water, so hydrolysis temperatures of up to 170 °C could be reached. At temperatures as low as 135 °C at an initial pressure of 14.6 atm, 3 equivalents of dihydrogen/ammonia-borane molecule were released. Isotope studies showed that approximately 2 equivalents originated from AB and one from water. Crucially, the reaction was very selective so that by ^{11}B NMR and MS no borazine formation could be detected. This type of reaction was further developed by combining the exothermic reaction of a nanoaluminium/water combustion with ammonia-borane dehydrogenation in a spatially separated reaction space.[164]

6.3. Direct Use of Ammonia-Borane in Fuel Cells

If ammonia-borane is used to generate hydrogen for a fuel cell, and hydrogen is then oxidized at the anode to water, the reaction could be made more efficient if ammonia-borane was oxidized directly. This concept was first proposed by Xu and co-workers,[165] who postulated that it should be possible to achieve a more negative potential and thereby generate more power from such a fuel cell and it should also be easier design it, because no separate compartments for fuel generation and electrolytic reduction would be needed. Under optimal conditions, the anodic oxidation reaction should be as follows:

$$NH_3 \cdot BH_3 + 6OH^- \rightarrow BO_2^- + NH_4^+ + 4H_2O + 6e^- \quad E^\circ = -1.216\ V \tag{26}$$

and the reduction of oxygen at the cathode could be described as follows:

$$^3/_2O_2 + 3H_2O + 6e^- \rightarrow 6OH^- \quad E^\circ = 0.40\ V \tag{27}$$

Thus, the cell potential would be up to 1.616 V with a high theoretical specific energy for the overall reaction of 8422.12 W h kg^{-1}. The authors noted another potential advantage, which is the regeneration of BO_2^- with MgH_2 to give BH_4^-,[166] which can be reconverted to ammonia-borane.[3] If ammonia-borane is used directly in an aqueous medium in the fuel cell, the hydrogen producing hydrolysis reaction (eq 28) is an unwanted side reaction, because the hydrides oxidized to H_2 are no longer available to donate electrons for power generation.

$$NH_3 \cdot BH_3 + 2H_2O \rightarrow BO_2^- + NH_4^+ + 3H_2 \tag{28}$$

Indeed, the anode evolved hydrogen under both open circuit and operational conditions, despite the fact that the conditions were alkaline. The authors further tested different electrode materials (Ta, Au, Ni, Cu, Pt) and morphologies (rod, wire, plate, mesh, or foam) at different concentrations, observing that all parameters influenced the open circuit potential. The cyclovoltammograms were complex and could only be partially interpreted. Nevertheless, a prototype of an ammonia-borane fuel cell with an open circuit potential (OCP) of up to −1.291 V (against a calomel ($HgCl_2$) electrode) was prepared. In two subsequent papers, Xu and co-workers presented more detailed analyses and a refined design of the initial ammonia-borane powered fuel cell (schematically represented in Figure 37).[167,169] Both cathode and anode were made out of carbon supported platinum, mixed with an ionomer solution of an anion exchange resin, deposited as a thin layer on a PTFE sheet. Between the electrodes there was an anion exchange membrane with porous carbon cloth on either side. The ammonia-borane solution (different concentrations in 2 M NaOH) was then pumped to the anode side, whereas the cathode was exposed to air. It was found that increasing the $NH_3 \cdot BH_3$ concentration led to an increasingly negative OCP (measured against a standard calomel electrode) of up to −1.05 V. This is lower than the theoretical value −1.216 V vs the normal hydrogen electrode (NHE) (−1.314 V vs Hg/HgO), which is likely to be due to unwanted hydrolysis/hydrogen generation. At higher temperatures, the performance was also increased, and an OCP of −1.12 V vs Hg/HgO at 318 K was found. One of the other major problems that need to be solved is the cell's rapidly decreasing performance at high current densities. The authors suspected that fuel crossover across the membrane may have been reposonsible for this issue. To investigate this postulate, they analyzed the electrodes of a used cell by SEM-EDX (scanning electron microscope, energy dispersive X-ray spectroscopy), where they indeed found nitrogen containing deposits on the cathode.[167]

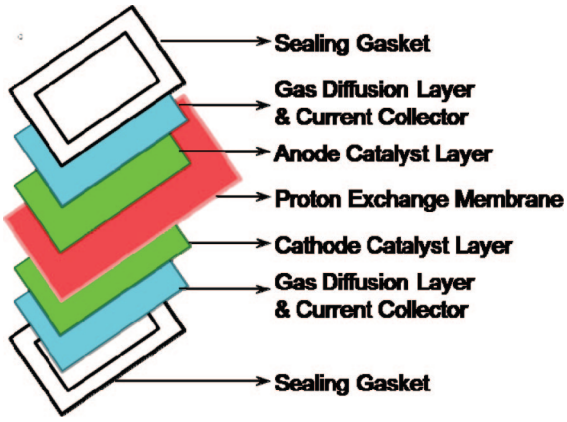

Figure 37. Schematic of a membrane fuel cell, adapted from ref 168.

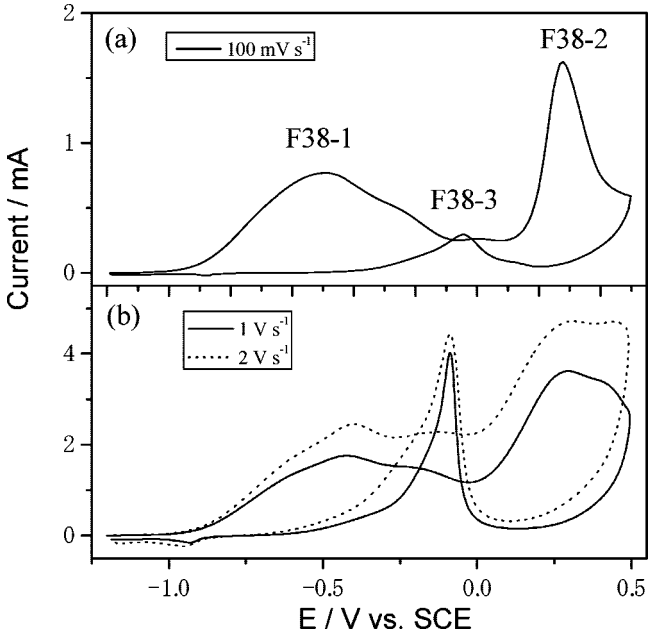

Figure 38. Cyclic volammetric response of 0.01 M $NH_3 \cdot BH_3$ in 2 M NaOH with 0.001 M CH_4N_2S present at a Au electrode at different scan rates. Reprinted with permission from ref 169. Copyright 2010, Qiang Xu, at the National Institute of Advanced Industrial Science and Technology (AIST), Japan.

A more detailed examination of the actual oxidation process of ammonia-borane at the anode was provided by cyclic voltammetry with a gold electrode.[169] Without any additives, these data were complex, as noted before, but the addition of thiourea as an inhibitor of H_2 evolution[170] allowed a cleaner and simpler electrochemical reaction (SCE = saturated calomel electrode). By careful comparison of the cyclovoltammograms of a 2 M NaOH solution without and with 0.001 M CH_4N_2S only to a 2 M NaOH solution with 0.01 M $NH_3 \cdot BH_3$ and with and without 0.001 M CH_4N_2S, the authors interpret peaks F38-1 and F38-2 tentatively with the following reactions (eqs 29−31)

Peak F38-1: Direct electrooxidation of $NH_3 \cdot BH_3$

$$NH_3 \cdot BH_3 + OH^- \rightarrow NH_3 + BH_3OH^- \quad (29)$$

$$BH_3OH^- + 6OH^- \rightarrow BO_2^- + 5H_2O + 6e^- \quad (30)$$

Peak 38-2: Formamide formation from thiourea

$$CH_4N_2S + 10OH^- \rightarrow SO_4^{2-} + H_2NC(O)NH_2 + 8e^- + 5H_2O \quad (31)$$

The anodic reaction peak F38-3 is seen during the reverse scan, where the reduction of the gold oxide layer led to the resumption of $NH_3 \cdot BH_3$ oxidation.

By analysis of the peak height of F38-1 at different concentrations of $NH_3 \cdot BH_3$ (so-called Tafel analysis), it was possible to determine that this peak arises due to a two-electron transfer step, which is substantially less than the theoretically possible six electrons. Xu and co-workers suggested that the effect of NH_4^+ on the electro-oxidation behavior of BH_3OH^- could be a reason for this difference but concluded that further studies are required.

Xu and co-workers also presented a related study, where they reported that carbon supported Fe@Pt core−shell nanoparticles could be employed as efficient electrocatalysts for ammonia-borane in an aqueous basic solution, which were up to 354% more active than commercial Pt/C catalysts.[171] Not only could these particles be recycled, but the fact that they contained Fe allowed magnetic separation of the catalyst, rendering this system highly practical.

7. Other Amine-Boranes and Alternatives to Ammonia-Borane

7.1. *N*-Methylamine-Borane Adducts

7.1.1. Synthesis and Basic Physical Properties

The syntheses of these materials follow standard routes as described in section 2 and will not be discussed in detail here. We merely provide a summary of the different methods for the interested reader.

N-Methylamine-borane could be prepared by salt metathesis from $MeNH_2 \cdot HCl$ with metal borohydrides MBH_4 (M = Li, Na, K) in a rotary mill to yield $MeNH_2 \cdot BH_3$.[172] The best results were obtained with $NaBH_4$ in THF, which gave 83% of $MeNH_2 \cdot BH_3$. It was also reported from a reaction of $BH_3 \cdot THF$ with $MeNH_2$ in THF at −78 °C in a 89% yield.[173] The chemical shift and B−H coupling constants in ^{11}B NMR spectroscopy (δ = −18.8 ppm, q, J_{BH} = 94 Hz) were similar to those of ammonia-borane (δ = −21.6 (q, J_{BH} = 95 Hz)).[9]

N,*N*-Dimethylamine-borane can be synthesized by the low temperature reaction of diborane and dimethylamine[174] or the reaction of dimethylamine with $BH_3 \cdot THF$.[9]

N,*N*,*N*-Trimethylamine-borane has been prepared by mixing $[Me_2NCH_2]I$ with $NaBH_4$ in neat conditions in 46% yield.[175] A more conventional route involved the reaction of trimethylamine with diborane.[176] The reaction of *N*,*N*,*N*-trimethylamine-borane and $BH_3 \cdot THF$ has not been reported but should be equally feasible.

7.1.2. Structures of N-Methylamine-Borane Adducts

The solid state structures for various amine-boranes have been elucidated; but as we are focusing on amine-boranes as a comparison to ammonia-borane in this review, we will only discuss *N*-methyl substituted congeners of the latter.

Table 9. Comparison of Structural and Physical Parameters of the *N*-Methylamine-Borane Adducts

property	$MeNH_2 \cdot BH_3$	$Me_2NH \cdot BH_3$	$Me_3N \cdot BH_3$
bond dissociation enthalpy in kcal/mol	35.0	36.4	34.8
crystal lattice	orthorhombic *Pnma*[a,b]	monoclinic $P2_1/c$[b]	rhombohedral $R3m$[b]
B−N bond, crystal structure	1.5936[b]	1.5965[b]	1.617[b]
B−N distance, GED	1.602(7) Å[b]	1.615(4) Å[b]	1.62 ± 0.05[c]
B−N distance, microwave	not determined	not determined	1.609 or 1.637[d] 1.638 ± 0.01[e] 1.656 ± 0.002[f]
dipole moment/D			
microwave	not determined	not determined	4.84 ± 0.1[g]
benzene, 25 °C	5.19[h]	4.87[h]	4.45[h] 4.62[i]
vapor pressure—enthalpies of vaporization[183]	18.8 ± 1.0[j]	18.5 ± 0.7[j]	13.6 ± 0.2[j]

[a] Reference 177. [b] Reference 178. [c] Reference 184. [d] Reference 185. [e] Reference 186. [f] Reference 187. [g] Reference 186. [h] Reference 188. [i] Reference 189. [j] Reference 190.

The existence of dihydrogen bonds in ammonia-borane in the solid state has been well-established (see section 3). It was therefore reasonable to assume that the closely related *N*-methyl substituted amine-boranes, $Me_nH_{3-n}N \cdot BH_3$ with $n = 1, 2$, would also exhibit this type of stabilizing bond, whereas the *N*,*N*,*N*-trimethylamine-borane would not. The first evidence for this was provided by vapor pressure measurements at various temperatures, which gave 79 and 77 kJ/mol (18.7 and 18.4 kcal/mol) as enthalpies of evaporation for $MeH_2N \cdot BH_3$ and $Me_2HN \cdot BH_3$, respectively, but a much reduced value of 57 kJ/mol (13.6 kcal/mol) for $Me_3N \cdot BH_3$. This fact cannot be explained as a result of their dipole moments, since these decrease with successive replacement of N−H by N−Me.

The first single crystal X-ray data of $MeNH_2 \cdot BH_3$ were presented by Bowden and co-workers,[177] which was essentially confirmed by later work by Downs, Parsons, and Rankin and co-workers.[178] (For comparison of different structural and physical parameters, see Table 9). A gas phase electron diffraction (GED) study for $MeNH_2 \cdot BH_3$ and $Me_2NH \cdot BH_3$ and single crystal X-ray diffraction for the whole $Me_nH_{3-n}N \cdot BH_3$ with $n = 1$, 2, and 3 series were also presented, supplemented by DFT studies. The gas-phase estimation of the geometries of these adducts is however fraught with difficulty. Not only did the value which was obtained vary when different techniques such as GED or microwave spectroscopy were used, it was also dependent on the selected data refinement, which is why many researchers in the field are relying increasingly on computational estimates. However, these are generally, and for amine-boranes in particular, functional and basis set dependent so that the unambiguous determination of exact reliable numbers in the gas phase seems impossible. Given the increasing bond dissociation enthalpies[179–181] with increasing Me substitution, which agree well with the increasing proton affinity of the corresponding Lewis bases (Table 9),[182] it was surprising that the actual geometries of the *N*-methylamine-borane adducts changed very little. For all adducts, the B−N bond distance was somewhat shortened in the crystal phase and mono- and dimethylated adducts showed significant hydrogen bonding. Contrary to ammonia-borane, which assumes a layered structure, the methyl congeners are more chainlike.

7.1.3. Thermal Decomposition of N-Methylamine-Borane Adducts

Insight into the mechanism of the thermal uncatalyzed hydrogen elimination of *N*-methylamine-borane was attempted by Beachley.[191] It was proposed that two molecules of *N*-methylamine-borane would initially form a thermally unstable salt **(i)**, which would then react with another equivalent to form the salt **(ii)** (eqs 32−35). This is turn would lose hydrogen to give a linear oligomer **(iii)**, which upon loss of another equivalent of hydrogen would form the cyclic trimer **(iv)**. The evidence presented for this mechanism is mainly based on the synthesis of intermediates **(i)** and **(ii)** and the observation of their reactions under thermal conditions.

$$2MeNH_2BH_3 \rightarrow \underset{\textbf{(i)}}{[MeNH_2-BH_2-NMeH_2]^+[BH_4]^-} \quad (32)$$

$$\textbf{(i)} + 2MeNH_2 \cdot BH_3 \rightarrow \underset{\textbf{(ii)}}{[MeNH_2-BH_2-NMeH_2-BH_2-NMeH_2]^+[BH_4]} + H_2 \quad (33)$$

$$\textbf{(ii)} \rightarrow \underset{\textbf{(iii)}}{H_3B-MeNH_2-BH_2-NMeNH_2-BH_2-NMeNH_2} + H_2 \quad (34)$$

$$\textbf{(iii)} \rightarrow \underset{\textbf{(iv)}}{(MeNH_2-BH_2)_3} + H_2 \quad (35)$$

While these studies were performed with great care, the analysis of these compounds at the time did not routinely include NMR spectroscopy and was mainly based on IR spectroscopy and elemental analysis. The ^{11}B NMR spectrum of salt (i) had already been reported,[192] and further characterizations by IR and, of the related chloride salt, also by PXRD had been reported.[191] However, there was no proof whether these materials were actually identical. In addition, no indication of purity was provided in either paper, which warrants caution with respect to the mechanistic conclusions that have been drawn.

More than 40 years after this study, the thermal decomposition of *N*-methylamine-borane was reinvestigated.[177] Its crystallographic phase was determined as orthorhombic at 113 K by single crystal X-ray diffraction, and contrary to the case of ammonia-borane, there was no phase transition up to 298 K. A thermal analysis of its decomposition was performed using TGA/DSC (Figure 39). Using a heating rate of 2 °C/min, a melt endotherm was found at 55 °C, followed by a large mass loss between 100 and 130 °C. This exceeded the mass loss expected for 1 equivalent of dihydrogen, and DSC showed that besides the exotherm, which was to be

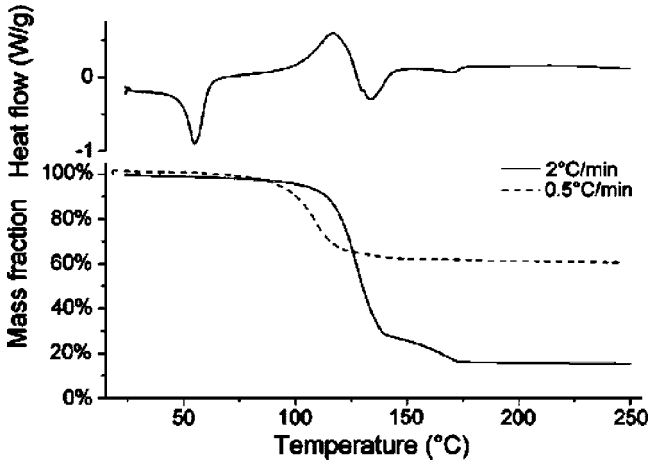

Figure 39. DSC (top) and TGA (bottom) for the thermal decomposition of *N*-methylamine-borane at 2 °C min^{-1} (TGA and DSC) and 0.5 °C min^{-1} (TGA only). Reprinted with permission from ref 177. Copyright 2008 Elsevier.

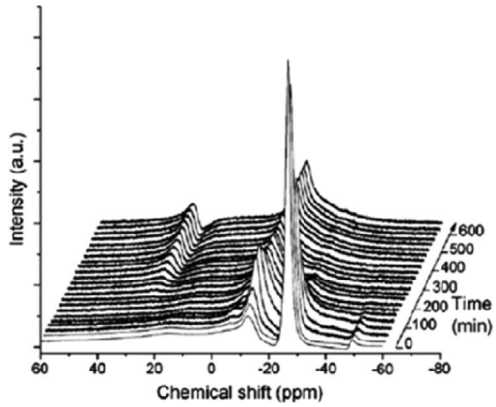

Figure 40. ^{11}B NMR spectra of the thermal decomposition reaction of *N*-methylamine-borane at 85 °C. Reprinted with permission from ref 177. Copyright 2008 Elsevier.

expected for the dehydrogenation reaction, an endotherm was present, which was attributed to mass loss through volatiles other than H_2. A further mass loss was observed between 130 and 190 °C, reducing the overall ceramic yield to less than 20%.

Mass spectroscopy of the volatiles was inconclusive, but ^{11}B NMR spectra of the reaction at 85 °C proved insightful (Figure 40). Initially, the most prominent peak was found at $\delta = -27$ ppm, which was attributed to the starting material, *N*-methylamine-borane, despite the fact that this is a significant upfield shift from $\delta = -18.4$ ppm observed at room temperature. The signal at $\delta = -48$ ppm was consistent with BH_4^-. Another signal at $\delta = -13$ ppm was not assigned; however, it is prominent throughout the reaction. This peak appeared to have a downfield shoulder, which was not commented upon, but from work on the polymerization of *N*-methylamine-borane,[193] it is well possible that poly(*N*-methylaminoborane) was observed. After 350 min, another signal at $\delta = 26$ ppm emerged, which was attributed to B-atoms in cross-linking positions.

Based on these findings, it was concluded that Beachley's mechanism appears largely correct, except that at higher temperatures cross-linking would take place as well. There was no evidence of borazine formation, which is in contrast to the work by Framery and Vaultier.[194] They heated a variety of *N*-substituted primary amine-borane adducts to 120 °C for 30 min and then to 200 °C for a further 60 min, and they purified the corresponding borazines by distillation. It therefore seems likely that borazines are the thermodynamic product whereas lower temperatures lead to kinetic products.

Table 10. Calculated Reaction Enthalpies at 298 K for the Dehydrogenation of the *N*-Methylamines

entry	reaction	ΔH in kcal/mol
1	$H_3N \cdot BH_3 \rightarrow H_2N{=}BH_2 + H_2$	−5.1[a]
2	$MeNH_2 \cdot BH_3 \rightarrow MeHN{=}BH_2 + H_2$	−3.5
3	$Me_2NH \cdot BH_3 \rightarrow Me_2N{=}BH_2 + H_2$	−1.8

[a] Reference 88.

The mechanism for the pyrolytic dehydrogenation of $Me_2NH \cdot BH_3$ was speculated to be a unimolecular process, involving only neutral species.[191] However, this mechanistic proposal was re-examined in more detail and provided evidence that solely an intramolecular mechanism could not be operating.[195] By mixing fully deuterated with nondeuterated *N*,*N*-dimethylamine-borane (or all other conceivable combinations of deuterated and nondeuterated substrates), heating the neat reaction mixture to 100 °C, and analyzing the gas in a MS, it was found that alongside H_2 and D_2, HD had been produced, which was evidence for an intermolecular dehydrogenation process. All necessary blank reactions were performed to rule out H−D scrambling in the gas itself or the starting materials. From these studies, KIEs of ($k_{N-H}/k_{N-D} = 3.5$; $k_{B-H}/k_{B-D} = 1.2$) were also obtained. The reaction was then postulated to occur via a dimer (eq 36), which could then lose another equivalent of hydrogen to produce a cyclic dimer.

$$2(CH_3)_2NH \cdot BH_3 \rightarrow (CH_3)_2NH \cdot BH_2{-}(CH_3)_2N \cdot BH_3 + H_2 \quad (36)$$

N,*N*-Dimethylamine-borane could be thermally dehydrocoupled to give the cyclic dimer $[Me_2N\text{-}BH_2]_2$ at 130 °C in the melt.[174] The thermal decomposition of this amine-borane adduct in the gas phase (with an applied vacuum) at thermolysis conditions ranging from 150 to 450 °C was also studied, and products were trapped in a cold trap at −196 °C.[9] Only trace amounts of the cyclic dimer were found, which led to the conclusion that its formation must be intermolecular, which would be kinetically inhibited at the low partial pressures employed during the experiment. This is in agreement with the earlier study by Ryschkewitsch and Wiggins.[195]

The thermochemistry for the dehydrogenation of the *N*-methylamine-boranes in the gas phase was investigated computationally using high accuracy coupled cluster methods.[196] Unsurprisingly, it was found that the dehydrogenation across the B−N bond is strongly favored over dehydrogenation across the N−C bond. Table 10 lists the calculated reaction enthalpies at 298 K.

7.2. Other Alternatives to Ammonia-Borane

There are a number of hydrogen releasing fuels which may be considered alternatives to ammonia-borane, including various metal hydrides[197] or metal borohydrides,[197a,198] but it is beyond the scope of this review to discuss them in detail.

Instead, were are only going to present comprehensively such compounds which still contain nitrogen and boron and are thus related to ammonia-borane.

7.2.1. Ammonia-Triborane

As an alternative substrate to ammonia-borane for hydrolytically generated dihydrogen ammonia-triborane, $NH_3B_3H_7$ was proposed.[199] The synthesis of this compound proved to be easy and scalable. Ammonia-triborane is significantly more soluble in water than ammonia-borane, thus decreasing the overall necessary weight of a potential appliance. It could be obtained in over 80% yield from the $[n\mathrm{BuN}_4][B_3H_8]$ salt (Scheme 11),[200] which was a considerable improvement compared to the first synthesis.[201] It showed two distinct signals by ^{11}B NMR, one at $\delta = -7.7$ ppm for *B2* and *B3* and another at $\delta = -32.8$ for *B1*. Dehydrogenation was effective with both 1 M HCl (7.85 equivalents of H_2 after 120 min) and various metal catalysts, the best being Rh/Al_2O_3 (approximately 7.5 equivalents after 25 min at 21 °C with 7 mol % catalyst).

Scheme 11. Synthesis of Ammonia-Triborane

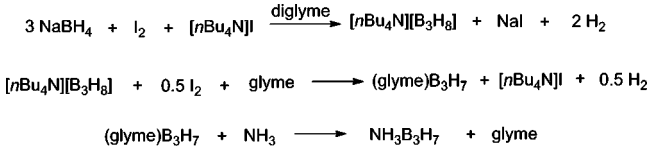

The first crystallographic single X-ray structure of ammonia-triborane showed two crystalline phases, an ordered monoclinic phase obtained at −45 °C and a disordered tetragonal form at 25 °C.[202] This phase transition was later determined more precisely by calorimetric measurements, where a first-order transition was found at 297.10 K.[203] When ammonia-triborane began to be considered as a potential rival for ammonia-borane for hydrogen storage applications, another, more detailed account appeared on this compound, which also included single crystal X-ray crystallographic data, combined with a computational DFT study.[204] In this paper an inconsistency between the crystal study and earlier DFT studies[205–207] could finally be resolved: all DFT calculations predicted a symmetrical C_s structure with one bridging hydrogen atom, as shown in Figure 41a. However, the crystal structure showed a highly unsymmetrical molecule, where the bridging hydrogen atom was much closer to one of the boron atoms than to the other (Figure 41b). Based on the knowledge that ammonia-borane has an extensive network of dihydrogen bonds in the solid state (see section 3), it was hypothesized that similar forces should be at work in the related ammonia-triborane, which would only become evident in the solid state and which would be overlooked in a gas-phase calculation. Therefore, dimeric structures were calculated, which indeed showed these dihydrogen bonds. Further evidence was obtained by calculating the corresponding *N*-mono- and *N*,*N*-dimethylammonia-triborane dimers, which showed the same effect, and crystallographically determining the 18-crown-6-adduct, which did not allow for dihydrogen bonding and showed a much more symmetrical bridge.

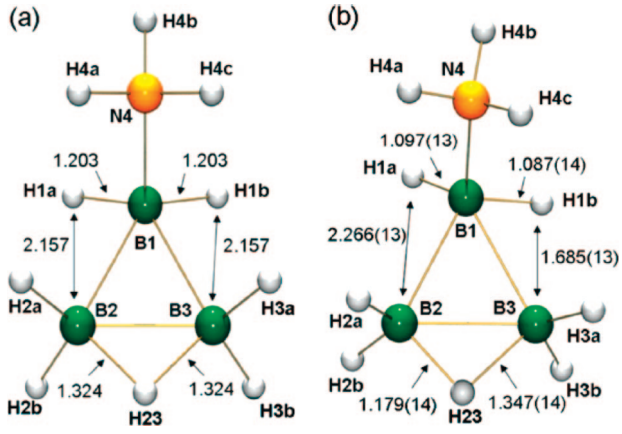

Figure 41. (a) DFT (B3LYP/6-31G(d)) optimized structure and (b) crystallographically redetermined structure of ammonia-triborane. Reprinted with permission from ref 204. Copyright 2009 American Chemical Society.

The *N*-methylamine adduct congeners of ammonia-triborane[208] and phosphine triborane[209] have also been investigated, but since there is at present no materials or hydrogen storage application for these adducts, they will not be discussed here.

Using localized orbital theory, the molecular and electronic structure of ammonia-triborane was reinvestigated.[210] This calculation largely confirmed the finding of earlier calculations by Lipscomb on similar systems in 1973,[211] which predicted that, besides the N→B_1 dative bond and the normal B−H and N−H bonds, the bridging hydrogen is bound by both B_2 and B_3 in a 3-center-2-electron bond similar to the bonding found for the bridging hydrogen atoms in diborane. The remaining two electrons, however, form a B−B−B 3-center-2-electron bond. At almost the same time, this molecule was analyzed by the quantum theory—atoms-in-molecules approach, electron localization function analysis, and natural bond orbital analysis, where qualitatively the same conclusion was reached.[212] Molecules of the type $B_3H_7EH_3$ (with E = N, P, As) were analyzed in the gas phase in a molecular orbital study.[213] Based on Sneddon's work,[204] these gas phase geometries are almost certainly perturbed in the solid state, but within limits, the molecular orbital comparison between the different donors in group 15 is nevertheless insightful. The bonding of the Lewis base to B_3H_7 was asymmetric via one of the boron atoms (B_1), which was expected to give the major bonding contribution (Figure 42). In the case of NH_3, the donor participated only by the $4a'$ HOMO, whereas, in the case of the higher homologs, PH_3 and AsH_3, there was also a participation by the na' HOMO and also the $(n-2)a'$ ($n = 7$ and 13, respectively). The energetically lower MO was much higher in energy in PH_3 and AsH_3, which allowed for the participation, whereas, in NH_3, no significant energetic overlap was found. Because this MO is filled and interacted with a filled MO on the B_3H_7 fragment, this interaction was destabilizing. This interaction contributed to the increasing lability of the complexes on descending group 15.

A second, destabilizing interaction between occupied molecular orbitals (2MO-4e) of donor and acceptor fragments with a'' symmetry was also described (Figure 43). This destabilizing influence increased from NH_3 to AsH_3 because the concerned orbitals became closer in energy, thus mixing more efficiently.

However, there was no comment on the possibility of a BBB bond nor were any actual values provided for the orbitals involved. There was also no mention of whether the isolated stabilizing effect, which was based on a classic Lewis acid/Lewis base interaction, was numerically different with NH_3, PH_3, or AsH_3, as one would expect and to which

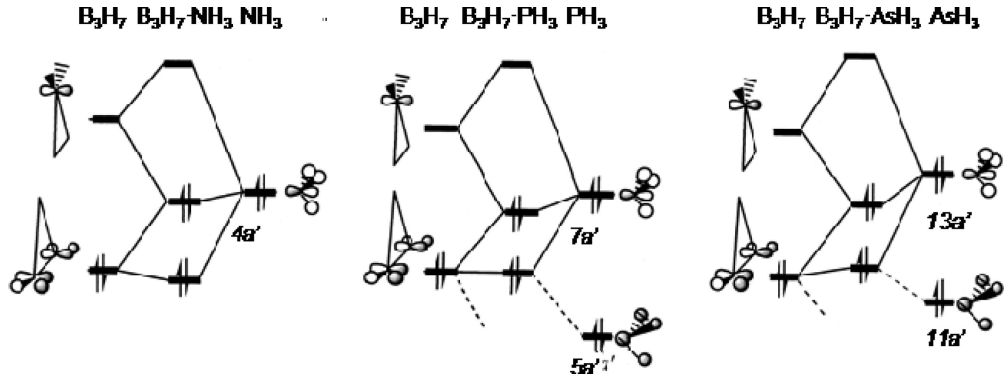

Figure 42. Fragmental analysis of the "*a′* " symmetry (symmetric with respect to horizontal mirror plane) molecular orbitals of (a) $B_3H_7NH_3$, (b) $B_3H_7PH_3$, and (c) $B_3H_7AsH_3$. Reprinted with permission from ref 213. Copyright 2002 American Chemical Society.

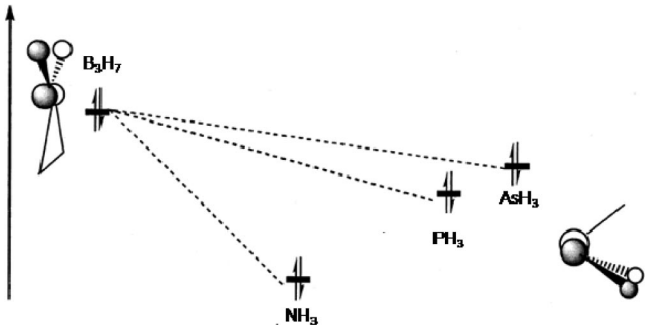

Figure 43. "*a″*" symmetry (antisymmetric with respect to horizontal mirror plane) MO energy level diagram for B_3H_7 and XH_3 (X) N, P, and As). Reprinted with permission from ref 213. Copyright 2002 American Chemical Society.

numerical extent the destabilizing factors play a role in the bonding situation of these molecules.

The thermal hydrogen release mechanism for ammonia-triborane was calculated in the gas phase.[214] Interestingly, the (nonhydrolytic) dihydrogen release was predicted to be endothermic (it is exothermic in ammonia-borane) to give aminotriborane. However, the barriers for this process and ammonia-triborane dissociation were predicted to be similar so that purely thermal (i.e., uncatalyzed) reactions are unlikely to render this a useful hydrogen storage material for these reaction conditions (as opposed to hydrolysis). Nevertheless, it has to be borne in mind that Miranda and Cedar showed convincingly how important the consideration of the crystal structure for accurate estimation of reactions occurring in solid state ammonia-borane is.[96] Combined with the insight that the crystal structure differs significantly from the gas phase structure, it is well possible that such computational studies which would consider intermolecular dihydrogen bonds could lead to different results.

7.2.2. Hydrazine-Monoborane and Hydrazine-Bisborane

Hydrazine-monoborane (HB) and hydrazine-bisborane (HBB) are both interesting amine-boranes in their own right, and due to their close relationship to ammonia-borane, these species have received increasing attention over the last ten years. Both can be prepared relatively easily by mixing dihydrazinium sulfate or hydrazinium sulfate, respectively, with sodium borohydride (eqs 37 and 38).[36]

HB:

$$(N_2H_5)_2SO_4 + 2NaBH_4 \rightarrow 2H_2N{-}NH_2 \cdot BH_3 + Na_2SO_4 + 2H_2 \quad (37)$$

HBB:

$$(N_2H_6)SO_4 + 2NaBH_4 \rightarrow H_3B \cdot H_2N{-}NH_2 \cdot BH_3 + 2H_2 + Na_2SO_4 \quad (38)$$

Two alternative routes for the synthesis of hydrazine monoborane exist.[215] In the first, magnesium chloride hexahydrate was reacted with 2 equivalents of sodium borohydride in hydrazine. The product hydrazine monoborane could be extracted with THF in 79% yield (eq 39)

$$MgCl_2 \cdot 6H_2O + 2NaBH_4 + 4H_2N - NH_2 \rightarrow 2H_2N - NH_2 \cdot BH_3 + 2H_2 + Mg(N_2H_3)_2 + 2NaCl \quad (39)$$

The second route involved the direct reaction of $MgCl_2 \cdot 4N_2H_4$ with $NaBH_4$ (eq 40) and gave a similar yield (83%).

$$MgCl_2 \cdot 4N_2H_4 + 2NaBH_4 \rightarrow 2H_2N - NH_2 \cdot BH_3 + 2H_2 + Mg(N_2H_3)_2 + 2NaCl \quad (40)$$

The intended product was analyzed by IR, melting point, and elemental analysis, but the exact nature of the other side products was not investigated, which makes the above equations an educated guess only. Instead of using the magnesium chloride complex of hydrazine, the reaction was optimized to allow for the use of the hydrochloride of hydrazine, $N_2H_4 \cdot HCl$.[216]

Their potential applications are similar to those discussed for ammonia-borane and include use as precursors to boron nitride, hydrogen storage materials, and reducing agents, in particular in the field of electroless plating and direct use as a propellant, for example for torpedoes. In this section, we will limit the discussion to the structure of these compounds and applications in which the B−N bond(s) is (are) preserved, because reductive solvolysis applications should follow the same principles as for ammonia-borane and, therefore, do not add fundamentally to the discussion.

Hydrazine-monoborane was analyzed by vibrational spectroscopy, which allowed the extraction of the force constants[217] and was complemented by infrared and Raman

spectroscopy of hydrazinebisborane.[218] However, compared to ammonia-borane, these compounds remain relatively unexplored.

Hydrazine-monoborane was computationally (DFT) found to have an unusual reactivity toward acids (Figure 44). While

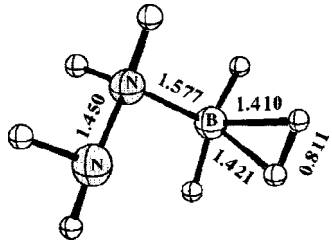

Figure 44. DFT calculated structure of the protonated hydrazine-monoborane. Reprinted with permission from ref 219. Copyright 1999 American Chemical Society.

an intuitive guess would lead most to believe that protonation would occur at the lone pair of the uncomplexed NH_2 moiety of the molecule, DFT calculations suggested that, in fact, protonation on the BH_3 moiety was 6.3 kcal lower in energy (in the gas phase).[219] Therefore, the B−H bond must have a greater proton affinity than the nitrogen lone pair. Similarly to the case of ammonia-borane, the calculated gas phase B−N bond length for the unprotonated hydrazine-monoborane (1.625 Å)[220] was considerably longer than the one obtained by single crystal X-ray crystallography (1.56 Å) and the unusual protonation behavior was interpreted as an indication that similar electrostatic forces could be at play, but it has to be borne in mind that gas phase calculations can be misleading, especially when charged species are investigated.

Hydrazine-bisborane has been investigated as a hydrogen storage material. Initially the thermal decomposition of this compound was studied, and while the dihydrogen yield of 10 wt % up to 150 °C is useful in principle, the material decomposed explosively at 160 °C, which would make it unsafe to use in hydrogen storage applications.[221] Hydrazine-monoborane on the other hand was not reported to explode to temperatures up to 200 °C.[36] It melted at 65 °C, at which temperature thermal decomposition commenced.[222] The hydrogen release was measured at different temperatures, and it was found that, at 140 °C, a total of about 6 wt % was released within 30 min.[221] As the use of alkaline and alkaline earth metal hydrides as additives to ammonia-borane moved into focus in the field of ammonia-borane research, the same principle was used by adding LiH as a 1:1 stoichiometric additive to HB form a mixture containing
14.5 wt % of dihydrogen. It was found that with this mixture, a total of 10 wt % was released at 150 °C within 12 min. The release kinetics with the additive were thus considerably faster than without and, in both cases (pure HB and HB/Li), the amount of fuel cell poisoning impurities, such as NH_3 (below 1%) and borazine (not detected), was very low.

Shortly after this work, a computational study of the hydrazine-monoborane (the initial focus of this contribution was the interaction of hydrazine and diborane or borane-alane) was reported.[223] It was found that, qualitatively, the hydrogen release mechanism was similar to that of ammonia-borane, because the NH_2 moiety of hydrazine-monoborane merely acted as a substituent and did not partake in the reaction itself. The central B−N bond was stabilized

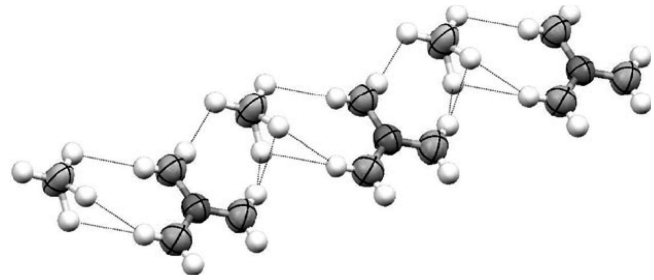

Figure 45. Single X-ray structure of guanidinium borohydride. Reprinted with permission from ref 224. Copyright 2009 RSC Publishing group.

by this substituent and the transition state for the release of dihydrogen was also higher than that for ammonia-borane. However, the authors noted that a Lewis acid such as AlH_3 may be catalytically active, similar to the catalytic effect BH_3 had on the dehydrogenation kinetics of ammonia-borane.[91]

7.2.3. Guanidinium Borohydride

Guanidinium borohydride represents a compound which is relatively closely related to ammonium borohydride and thus ammonia-borane, and may have useful hydrogen storage properties.[224] Guanidinium borohydride was synthesized by Titov and co-workers by the salt metathesis reaction of bisguanidinium sulfate and sodium borohydride in *i*PrOH in 65% yield (eq 41)[225] or by the metathesis reaction of bisguanidinium carbonate and calcium diborohydride in water (eq 42).[226]

$$[C(NH_2)_3]_2SO_4 + 2NaBH_4 \rightarrow 2[C(NH_2)_3]BH_4 + Na_2SO_4 \quad (41)$$

$$[C(NH_2)_3]_2CO_3 + Ca(BH_4)_2 \rightarrow 2[C(NH_2)_3]BH_4 + CaCO_3 \quad (42)$$

Analyses on the properties of this novel compound found that heating at 100 °C for a few hours led to release of hydrogen and the formation of $CN_3H_4BH_2$, which at 400 °C decomposed to give a gas and a brown ceramic.[226] The enthalpy of formation $\Delta H°$ of $(CN_3H_6)BH_4$ was determined to be -26.5 ± 1.2 kcal/mol.[227] It is of practical use that guanidinium borohydride is air stable and soluble in a variety of polar solvents such as liquid NH_3, H_2O, MeOH, and EtOH with little solvolysis, although it was found to be insoluble in Et_2O, benzene, and hexane.[228] Guanidinium borohydride was found to start decomposing at 100 °C and gave unidentified BN polymer at 400 °C.[228] In order to gain a clearer understanding of the compound, a single crystal X-ray analysis was performed, which revealed a dense dihydrogen network similar to ammonia-borane (Figure 45).[224]

As guanidinium borohydride contains 13.5 wt % of active hydrogen, its thermal properties were reinvestigated with a view to assessing it as a potential hydrogen storage material. The calorimetric analysis by DSC of guanidinium borohydride at a heating rate of 8 °C min^{-1} showed a narrow exotherm at 110 °C before a relatively broad exothermic peak to about 175 °C with a mass loss of about 13−14% up to this temperature (Figure 46).

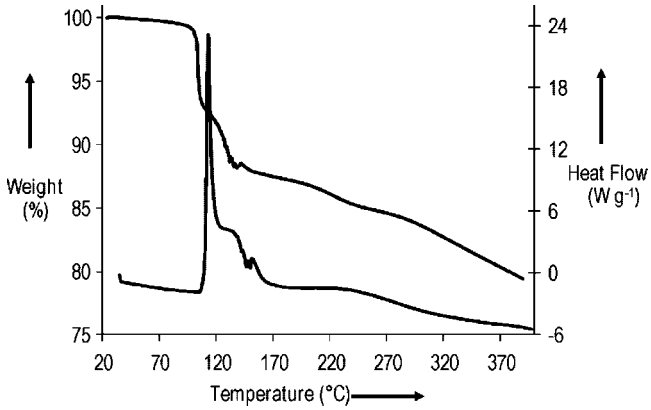

Figure 46. Thermogravimetric and calorimetric analysis of guanidinium borohydride. Reprinted with permission from ref 224. Copyright 2009 RSC Publishing group.

When ignited, neat guanidinium borohydride decomposed in a self-sustaining reaction while rapidly generating hydrogen gas. However, some residual ammonia (3−5%) was also observed, which would be detrimental for fuel cells but could not be prevented even with the addition of various hydrides (MgH_2, $NaBH_4$, $LiAlH_4$, Me_4NBH_4). However, the purity could be improved upon with the additive ethylenediamine bisborane. It is possible that further optimization on the hydrogen release properties of this compound will make it an interesting alternative to ammonia-borane.

7.2.4. Ammonium Borohydride

At first glance, ammonium borohydride would appear as an even more promising hydrogen storage material, based on the calculation that it contains up to 24.3 wt % of H_2. Ammonium borohydride was first prepared in 1958.[229] It is a white crystalline solid with a rock salt structure,[230] which was found to decompose slowly above −40 °C to the diammoniate of diborane, with a half-life of 6 h at 25 °C.[229] Nevertheless, ammonium borohydride and its decomposition product could be analyzed by Raman spectroscopy in liquid ammonia.[231] This thermodynamic instability was calculated to be around 37 kcal/mol[232] (or $\Delta H_{(0\,K)} = -16.8$ kcal/mol using high level coupled cluster methods),[88] and the potential energy surface for this salt was assessed.[233] It has been suggested that, in the salt, there is initially a dihydrogen bond between a protic H on NH_4^+ and a hydridic H on BH_4^-, which, due to electrostatic forces (field effects) react to give two molecules coordinated to dihydrogen.[234] Despite its instability, the high hydrogen content of ammonium borohydride is so attractive that there has been an attempt to study its thermal decomposition by means of DSC and TGA, coupled with mass spectrometry using a heating rate of 1 °C/min.[230] It was found that ammonium borohydride decomposed in three distinct steps, all of them exotherms (Figure 47). The first, at about 53 °C, leading to a mass loss of 6.5 wt %, was attributed to the decomposition into ammonia-borane and hydrogen, the latter of which was analyzed by MS. This was then followed by a second step, at about 85 °C, leading to a further loss of 6 wt % dihydrogen, presumably giving polyaminoborane, followed by a third step at 130 °C, concomitant with 9 wt % loss of hydrogen, with polyiminoborane type species as the solid products. MS showed that, for these steps, hydrogen was again the major product, with traces of borazine being found for the last step.

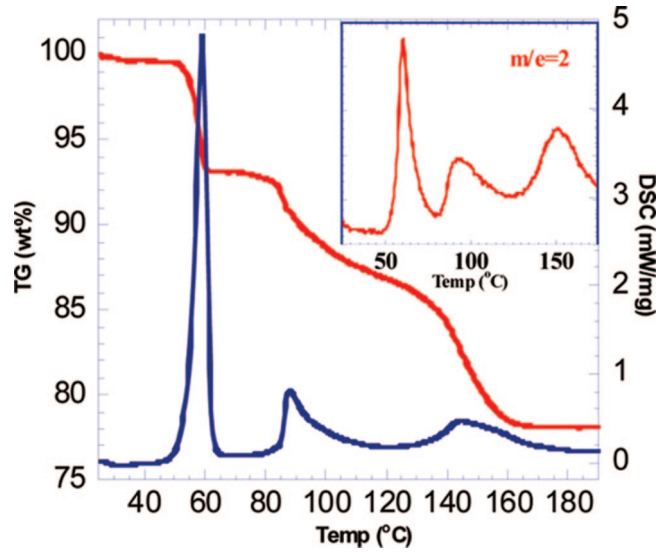

Figure 47. DSC-TGA-MS data for decomposition of ammonium borohydride, $[NH_4][BH_4]$, heated at 1 °C/min, three distinct steps for hydrogen release are visible: step 1, $T_d = 53$ °C, mass loss 6.5%, ΔH ca.−40 kJ/mol; step 2, $T_d = 85$ °C, mass loss 6.0%, ΔH ca.−15 kJ/mol; step 3,$T_d = 130$ °C, mass loss 9%, ΔH ca. −13 kJ/mol. Reproduced with permission from ref 230. Copyright 2009 American Chemical Society.

In order to determine whether the diammoniate of diborane played a role in the observed decomposition process, ammonia-borane and ammonium borohydride were mixed, which led to the immediate formation of DADB. It was therefore hypothesized that the rate determining step may be hydrogen and ammonia-borane formation, the latter of which then reacts with further ammonium borohydride to give hydrogen and DADB. In order for this compound to be a safe and practical hydrogen storage material, it will be necessary to find possibilities to stabilize the compound at ambient temperature, perhaps by using additives or incorporating it into a scaffold with reaction retarding properties. Chemical modifications, for example exchanging a protic H atom on nitrogen for an alkali or earth alkali metal, might also lead to useful materials, but to our knowledge, this approach has not been explored to date.

Higher congeners of group 13 group 15 $[XH_4][YH_4]$ salts have also been computationally assessed, but since the results do not reflect the experimental results for ammonium borohydride, it is not certain how much predictive power can be ascribed to this study.[235]

8. Regeneration of Ammonia-Borane Spent Fuel

Despite the large amount of research into the release of dihydrogen from ammonia-borane, as of early 2010, there have been only a few reports on strategies to tackle the need for spent fuel to be regenerated. In fact, there are only three papers apart from conference papers and patents. The first by Ramachandran and co-workers discussed a system in which ammonia-borane was subjected to transition metal-catalyzed solvolysis to yield $[NH_4][B(OMe)_4]$, which could be converted back to ammonia-borane at ambient temperature using NH_4Cl and $LiAlH_4$, releasing another equivalent of

Scheme 12. Regeneration of Solvolysis Product of Ammonia-Borane

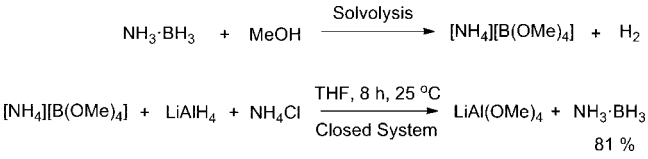

Scheme 13. Strategy for the Regeneration of Ammonia-Borane in Six Distinct Processes[a]

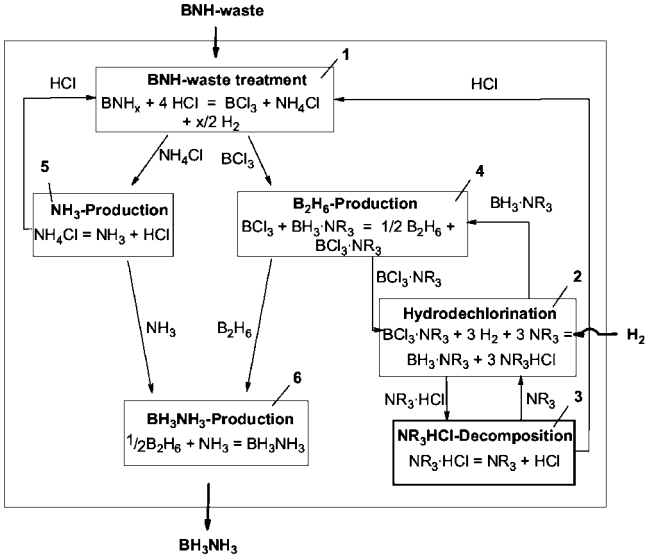

[a] Reprinted with permission from ref 236. Copyright 2008 Elsevier.

hydrogen (Scheme 12).[4] At the time of writing, there is no procedure published to convert the oxidation product, $[Al(OMe)_4]$, back to the complex hydride, and it must to be demonstrated that this is indeed a feasible process.

The two other publications deal with the regeneration of spent ammonia-borane fuel where there are no B−O bonds present. It is clear that not all 3 equivalents of hydrogen should be released from ammonia-borane, because the resulting boron nitride is chemically extremely inert and the energy needed to reduce it would outweigh all potential benefits of using ammonia-borane as a hydrogen storage material. The first basic concept relies on the initial waste treatment with HCl (step 1 in Scheme 13) as a superacid mixture with $AlCl_3$.[236] This step was partly developed based on a report by Sneddon which is yet to appear in the peer reviewed literature.[237] The most challenging step would then be the diborane generation from BCl_3 (step 4 in Scheme 13), which has been achieved, but only at prohibitively high temperatures (600−750 °C), electrolytically or using other hydrides, which is either too energy consuming or simply creates a new problem of generating hydrides. It was pointed out, however, that addition of base could shift the equilibrium to the reaction product side by complexing the HCl side product (eq 43), which would allow the process to proceed at lower temperatures.

$$BCl_3 \cdot NR_3 + 3H_2 + 3NR_3 \rightarrow BH_3 \cdot NR_3 + 3NR_3 \cdot HCl \quad (43)$$

However, this process was merely suggested and not rigorously analyzed by experimental means to determine whether it is actually feasible. Both NH_4Cl from the first decomposition step and the HCl·base adduct from the diborane regeneration pathway (step 2 in Scheme 13) are then proposed to thermally decompose to regenerate HCl for the initial waste treatment and ammonia for the reaction with diborane (steps 3 and 5 in Scheme 13).

Scheme 14. Possible Regeneration Pathway for Spent Ammonia-Borane Fuel

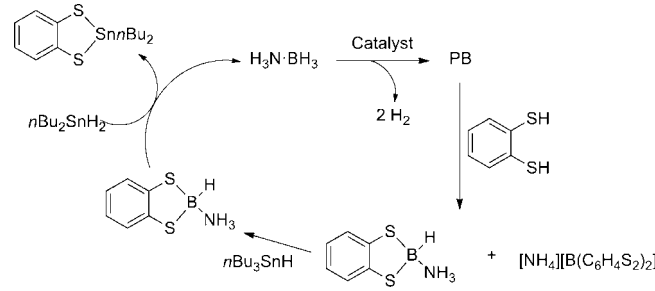

Table 11. Efficiency Estimates for AB Regeneration

regeneration process	efficiency (0% heat recovery)
$[NH_4][B(OMe)_4] + 3H_2 \rightarrow NH_3 \cdot BH_3 + 4MeOH$	46%
$^1/_3B_3N_3H_6 + 2H_2 \rightarrow NH_3 \cdot BH_3$	65%

A better developed regeneration cycle was put forward which used a DFT approach to determine a reagent that might convert the spent fuel, which mainly consists of polyborazylene (PB), to a more useful and clearly defined compound.[238] As a model for PB, borazine was used, and it was found that a reaction with 1,2-benzenedithiol had an exothermic reaction enthalpy of −20.4 kcal/mol in the condensed phase. Indeed, when 1,2-benzenedithiol was reacted with PB under reflux conditions in THF, the formation of $(C_6H_4S_2)BH \cdot (NH_3)$ (^{11}B NMR: $\delta = -5.6$, d, $^1J_{B-H} = 128$ Hz) and $[NH_4][B(C_6H_4S_2)_2]$ ($\delta = 10.5$ ppm, s) was observed. While the structure of the former compound could be proven by independent analysis, for the second one, this was not possible and chemical shift calculations by DFT and a comparison with $Li[B(C_6H_4S_2)_2]$ had to suffice. Using excess Bu_3SnH at 60 °C in THF, this salt could then be transformed into $(C_6H_4S_2)BH \cdot (NH_3)$ as well, which could be transformed back into ammonia-borane and $C_6H_4S_2Sn(n\text{Bu})_2$ using $n\text{Bu}_2\text{SnH}_2$ (Scheme 14).

Although this process still had some issues with side products, the use of toxic tin hydrides, the less than optimum overall yield of recycled ammonia-borane (67%), and the lack of scalability due to instability of Bu_2SnH_2, this important contribution was the first demonstration that relatively efficient ammonia-borane regeneration might be within reach. (For a comparison with Ramachandran's approach,[4] see Table 11.) Indeed, it could be shown that the process could be improved by inducing an amine exchange step after the digestion with Me_3N, which allowed for the much less problematic use of $n\text{Bu}_3\text{SnH}$ as a reductant.[239] The resulting products (**a** and **b**) (Scheme 15) could then be treated with HCl to give $n\text{Bu}_3\text{SnCl}$ and the *o*-benzenedithiol, which can be reused for the digestion. It could be shown that $n\text{Bu}_3\text{SnCl}$ could be transformed into the corresponding formate, which can be reduced to give $n\text{Bu}_3\text{SnH}$,[240] thus closing the catalytic cycle (Scheme 15).

From an engineering point of view, the transport properties of ammonia-borane spent fuel are of crucial importance. For this purpose, the viscoelastic properties of spent fuel from ammonia-borane hydrolysis, ammonia-

Scheme 15. Regeneration of AB with Tin Recycle and *ortho*-Benzenethiol Recovery

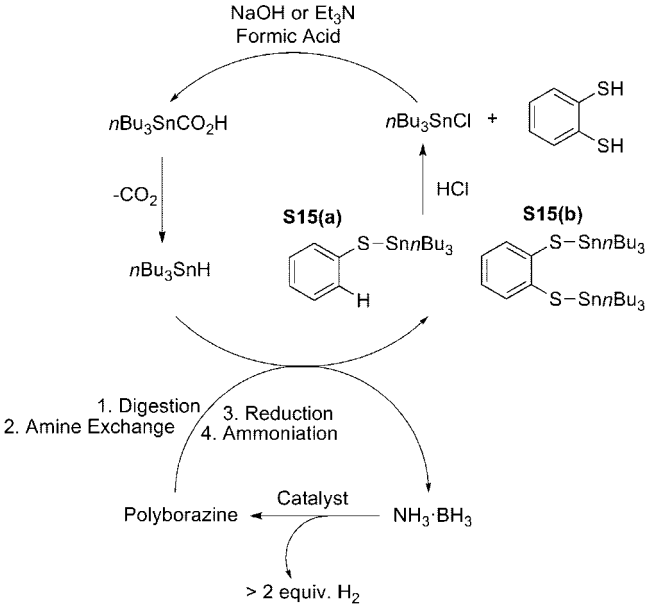

borane thermolysis, and ammonia-borane hydrothermolysis were compared.[241] The ammonia-borane hydrolysis spent fuel was found to be more transportable (smaller stiffness and larger mobility equal to smaller viscous damping) than comparable samples obtained from sodium borohydride spent fuel. Ammonia-borane fuels obtained from neat thermolysis and hydrothermolysis proved to be more transportable than those obtained in ionic liquids. The thermal history of the fuel also played a crucial role. For example, samples obtained at higher dehydrogenation temperature proved to be more transportable than those obtained at lower temperature.

9. Conclusion

Research on ammonia-borane as a potential hydrogen storage material has intensified since 2005 and is a highly active and exciting area. Initial efforts were focused on understanding the structure and physical properties of ammonia-borane itself and the dehydrogenation of this species. It soon emerged that in order to obtain clean hydrogen suitable for fuel cell applications at useful temperatures and hydrogen release rates, catalytic processes were required. Here, the approaches range from transition metal catalysis, to acid and base catalysis, to the use of ionic liquids and catalyzed solvolysis. A further active area is the enhancement of hydrogen generation by incorporation of ammonia-borane into a variety of scaffolds, and substantial efforts are being made to understand the structural changes imposed by the large interior surface of these scaffolds and ammonia-borane. Another promising avenue which has been explored is the chemical modification of this compound to produce amidoboranes. By comparison, the regeneration of spent fuel has received much less attention and only recently have potentially workable approaches been published. It is to be expected that this last area will gain more impetus if ammonia-borane is to make the transition from a potential portable hydrogen storage compound to an industrially viable species with a significant role in the hydrogen economy.

Table A1. Solubility

solvent	solubility ($g_{NH3\cdot BH3}$/100 $g_{solvent}$)	ref
ammonia	260	242
water	33.6	242
Et_2O	0.74	242
EtOH	6.5	242
*i*PrOH	4	242
*i*BuOH	1	242

Table A2. Dipole Moment

method	value/D	ref
microwave, vapor	5.216 ± 0.017	25
dielectric constant, in dioxane	4.88 ± 0.1	243

Table A3. Calculated Electron Affinity in eV

molecule	EA (eV)
$H_2N{=}BH_2$	−0.41
$H_2N\cdot BH_3$	2.25
$H_3N\cdot BH_2$	−0.05
$H_3N\cdot BH_3$	−0.03

Table A4. Calculated Hydride Affinities at 0 K in kcal/mol

reaction	
$H_2B{=}NH_2 + H^- \rightarrow H_3B{-}NH_2^-$	37.0
$H_2B{=}NH_2 + H^- \rightarrow H_2B{-}NH_3^-$	−20.2
$H_2B{-}NH_3 + H^- \rightarrow H_3B{-}NH_3^-$	84.9
$H_3B{-}NH_2 + H^- \rightarrow H_3B{-}NH_3^-$	78.4

Table A5. Calculated Adiabatic Ionization Potentials at 0 K

molecule	IE (eV)
$H_2N{=}BH_2$	10.62
$H_3N{=}BH_2$	5.65
$H_3N\cdot BH_3$	9.29

Table A6. Calculated Proton Affinities at 298 K in kcal/mol

reaction	298 K
$H_2B\cdot NH_2 + H^+ \rightarrow H_2B\cdot NH_3^+$	180.4
$H_2B\cdot NH_3 + H^+ \rightarrow H_3B\cdot NH_3^+$	201.3
$H_3B\cdot NH_2 + H^+ \rightarrow H_3B\cdot NH_3^+$	194.8
$H_3B\cdot NH_3 + H^+ \rightarrow H_4B\cdot NH_3^+$	192.1

Table A7. Calculated Adiabatic Bond Dissociation Energies at 0 and 298 K in kcal/mol

reaction	0 K	298 K
$H_2BNH_2 \rightarrow H_2BNH + H$	111.8	113.9
$H_3BNH_2 \rightarrow H_2BNH_2 + H$	2.4	3.6
$H_2B\cdot NH_3 \rightarrow H_2BNH_2 + H$	−4.1	−2.9
$H_3B\cdot NH_3 \rightarrow H_2BNH_3 + H$	100.5	102.0
$H_3B\cdot NH_3 \rightarrow H_3BNH_2 + H$	94.0	95.5

Table A8. Reported Metal Catalyzed Dehydrogenation/Hydrolysis Reactions for the Production of Dihydrogen

entry	amine-borane	catalyst	solvent	equiv of H_2 released	T^b/°C	time	ref
1	tBuNH$_2$·BH$_3$ Me$_3$N·BH$_3$	10% Pd/C (50% wet)	MeOH	approx 3	30	100 min 20 h	157, 245
2	various	10% Pd/C (50% wet), Raney Ni (5 mol %)	H_2O, various alcohols	high efficiency	20	5 min (MeOH) to −190 min (tBuOH)	246, 247
3	H_3N·BH_3 (1 M)	Pt (20% on C) (2 mol %)	H_2O	approx 3	20	2 min	158
		PtO_2 (2 mol %)		approx 3		8 min	
		Pt black (2 mol %)		approx 3		12 min	
		K_2PtCl_4 (2 mol %)		approx 3		19 min	
		[Rh(1,5-COD)(μ-Cl)]$_2$ (2 mol %)		approx 2.6		15 min	
		Pd (2 mol %)		approx 2.6		250 min	
4	H_3N·BH_3	Dowex (12 wt %) CO_2	H_2O	approx 2.8; no starting material left	20	8 min 7 days	248
5	H_3N·BH_3	Co (10% on C) (2 mol %)	H_2O	approx 2.9	20	60 min	249
		Ni (10% on γ-Al_2O_3) (2 mol %)		approx 2.9		60 min	
6	H_3N·BH_3	$Ni_{0.88}Pt_{0.12}$ hollow sphere (2 mol %)	H_2O	approx 3	20	30 min	161
7	H_3N·BH_3	Rh colloids (1 mol %)	H_2O	approx 2.8	20	40 s	250
		Ir colloids (1 mol %)		approx 3		105 min	
		Co colloids (1 mol %)		approx 3		60 min	
8	H_3N·BH_3 (2 M)	$RuCl_3$ (0.5 mol %)	MeOH	approx 3	25	5 min	4
		$NiCl_2$ (2 mol %)				60 min	
		$CoCl_2$ (2 mol %)				40 min	
		Pd/C (2 mol %)				90 min	
		Raney Ni (2 mol %)				50 min	
		$PdCl_2$ (2 mol %)				110 min	
		$RhCl_3$ (2 mol %)				<10 min	
9	H_3N·BH_3 (0.16 M)	amorphous Fe nanoparticles (0.1 mol %)	H_2O	approx 3	20	8 min	162
10	H_3N·BH_3 (16 M)	K_2PtCl_6 (0.1 mol %)	H_2O, D_2O	approx 3	25	330 min	251
11	H_3N·BH_3 (0.32 M)	nanoclusters of Ru, Rh, Pt, Pd, Au, supported on γ-Al_2O_3, C, SiO_2; 2 wt % (Pd, Au also reported but less effective)	H_2O	approx 3	20	<3 min	252
12	H_3N·BH_3	PtM/C (M = Ir, Ru, Co, Cu, Sn, Au, Ni. metal content: 20 wt %)	H_2O	2.5−2.9	20	10−140 min	253
	(0.02 M)	(NiM/C; M = Au, Ag, Cu, Sn, Co. metal content: 20 wt %)		2.6−2.9	20	25−400 min	
13	H_3N·BH_3 (0.025 M)	$NiCl_2$·$6H_2O$ (7 mol %)	H_2O	2.7	20	125 min[a]	254
		$CoCl_2$·$6H_2O$ (7 mol %)				45 min[a]	
		$CuCl_2$·$6H_2O$ (7 mol %)				250 min	
		amorphous Cu, Ag, Au nanoparticles				40−60 min	
14	H_3N·BH_3	Cu nanoparticles (15 mol %)	H_2O,	1.1	20	93−100 min	255
	(0.03 M)	Cu@Cu_2O core shell nanoparticles (15 mol %)	MeOH	1.7			
		Cu_2O nanoparticles −(15 mol %)		2.1			
15	H_3N·BH_3 (0.12 M)	Rh on different supports, best on TiO_2, 1 wt %; catalyst loading 0.05 mol %	H_2O	2.7 equiv	40	7 min	256
16	H_3N·BH_3 (1 M)	$Ni_{60}Co_{20}Cu_{20}$/active carbon fiber 10 wt %, and others tested in high throughput screening	H_2O	approx 3	25	40 min	257
17	H_3N·BH_3	Co−Co_2B nanocomposite, 20 mol %	MeOH	3	25	2.5 min	258
	0.75 M	Ni−Ni_3B nanocomposite; 20 mol %		3	25	4.2 min	
18	H_3N·BH_3 (100 mM)	poly(4-styrenesulfonic acid-*co*-maleic acid), stabilized ruthenium(0) and palladium(0) nanoclusters; polymer/metal various ratios, Ru 0.7 mol %, Pd 1 mol %	H_2O	efficiency given in rate constants	25	efficiency given in rate constants	259
19	H_3N·BH_3 (300 mM)	starch stabilized Ni nanoparticles; 0.1 mol %	H_2O	approx 3	20	6 min	260
20	H_3N·BH_3 (100 mM)	poly(*N*-vinyl-2-pyrrolidone) stabilized Co nanoparticles, 1−3 mol %	H_2O	efficiency given in rate constants	various	efficiency given in rate constants	261
21	H_3N·BH_3 (100 mM)	zeolite framework stabilized rhodium(0) nanoclusters; 0.8 mol % Rh	H_2O	approx 3	25	5 min	262
22	H_3N·BH_3 (160 mM)	nickel clusters contained within silica nanospheres (20−30 nm); 1−5 mol %	H_2O	2.9−3 equiv	20	22−75 min	263
23	H_3N·BH_3 (260 mM)	Ru/C; 0.2 mol %	H_2O	approx 3	16−55 25 20	50−3 min 17 min	264
24	H_3N·BH_3 (160 mM)	nickel catalyst stabilized by poly(*N*-vinyl-2-pyrrolidone); $NaBH_4$ as coreductant; 10 mol % Ni	H_2O	2.7	25	9 min	265
25	H_3N·BH_3 (100 mM)	laureate stabilized Ru(0) nanoclusters, 2 mol %	H_2O	approx 3	25	5 min	266
26	H_3N·BH_3 (670 mM)	Co deposited by electroless plating on Ni foam Cu sheet	H_2O, pH = 9	no full conversion measured; 0.43 equiv/10 min; 0.1 equiv/10 min	30	n/a	267
27	H_3N·BH_3 (100 mM)	zeolite confined Cu(0) nanoclusters; 2 mol %	H_2O	approx 3	25	130 min	268
28	H_3N·BH_3 (800 mM)	zeolite confined Rh(0) nanoclusters; 0.08 wt % Rh; other conditions also tested	MeOH	approx 1.8; no full conversion measured	25	50 min	269
29	H_3N·BH_3 (330 mM)	3 wt % Ru on carbon, various particle sizes; 0.2 mol % Ru	H_2O	3	26	10 min	270
30	H_3N·BH_3 (200 mM)	monodisperse Ni nanoparticles, 4 mol % Ni	H_2O	3	25	10 min	271

Table A8 Continued

entry	amine-borane	catalyst	solvent	equiv of H_2 released	T^b/°C	time	ref
31	$H_3N{\cdot}BH_3$ (200 mM)	poly(*N*-vinyl-2-pyrrolidone) (PVP)-stabilized palladium(0) nanoclusters	MeOH	efficiency given in rate constants	various	efficiency given in rate constants	272
32	$H_3N{\cdot}BH_3$ (100 mM)	2 mM intrazeolite cobalt(0) nanoclusters with 0.85 wt % of Co, corresponding to 2 mol %, and various other loadings	H_2O	ca. 2.3	25	33.3 h	273
33	$H_3N{\cdot}BH_3$ (solid)	$CoCl_2$, 2.6 mol %	H_2O (stochiometric)	ca. 2.7	25	15 min	274
34	$H_3N{\cdot}BH_3$ (152 mM)	bimetallic Au−Ni nanoparticles embedded in SiO_2 nanospheres, Au/AB = 0.019, Ni/AB = 0.065	H_2O	ca. 2.9	18	14 min	275
35	$H_3N{\cdot}BH_3$ (0.17 mM)	magnetically recyclable hollow Co−B nanospindles from poly(styrene-*co*-methacrylic acid) and $Co(OAc)_2$ with KBH_4, 5 mg of catalyst to 8.3 mmol of ammonia-borane, metal loading not presented.	H_2O	3	25	30 min	276
36	$H_3N{\cdot}BH_3$ (260 mM)	magnetically recyclable Au@Co core−shell nanoparticles, 2 mol %	H_2O	3	25	11 min	277
37	$H_3N{\cdot}BH_3$ (25 mM)	nanoparticle-assembled Co−B thin film, 10 mg of catalyst for 3.75 mmol of catalyst	H_2O	2.9	25	11 min	278
38	$H_3N{\cdot}BH_3$ (100 mM)	zeolite confined palladium(0) nanoclusters 3 mol %	H_2O	3	25	15 min	279

[a] Excluding an induction period. [b] If the paper gives "room temperature", we give 20 °C.

10. Abbreviations

AB	ammonia-borane
BCDB	*B*-(cyclodiborazanyl)aminoborohydride
CDB	cyclodiborazane
CPMAS	cross-polarization magic angle spinning
CTB	cyclotriborazane
DADB	diammoniate of diborane $[H_2B(NH_3)_2]BH_4$
DFT	density functional theory
DSC	differential scanning calorimetry
DTA	differential thermal analysis
ETP	emission thermophotometry
FT	Fourier transform
GC	gas chromatography
GED	gas phase electron diffraction
HB	hydrazine-monoborane
HBB	hydrazine-bisborane
HFBS	high flux backscattering spectrometer
IINS	inelastic incoherent neutron scattering
INS	inelastic neutron scattering
IR	infrared
IRC	intrinsic reaction coordinate
MAS	magic angle spinning
MOF	metal−organic framework
MS	mass spectrometry
NHE	normal hydrogen electrode
NMR	nuclear magnetic resonance
OCP	open circuit potential
PAB	polyaminoborane
PB	polyborazylene
PEEK	polyether ether ketone
PSA	poly(styrene-co-methacrylic acid)
PXRD	powder X-ray diffraction
SAB	sodium amidoborane
SCE	saturated calomel electrode
SCRF	self-consistent reaction field
SEM-EDX	scanning electron microscope, energy-dispersive X-ray spectroscopy
TEM-SAED	transmission electron microscopy, selective area diffraction
TG	thermogravimetry
TGA	thermogravimetric analysis
TPD	temperature programmed desorption
TS	transition state
WAXS	wide-angle X-ray scattering
XPS	photoelectron X-ray spectroscopy
XRD	X-ray diffraction

11. Appendix: Ammonia-borane—Various Physical Parameters

Various other physical parameters have been measured for ammonia-borane. While they add only incrementally to the understanding of this important molecule, the information may be useful for any given application and will be listed without further comment in Tables A1 and A2.

Besides the many computational studies dealing with the structure of ammonia-borane discussed in the previous section, Dixon and co-workers contributed a high accuracy coupled cluster study on some fundamental thermochemical properties of ammonia-borane and its dehydrogenated congeners.[244] While the discussion of the individual results is beyond the scope of this review, we will give a selection of the (subjectively) most important values in Tables A3−A7.

12. References

(1) Staubitz, A.; Robertson, A. P. M.; Sloan, M. E.; Manners, I. *Chem. Rev.* **2010**, *10*, http://dx.doi.org/10.1021/cr100105a.

(2) (a) Karkamkar, A.; Aardahl, C.; Autrey, T. *Mater. Matters* **2007**, *2*, 6; available at http://www.sigmaaldrich.com/materialsscience/learning-center/material-matters.html. (b) Peng, B.; Chen, J. *Energy Environ. Sci.* **2008**, *1*, 479. (c) Stephens, F. H.; Pons, V.; Baker, R. T. *Dalton Trans.* **2007**, 2613. (d) Smythe, N. C.; Gordon, J. C. *Eur. J. Inorg. Chem.* **2010**, 509.

(3) Shore, S. G.; Parry, R. W. *J. Am. Chem. Soc.* **1955**, *77*, 6084.

(4) Ramachandran, P. V.; Gagare, P. D. *Inorg. Chem.* **2007**, *46*, 7810.

(5) Heldebrant, D. J.; Karkamkar, A.; Linehan, J. C.; Autrey, T. *Energy Environ. Sci.* **2008**, *1*, 156.

(6) Hu, M. G.; Van Paasschen, J. M.; Geanangel, R. A. *J. Inorg. Nucl. Chem.* **1977**, *39*, 2147.

(7) Shore, S. G.; Böddeker, K. W. *Inorg. Chem.* **1964**, *3*, 914.

(8) (a) Mayer, E. *Inorg. Chem.* **1972**, *11*, 866. (b) For computational studies of this reaction, see: (b) McKee, M. L. *J. Phys. Chem.* **1992**,

96, 5380. (c) Nguyen, V. S.; Matus, M. H.; Nguyen, M. T.; Dixon, D. A. *J. Phys. Chem. A* **2008**, *112*, 9946.
(9) Jaska, C. A.; Temple, K.; Lough, A. J.; Manners, I. *J. Am. Chem. Soc.* **2003**, *125*, 9424.
(10) Mayer, E. *Inorg. Chem.* **1973**, *12*, 1954.
(11) Burnett, L. J.; Muller, B. H. *J. Chem. Eng. Data* **1970**, *15*, 154.
(12) Merino, G.; Bakhmutov, V. I.; Vela, A. *J. Phys. Chem. A* **2002**, *106*, 8491.
(13) Hoon, C. F.; Reynhardt, E. C. *J. Phys. C* **1983**, *16*, 6129.
(14) Klooster, W. T.; Koetzle, T. F.; Siegbahn, P. E. M.; Richardson, T. B.; Crabtree, R. H. *J. Am. Chem. Soc.* **1999**, *121*, 6337.
(15) Bowden, M. E.; Gainsford, G. J.; Robinson, W. T. *Aust. J. Chem.* **2007**, *60*, 149.
(16) Filinchuk, Y.; Nevidomskyy, A. H.; Chernyshov, D.; Dmitriev, V. *Phys. Rev. B: Condens. Matter Mater. Phys.* **2009**, *79*, 214111/1.
(17) Hess, N. J.; Bowden, M. E.; Parvanov, V. M.; Mundy, C.; Kathmann, S. M.; Schenter, G. K.; Autrey, T. *J. Chem. Phys.* **2008**, *128*, 034508/1.
(18) Yang, J. B.; Lamsal, J.; Cai, Q.; James, W. J.; Yelon, W. B. *Appl. Phys. Lett.* **2008**, *92*, 091916/1.
(19) Hess, N. J.; Schenter, G. K.; Hartman, M. R.; Daemen, L. L.; Proffen, T.; Kathmann, S. M.; Mundy, C. J.; Hartl, M.; Heldebrant, D. J.; Stowe, A. C.; Autrey, T. *J. Phys. Chem. A* **2009**, *113*, 5723.
(20) Allis, D. G.; Kosmowski, M. E.; Hudson, B. S. *J. Am. Chem. Soc.* **2004**, *126*, 7756.
(21) Thorne, L. R.; Suenram, R. D.; Lovas, F. J. *J. Chem. Phys.* **1983**, *78*, 167.
(22) Smith, J.; Seshadri, K. S.; White, D. *J. Mol. Spectrosc.* **1973**, *45*, 327.
(23) Dillen, J.; Verhoeven, P. *J. Phys. Chem. A* **2003**, *107*, 2570.
(24) Bühl, M.; Steinke, T.; Schleyer, P. v. R.; Boese, R. *Angew. Chem., Int. Ed.* **1991**, *30*, 1160.
(25) Suenram, R. D.; Thorne, L. R. *Chem. Phys. Lett.* **1981**, *78*, 157.
(26) Kathmann, S. M.; Parvanov, V.; Schenter, G. K.; Stowe, A. C.; Daemen, L. L.; Hartl, M.; Linehan, J.; Hess, N. J.; Karkamkar, A.; Autrey, T. *J. Chem. Phys.* **2009**, *130*, 024507/1.
(27) Safford, G. J.; Taylor, T. I.; Rustad, B. M.; Havens, W. W., Jr. *Phys. Rev.* **1960**, *119*, 1291.
(28) If we consider the vibrational spectra of (for simplification) diatomic molecules, the potential energy curve can be described as a first approximation by Hooke's law, where $V(x) = {}^1/_2kx^2$ with $V =$ potential energy, $x =$ distance form equilibrium distance, and $k =$ force constant. However, such a model is unrealistic, as it will not allow dissociation of the molecule, gives equidistant energy levels, and does not adequately allow for internuclear repulsion. A more realistic approach is the use of a Morse potential, where not only the latter is accounted for, but the energy levels move closer and closer together, the higher the energy, and asymptotically approach the dissociation energy. The shape of this potential is not symmetrical with respect to the equilibrium distance but allows for much larger elongations, the closer in energy the system is to the dissociation energy than the harmonic oscillator. Therefore, the larger the anharmonicity of a system, i.e. the higher the anharmonicity constant, the smaller the dissociation energy. See, for example: (a) Wedler, G. *Lehrbuch der Physikalischen Chemie*, 4th ed.; Wiley VCH: 1997; or (b) Yadav, M. S. *A Textbook of Spectroscopy*, 2nd ed.; J. L. Kumar for Anmol Publications Pvt. Ltd.: New Delhi, 2003.
(29) Brown, C. M.; Jacques, T. L.; Hess, N. J.; Daemen, L. L.; Mamontov, E.; Linehan, J. C.; Stowe, A. C.; Autrey, T. *Physica B* **2006**, *385−386*, 266.
(30) Bée, M. *Chem. Phys.* **2003**, *292*, 121.
(31) Reynhardt, E. C.; Hoon, C. F. *J. Phys. C* **1983**, *16*, 6137.
(32) Penner, G. H.; Chang, Y. C. P.; Hutzal, J. *Inorg. Chem.* **1999**, *38*, 2868.
(33) Taylor, R. C.; Cluff, C. L. *Nature* **1958**, *182*, 390.
(34) Taylor, R. C. *Adv. Chem. Ser.* **1964**, *42*, 59.
(35) Rice, B.; Galiano, R. J.; Lehmann, W. J. *J. Phys. Chem.* **1957**, *61*, 1222.
(36) Goubeau, J.; Ricker, E. *Z. Anorg. Allg. Chem.* **1961**, *310*, 123.
(37) Clague, A. D. H.; Danti, A. *Spectrochim. Acta, Part A* **1967**, *23*, 2359.
(38) (a) Dunkin, I. R. *Chem. Soc. Rev.* **1980**, *9*, 1. (b) Hermann, T. S. *Appl. Spectrosc.* **1969**, *23*, 461. (c) Wehry, E. L.; Mamantov, G. *Anal. Chem.* **1979**, *51*, 643A.
(39) Trudel, S.; Gilson, D. F. R. *Inorg. Chem.* **2003**, *42*, 2814.
(40) Custelcean, R.; Dreger, Z. A. *J. Phys. Chem. B* **2003**, *107*, 9231.
(41) Taylor, R. C.; Gabelnick, H. S.; Aida, K.; Amster, R. L. *Inorg. Chem.* **1969**, *8*, 605.
(42) Nxumalo, L. M.; Andrzejak, M.; Ford, T. A. *Vib. Spectrosc.* **1996**, *12*, 221.
(43) Lin, Y.; Mao, W. L.; Drozd, V.; Chen, J.; Daemen, L. L. *J. Chem. Phys.* **2008**, *129*, 234509/1.
(44) Chellappa, R. S.; Somayazulu, M.; Struzhkin, V. V.; Autrey, T.; Hemley, R. J. *J. Chem. Phys.* **2009**, *131*, 224515/1.
(45) Cho, H.; Shaw, W. J.; Parvanov, V.; Schenter, G. K.; Karkamkar, A.; Hess, N. J.; Mundy, C.; Kathmann, S.; Sears, J.; Lipton, A. S.; Ellis, P. D.; Autrey, S. T. *J. Phys. Chem. A* **2008**, *112*, 4277.
(46) Gervais, C.; Babonneau, F.; Maquet, J.; Bonhomme, C.; Massiot, D.; Framery, E.; Vaultier, M. *Magn. Reson. Chem.* **1998**, *36*, 407.
(47) Gunaydin-Sen, O.; Achey, R.; Dalal, N. S.; Stowe, A.; Autrey, T. *J. Phys. Chem. B* **2007**, *111*, 677.
(48) Yannoni, C. S. *Acc. Chem. Res.* **1982**, *15*, 201.
(49) Paolone, A.; Palumbo, O.; Rispoli, P.; Cantelli, R.; Autrey, T. *J. Phys. Chem. C* **2009**, *113*, 5872.
(50) Wolf, G.; van Miltenburg, J. C.; Wolf, U. *Thermochim. Acta* **1998**, *317*, 111.
(51) Morrison, C. A.; Siddick, M. M. *Angew. Chem., Int. Ed.* **2004**, *43*, 4780.
(52) (a) Cramer, C. J.; Gladfelter, W. L. *Inorg. Chem.* **1997**, *36*, 5358. (b) Kulkarni, S. A. *J. Phys. Chem.* **1998**, *102*, 7704. (c) Li, J.; Zhao, F.; Jing, F. *J. Chem. Phys.* **2002**, *116*, 25. (d) Richardson, T.; de Gala, S.; Crabtree, R. H.; Siegbahn, P. E. M. *J. Am. Chem. Soc.* **1995**, *117*, 12875. (e) Popelier, P. L. A. *J. Phys. Chem. A* **1998**, *102*, 1873. (f) Meng, Y.; Zhou, Z.; Duan, C.; Wang, B.; Zhong, Q. *THEOCHEM* **2005**, *713*, 135.
(53) Mo, Y.; Song, L.; Wu, W.; Zhang, Q. *J. Am. Chem. Soc.* **2004**, *126*, 3974.
(54) [http://www1.eere.energy.gov/vehiclesandfuels/pdfs/program/hydrogen_storage_roadmap.pdf.].
(55) IOR energy http://www.ior.com.au/ecflist.html retrieved May 10th, 2010.
(56) Graetz, J. *Chem. Soc. Rev.* **2009**, *38*, 73.
(57) Hamilton, C. W.; Baker, R. T.; Staubitz, A.; Manners, I. *Chem. Soc. Rev.* **2009**, *38*, 279.
(58) For some recent reviews of materials other than ammonia-borane, see: (a) Wu, H. *ChemPhysChem* **2008**, *9*, 2157. (b) Gregory, D. H. *J. Mater. Chem.* **2008**, *18*, 2321. (c) Sakintuna, B.; Lamari-Darkrim, F.; Hirscher, M. *Int. J. Hydrogen Energy* **2007**, *32*, 1121. (d) Bououdina, M.; Grant, D.; Walker, G. *Int. J. Hydrogen Energy* **2006**, *31*, 177.
(59) Marder, T. B. *Angew. Chem., Int. Ed.* **2007**, *46*, 8116.
(60) (a) Chen, P.; Zhu, M. *Mater. Today* **2008**, *11* (12), 36. (b) Irvine, J. *J. Mater. Chem.* **2008**, *18*, 2295. (c) Felderhoff, M.; Weidenthaler, C.; von Helmolt, R.; Eberle, U. *Phys. Chem. Chem. Phys.* **2007**, *9*, 2643. (d) Sigma-Aldrich "*Mater. Matters*" special issue 2007, Volume 2, Number 2, http://www.scribd.com/doc/12703635/Hydrogen-Storage-Materials-Material-Matters-v2n2-.
(61) Wise, S. S.; Margrave, J. L.; Feder, H. M.; Hubbard, W. N. *J. Phys. Chem.* **1966**, *70*, 7.
(62) Hu, M. G.; Geanangel, R. A.; Wendlandt, W. W. *Thermochim. Acta* **1978**, *23*, 249.
(63) Sit, V.; Geanangel, R. A.; Wendlandt, W. W. *Thermochim. Acta* **1987**, *113*, 379.
(64) Geanangel, R. A.; Rabalais, J. W. *Inorg. Chim. Acta* **1985**, *97*, 59.
(65) Wolf, G.; Baumann, J.; Baitalow, F.; Hoffmann, F. P. *Thermochim. Acta* **2000**, *343*, 19.
(66) Baitalow, F.; Baumann, J.; Wolf, G.; Jaenicke-Rö*β*ler, K.; Leitner, G. *Thermochim. Acta* **2002**, *391*, 159.
(67) Rassat, S. D.; Aardahl, C. L.; Autrey, T.; Smith, R. S. *Energy Fuels* **2010**, *24*, 2596.
(68) (a) A good indication of whether pure boron nitride has been obtained is the IR spectrum: Often, authors cite WAXS data as proof, where BN can indeed be identified, but impurities, where some N−H bonds remain, may not be visible. They can be identified by a prominent N−H stretch band around 3100−3400 cm^{-1}. (b) *Gmelin Handbuch der Anorganischen Chemie, Boron Nitride. B−N−C Heterocylces. Polymeric B−N Compound*; Springer-Verlag: New York, 1974. (c) K. A. Schwetz, A. L. *Ullmann's Encyclopedia of Industrial Chemistry*; VCH: Deerfield Beach, 1985. (d) Kim, D.-P.; Moon, K.-T.; Kho, J.-G.; Economy, J.; Gervais, C.; Babonneau, F. *Polym. Adv. Technol.* **1999**, *10*, 702.
(69) Carpenter, J. D.; Ault, B. S. *Chem. Phys. Lett.* **1992**, *197*, 171.
(70) Kuznesof, P. M.; Shriver, D. F.; Stafford, F. E. *J. Am. Chem. Soc.* **1968**, *90*, 2557.
(71) Mohajeri, N.; T-Raissi, A.; Ramasamy, K. K. *Thermochim. Acta* **2007**, *452*, 28.
(72) Geanangel, R. A.; Wendlandt, W. W. *Thermochim. Acta* **1985**, *86*, 375.
(73) The thermal dehydrogenation of borazine to form boron nitride has elicited considerable interest due to the material properties of boron nitride. While this expands the chemical knowledge of formally the third dehydrogenation step of ammonia-borane, this is of no interest for hydrogen storage purposes, as, firstly, borazine is a fuel cell poison and, secondly, formation of boron nitride as a thermodynamically extremely stable product makes recycling impossible. Readers who

are interested in this aspect of ammonia-borane chemistry are referred to, for example: (a) Laubengayer, A. W.; Moews, P. C., Jr.; Porter, R. F. *J. Am. Chem. Soc.* **1961**, *83*, 1337. (b) Fazen, P. J.; Beck, J. S.; Lynch, A. T.; Remsen, E. E.; Sneddon, L. G. *Chem. Mater.* **1990**, *2*, 96. (c) Fazen, P. J.; Remsen, E. E.; Beck, J. S.; Carroll, P. J.; McGhie, A. R.; Sneddon, L. G. *Chem. Mater.* **1995**, *7*, 1942.

(74) Baumann, J.; Baitalow, F.; Wolf, G. *Thermochim. Acta* **2005**, *430*, 9.
(75) Stowe, A. C.; Shaw, W. J.; Linehan, J. C.; Schmid, B.; Autrey, T. *Phys. Chem. Chem. Phys.* **2007**, *9*, 1831.
(76) Bowden, M.; Autrey, T.; Brown, I.; Ryan, M. *Curr. Appl. Phys.* **2008**, *8*, 498.
(77) Heldebrant, D. J.; Karkamkar, A.; Hess, N. J.; Bowden, M.; Rassat, S.; Zheng, F.; Rappe, K.; Autrey, T. *Chem. Mater.* **2008**, *20*, 5332.
(78) Geanangel, R. A.; Wendlandt, W. W. *Thermochim. Acta* **1987**, *113*, 383.
(79) Price, F. P. *J. Am. Chem. Soc.* **1951**, *73*, 2141.
(80) Baitalow, F.; Wolf, G.; Grolier, J. P. E.; Dan, F.; Randzio, S. L. *Thermochim. Acta* **2006**, *445*, 121.
(81) Nylén, J.; Sato, T.; Soignard, E.; Yarger, J. L.; Stoyanov, E.; Häussermann, U. *J. Chem. Phys.* **2009**, *131*, 104506/1.
(82) Wang, S.; Mao, W. L.; Autrey, T. *J. Chem. Phys.* **2009**, *131*, 144508/1.
(83) Palumbo, O.; Paolone, A.; Rispoli, P.; Cantelli, R.; Autrey, T. *J. Power Sources* **2010**, *195*, 1615.
(84) Wang, J. S.; Geanangel, R. A. *Inorg. Chim. Acta* **1988**, *148*, 185.
(85) Shaw, W. J.; Linehan, J. C.; Szymczak, N. K.; Heldebrant, D. J.; Yonker, C.; Camaioni, D. M.; Baker, R. T.; Autrey, T. *Angew. Chem., Int. Ed.* **2008**, *47*, 7493.
(86) Schellenberg, R.; Kriehme, J.; Wolf, G. *Thermochim. Acta* **2007**, *457*, 103.
(87) Himmel, H. J.; Schnöckel, H. *Chem.—Eur. J.* **2002**, *8*, 2397.
(88) Dixon, D. A.; Gutowski, M. *J. Phys. Chem. A* **2005**, *109*, 5129.
(89) Sana, M.; Leroy, G. *Int. J. Quantum Chem.* **1993**, *48*, 89.
(90) (a) Li, Q. S.; Zhang, J.; Zhang, S. *Chem. Phys. Lett.* **2005**, *404*, 100. (b) Zhang, J.; Zhang, S.; Li, Q. S. *THEOCHEM* **2005**, *717*, 33.
(91) Nguyen, M. T.; Nguyen, V. S.; Matus, M. H.; Gopakumar, G.; Dixon, D. A. *J. Phys. Chem. A* **2007**, *111*, 679.
(92) Weismiller, M. R.; van Duin, A. C. T.; Lee, J.; Yetter, R. A. *J. Phys. Chem. A* **2010**, *114*, 5485.
(93) Zimmerman, P. M.; Paul, A.; Zhang, Z.; Musgrave, C. B. *Inorg. Chem.* **2009**, *48*, 1069.
(94) Pons, V.; Baker, R. T.; Szymczak, N. K.; Heldebrant, D. J.; Linehan, J. C.; Matus, M. H.; Grant, D. J.; Dixon, D. A. *Chem. Commun.* **2008**, 6597.
(95) Nguyen, V. S.; Matus, M. H.; Grant, D. J.; Nguyen, M. T.; Dixon, D. A. *J. Phys. Chem. A* **2007**, *111*, 8844.
(96) Miranda, C. R.; Ceder, G. *J. Chem. Phys.* **2007**, *126*, 184703/1.
(97) Jaska, C. A.; Temple, K.; Lough, A. J.; Manners, I. *Chem. Commun.* **2001**, 962.
(98) Denney, M. C.; Pons, V.; Hebden, T. J.; Heinekey, D. M.; Goldberg, K. I. *J. Am. Chem. Soc.* **2006**, *128*, 12048.
(99) Göttker-Schnetmann, I.; White, P.; Brookhart, M. *J. Am. Chem. Soc.* **2004**, *126*, 1804.
(100) Böddeker, K. W.; Shore, S. G.; Bunting, R. K. *J. Am. Chem. Soc.* **1966**, *88*, 4396.
(101) Hebden, T. J.; Denney, M. C.; Pons, V.; Piccoli, P. M. B.; Koetzle, T. F.; Schultz, A. J.; Kaminsky, W.; Goldberg, K. I.; Heinekey, D. M. *J. Am. Chem. Soc.* **2008**, *130*, 10812.
(102) Paul, A.; Musgrave, C. B. *Angew. Chem., Int. Ed.* **2007**, *46*, 8153.
(103) Keaton, R. J.; Blacquiere, J. M.; Baker, R. T. *J. Am. Chem. Soc.* **2007**, *129*, 1844.
(104) (a) Yang, X.; Hall, M. B. *J. Am. Chem. Soc.* **2008**, *130*, 1798. (b) Zimmerman, P. M.; Paul, A.; Zhang, Z.; Musgrave, C. B. *Angew. Chem., Int. Ed.* **2009**, *48*, 2201. (c) Zimmerman, P. M.; Paul, A.; Musgrave, C. B. *Inorg. Chem.* **2009**, *48*, 5418.
(105) Blaquiere, N.; Diallo-Garcia, S.; Gorelsky, S. I.; Black, D. A.; Fagnou, K. *J. Am. Chem. Soc.* **2008**, *130*, 14034.
(106) Käss, M.; Friedrich, A.; Drees, M.; Schneider, S. *Angew. Chem., Int. Ed.* **2009**, *48*, 905.
(107) (a) Li, T.; Churlaud, R.; Lough, A. J.; Abdur-Rashid, K.; Morris, R. H. *Organometallics* **2004**, *23*, 6239. (b) Clapham, S. E.; Hadzovic, A.; Morris, R. H. *Coord. Chem. Rev.* **2004**, *248*, 2201. (c) Abdur-Rashid, K.; Clapham, S. E.; Hadzovic, A.; Harvey, J. N.; Lough, A. J.; Morris, R. H. *J. Am. Chem. Soc.* **2002**, *124*, 15104.
(108) Stephens, F. H.; Baker, R. T.; Matus, M. H.; Grant, D. J.; Dixon, D. A. *Angew. Chem., Int. Ed.* **2007**, *46*, 746.
(109) Miller, A. J. M.; Bercaw, J. E. *Chem. Commun.* **2010**, *46*, 1709.
(110) (a) Stephan, D. W. *Dalton Trans.* **2009**, 3129. (b) Stephan, D. W. *Org. Biomol. Chem.* **2008**, *6*, 1535. (c) Power, P. P. *Nature* **2010**, *463*, 171. (d) Stephan, D. W.; Erker, G. *Angew. Chem., Int. Ed.* **2010**, *49*, 46.
(111) Guo, Y.; He, X.; Li, Z.; Zou, Z. *Inorg. Chem.* **2010**, *49*, 3419.
(112) Vajo, J. J.; Olson, G. L. *Scr. Mater.* **2007**, *56*, 829.
(113) Dornheim, M.; Eigen, N.; Barkhordarian, G.; Klassen, T.; Bormann, R. *Adv. Eng. Mater.* **2006**, *8*, 377.
(114) Huot, J.; Liang, G.; Schulz, R. *Appl. Phys. A: Mater. Sci. Process.* **2001**, *72*, 187.
(115) Gutowska, A.; Li, L.; Shin, Y.; Wang, C. M.; Li, X. S.; Linehan, J. C.; Smith, R. S.; Kay, B. D.; Schmid, B.; Shaw, W.; Gutowski, M.; Autrey, T. *Angew. Chem., Int. Ed.* **2005**, *44*, 3578.
(116) Feaver, A.; Sepehri, S.; Shamberger, P.; Stowe, A.; Autrey, T.; Cao, G. *J. Phys. Chem. B* **2007**, *111*, 7469.
(117) Wang, L.-Q.; Karkamkar, A.; Autrey, T.; Exarhos, G. J. *J. Phys. Chem. C* **2009**, *113*, 6485.
(118) Paolone, A.; Palumbo, O.; Rispoli, P.; Cantelli, R.; Autrey, T.; Karkamkar, A. *J. Phys. Chem. C* **2009**, *113*, 10319.
(119) Kim, H.; Karkamkar, A.; Autrey, T.; Chupas, P.; Proffen, T. *J. Am. Chem. Soc.* **2009**, *131*, 13749.
(120) Sepehri, S.; Feaver, A.; Shaw, W. J.; Howard, C. J.; Zhang, Q.; Autrey, T.; Cao, G. *J. Phys. Chem. B* **2007**, *111*, 14285.
(121) Servoss, R. R.; Clark, H. M. *J. Chem. Phys.* **1957**, *26*, 1179.
(122) Sepehri, S.; García, B. B.; Zhang, Q.; Cao, G. *Carbon* **2009**, *47*, 1436.
(123) Sepehri, S.; García, B. B.; Cao, G. *Eur. J. Inorg. Chem.* **2009**, 599.
(124) Li, Z.; Zhu, G.; Lu, G.; Qiu, S.; Yao, X. *J. Am. Chem. Soc.* **2010**, *132*, 1490.
(125) Zhao, J.; Shi, J.; Zhang, X.; Cheng, F.; Liang, J.; Tao, Z.; Chen, J. *Adv. Mater.* **2010**, *22*, 394.
(126) Perut, C.; Gauthier, C. SNPE, Fr. Application: FR, FR, 2003.
(127) Hélary, J.; Salandre, N.; Saillard, J.; Poullain, D.; Beaucamp, A.; Autissier, D. *Int. J. Hydrogen Energy* **2009**, *34*, 169.
(128) Kalidindi, S. B.; Joseph, J.; Jagirdar, B. R. *Energy Environ. Sci.* **2009**, *2*, 1274.
(129) Xiong, Z.; Chua, Y.; Wu, G.; Wang, L.; Wong, M. W.; Kam, Z. M.; Autrey, T.; Kemmitt, T.; Chen, P. *Dalton Trans.* **2010**, *39*, 720.
(130) Graham, K. R.; Kemmitt, T.; Bowden, M. E. *Energy Environ. Sci.* **2009**, *2*, 706.
(131) Bluhm, M. E.; Bradley, M. G.; Butterick, R., III; Kusari, U.; Sneddon, L. G. *J. Am. Chem. Soc.* **2006**, *128*, 7748.
(132) Neiner, D.; Karkamkar, A.; Linehan, J. C.; Arey, B.; Autrey, T.; Kauzlarich, S. M. *J. Phys. Chem. C* **2009**, *113*, 1098.
(133) De Benedetto, S.; Carewska, M.; Cento, C.; Gislon, P.; Pasquali, M.; Scaccia, S.; Prosini, P. P. *Thermochim. Acta* **2006**, *441*, 184.
(134) Bluhm, M. E.; Bradley, M. G.; Sneddon, L. G. *Prepr. Symp.—Am. Chem. Soc., Div. Fuel Chem.* **2006**, *51*, 571.
(135) Diyabalanage, H. V. K.; Shrestha, R. P.; Semelsberger, T. A.; Scott, B. L.; Bowden, M. E.; Davis, B. L.; Burrell, A. K. *Angew. Chem., Int. Ed.* **2007**, *46*, 8995.
(136) Schlesinger, H. I.; Burg, A. B. *J. Am. Chem. Soc.* **1938**, *60*, 290.
(137) Xiong, Z.; Yong, C. K.; Wu, G.; Chen, P.; Shaw, W.; Karkamkar, A.; Autrey, T.; Jones, M. O.; Johnson, S. R.; Edwards, P. P.; David, W. I. F. *Nat. Mater.* **2008**, *7*, 138.
(138) Addition of 10% $LiNH_2$ to AB was observed to lower the dehydrogenation temperature and increase the hydrogen yield by Sneddon and co-workers, which was published as a preliminary result in: *New Methods for Promoting Amineborane Dehydrogenation/Regeneration Reactions*; Sneddon, L. G., Ed.; DoE Hydrogen Program, FY, Annual Progress Report, Section IV.B.4g; 2006; p 418.
(139) Xiong, Z.; Wu, G.; Chua, Y. S.; Hu, J.; He, T.; Xu, W.; Chen, P. *Energy Environ. Sci.* **2008**, *1*, 360.
(140) Ramzan, M.; Silvearv, F.; Blomqvist, A.; Scheicher, R. H.; Lebègue, S.; Ahuja, R. *Phys. Rev. B* **2009**, *79*, 132102/1.
(141) Fijalkowski, K. J.; Grochala, W. *J. Mater. Chem.* **2009**, *19*, 2043.
(142) Kang, X.; Fang, Z.; Kong, L.; Cheng, H.; Yao, X.; Lu, G.; Wang, P. *Adv. Mater.* **2008**, *20*, 2756.
(143) Xiong, Z.; Chua, Y. S.; Wu, G.; Xu, W.; Chen, P.; Shaw, W.; Karkamkar, A.; Linehan, J.; Smurthwaite, T.; Autrey, T. *Chem. Commun.* **2008**, 5595.
(144) Wu, C.; Wu, G.; Xiong, Z.; David, W. I. F.; Ryan, K. R.; Jones, M. O.; Edwards, P. P.; Chu, H.; Chen, P. *Inorg. Chem.* **2010**, *49*, 4319.
(145) Li, L.; Yao, X.; Sun, C.; Du, A.; Cheng, L.; Zhu, Z.; Yu, C.; Zou, J.; Smith, S. C.; Wang, P.; Cheng, H.-M.; Frost, R. L.; Lu, G. Q. *Adv. Funct. Mater.* **2009**, *19*, 265.
(146) Lee, T. B.; McKee, M. L. *Inorg. Chem.* **2009**, *48*, 7564.
(147) Kim, D. Y.; Singh, N. J.; Lee, H. M.; Kim, K. S. *Chem.—Eur. J.* **2009**, *15*, 5598.
(148) Kang, X.; Ma, L.; Fang, Z.; Gao, L.; Luo, J.; Wang, S.; Wang, P. *Phys. Chem. Chem. Phys.* **2009**, *11*, 2507.
(149) Wu, H.; Zhou, W.; Yildirim, T. *J. Am. Chem. Soc.* **2008**, *130*, 14834.
(150) Armstrong, D. R.; Perkins, P. G.; Walker, G. T. *THEOCHEM* **1985**, *122*, 189.
(151) Spielmann, J.; Jansen, G.; Bandmann, H.; Harder, S. *Angew. Chem., Int. Ed.* **2008**, *47*, 6290.
(152) Spielmann, J.; Harder, S. *J. Am. Chem. Soc.* **2009**, *131*, 5064.

(153) Spielmann, J.; Bolte, M.; Harder, S. *Chem. Commun.* **2009**, 6934.
(154) Zhang, Q.; Tang, C.; Fang, C.; Fang, F.; Sun, D.; Ouyang, L.; Zhu, M. *J. Phys. Chem. C* **2010**, *114*, 1709.
(155) Dou, D.; Ketchum, D. R.; Hamilton, E. J. M.; Florian, P. A.; Vermillion, K. E.; Grandinetti, P. J.; Shore, S. G. *Chem. Mater.* **1996**, *8*, 2839.
(156) Himmelberger, D. W.; Yoon, C. W.; Bluhm, M. E.; Carroll, P. J.; Sneddon, L. G. *J. Am. Chem. Soc.* **2009**, *131*, 14101.
(157) Couturier, M.; Tucker, J. L.; Andresen, B. M.; Dubé, P.; Brenek, S. J.; Negri, J. T. *Tetrahedron Lett.* **2001**, *42*, 2285.
(158) Chandra, M.; Xu, Q. *J. Power Sources* **2006**, *156*, 190.
(159) (a) Xu, Q.; Chandra, M. *J. Alloys Compd.* **2007**, *446*−*447*, 729. (b) Wang, P.; Kang, X.-D. *Dalton Trans.* **2008**, 5400. (c) Umegaki, T.; Yan, J.-M.; Zhang, X.-B.; Shioyama, H.; Kuriyama, N.; Xu, Q. *Int. J. Hydrogen Energy* **2009**, *34*, 2303.
(160) Özkar, S. *Appl. Surf. Sci.* **2009**, *256*, 1272.
(161) Cheng, F.; Ma, H.; Li, Y.; Chen, J. *Inorg. Chem.* **2007**, *46*, 788.
(162) Yan, J.-M.; Zhang, X.-B.; Han, S.; Shioyama, H.; Xu, Q. *Angew. Chem., Int. Ed.* **2008**, *47*, 2287.
(163) Diwan, M.; Diakov, V.; Shafirovich, E.; Varma, A. *Int. J. Hydrogen Energy* **2008**, *33*, 1135.
(164) Diwan, M.; Hanna, D.; Varma, A. *Int. J. Hydrogen Energy* **2010**, *35*, 577.
(165) Zhang, X.-B.; Han, S.; Yan, J.-M.; Chandra, M.; Shioyarna, H.; Yasuda, K.; Kuriyama, N.; Kobayashi, T.; Xu, Q. *J. Power Sources* **2007**, *168*, 167.
(166) Li, Z. P.; Morigazaki, N.; Liu, B. H.; Suda, S. *J. Alloys Compd.* **2003**, *349*, 232.
(167) Zhang, X.-B.; Yan, J.-M.; Han, S.; Shioyama, H.; Yasuda, K.; Kuriyama, N.; Xu, Q. *J. Power Sources* **2008**, *182*, 515.
(168) Weidner, J. W.; Sethuraman, V. A.; Van Zee, J. W. *Electrochem. Soc. Interface* **2003**, *Winter 2003*, 40.
(169) Zhang, X.-B.; Han, S.; Yan, J.-M.; Shioyama, H.; Kuriyama, N.; Kobayashi, T.; Xu, Q. *Int. J. Hydrogen Energy* **2009**, *34*, 174.
(170) (a) Conway, B. E.; Barber, J. H.; Gao, L.; Qian, S. Y. *J. Alloys Compd.* **1997**, *253*, 475. (b) Gyenge, E. *Electrochim. Acta* **2004**, *49*, 965 and 1875.
(171) Zhang, X.-B.; Yan, J.-M.; Han, S.; Shioyama, H.; Xu, Q. *J. Am. Chem. Soc.* **2009**, *131*, 2778.
(172) Volkov, V. V.; Myakishev, K. G. *Izv. Sib. Otd. Akad. Nauk SSSR, Ser. Khim. Nauk* **1988**, 140.
(173) Jaska, C. A.; Dorn, H.; Lough, A. J.; Manners, I. *Chem.*−*Eur. J.* **2003**, *9*, 271.
(174) Burg, A. B.; Randolph, C. L., Jr. *J. Am. Chem. Soc.* **1949**, *71*, 3451.
(175) Gaines, D. F.; Coons, D. E. *Inorg. Chem.* **1986**, *25*, 364.
(176) Köster, R.; Binger, P.; Dahlhoff, W. V. *Synth. React. Inorg. Met.-Org. Chem.* **1973**, *3*, 359.
(177) Bowden, M. E.; Brown, I. W. M.; Gainsford, G. J.; Wong, H. *Inorg. Chim. Acta* **2008**, *361*, 2147.
(178) Aldridge, S.; Downs, A. J.; Tang, C. Y.; Parsons, S.; Clarke, M. C.; Johnstone, R. D. L.; Robertson, H. E.; Rankin, D. W. H.; Wann, D. A. *J. Am. Chem. Soc.* **2009**, *131*, 2231.
(179) Haaland, A. *Angew. Chem., Int. Ed.* **1989**, *28*, 992.
(180) McCoy, R. E.; Bauer, S. H. *J. Am. Chem. Soc.* **1956**, *78*, 2061.
(181) Burg, A. B.; Fu, Y.-C. *J. Am. Chem. Soc.* **1966**, *88*, 1147.
(182) Smith, B. J.; Radom, L. *J. Phys. Chem.* **1995**, *99*, 6468.
(183) For a variety of values for these amine-boranes at different temperatures/pressures, see: Schlesinger, H. I.; Ritter, D. M.; Burg, A. B. *J. Am. Chem. Soc.* **1938**, *60*, 1296.
(184) Bauer, S. H. *J. Am. Chem. Soc.* **1937**, *59*, 1804.
(185) Durig, J. R.; Li, Y. S.; Odom, J. D. *THEOCHEM* **1973**, *16*, 443.
(186) Cassoux, P.; Kuczkowski, R. L.; Bryan, P. S.; Taylor, R. C. *Inorg. Chem.* **1975**, *14*, 126.
(187) Iijima, K.; Adachi, N.; Shibata, S. *Bull. Chem. Soc. Jpn.* **1984**, *57*, 3269.
(188) Nöth, H.; Beyer, H. *Chem. Ber.* **1960**, *93*, 939.
(189) Bax, C. M.; Katritzky, A. R.; Sutton, L. E. *J. Chem. Soc.* **1958**, 1258.
(190) Alton, E. R.; Brown, R. D.; Carter, J. C.; Taylor, R. C. *J. Am. Chem. Soc.* **1959**, *81*, 3550.
(191) Beachley, O. T., Jr. *Inorg. Chem.* **1967**, *6*, 870.
(192) Shore, S. G.; Hickam, C. W., Jr.; Cowles, D. *J. Am. Chem. Soc.* **1965**, *87*, 2755.
(193) Staubitz, A.; Soto, A. P.; Manners, I. *Angew. Chem., Int. Ed.* **2008**, *47*, 6212.
(194) Framery, E.; Vaultier, M. *Heteroat. Chem.* **2000**, *11*, 218.
(195) Ryschkewitsch, G. E.; Wiggins, J. W. *Inorg. Chem.* **1970**, *9*, 314.
(196) Grant, D. J.; Matus, M. H.; Anderson, K. D.; Camaioni, D. M.; Neufeldt, S. R.; Lane, C. F.; Dixon, D. A. *J. Phys. Chem. A* **2009**, *113*, 6121.
(197) (a) Shevlin, S. A.; Guo, Z. X. *Chem. Soc. Rev.* **2009**, *38*, 211. (b) Eigen, N.; Keller, C.; Dornheim, M.; Klassen, T.; Bormann, R. *Scr. Mater.* **2007**, *56*, 847. (c) Schüth, F.; Bogdanovič, B.; Felderhoff, M. *Chem. Commun.* **2004**, *20*, 2249. (d) Güther, V.; Otto, A. *J. Alloys Compd.* **1999**, *293*−*295*, 889.
(198) (a) Demirci, U. B.; Miele, P. *Energy Environ. Sci.* **2009**, *2*, 627. (b) Soloveichik, G. L. *Mater. Matters* **2007**, *2*, 11.
(199) Yoon, C. W.; Sneddon, L. G. *J. Am. Chem. Soc.* **2006**, *128*, 13992.
(200) (a) Ryschkewitsch, G. E.; Nainan, K. C. *Inorg. Synth.* **1974**, *15*, 113. (b) Nainan, K. C.; Ryschkewitsch, G. E. *Inorg. Nucl. Chem. Lett.* **1970**, *6*, 765.
(201) Kodama, G.; Parry, R. W.; Carter, J. C. *J. Am. Chem. Soc.* **1959**, *81*, 3534.
(202) Nordman, C. E.; Reimann, C. *J. Am. Chem. Soc.* **1959**, *81*, 3538.
(203) Westrum, E. F., Jr.; Levitin, N. E. *J. Am. Chem. Soc.* **1959**, *81*, 3544.
(204) Yoon, C. W.; Carroll, P. J.; Sneddon, L. G. *J. Am. Chem. Soc.* **2009**, *131*, 855.
(205) Mebel, A. M.; Musaev, D. G.; Morokuma, K. *Chem. Phys. Lett.* **1993**, *214*, 69.
(206) McKee, M. L. *Inorg. Chem.* **1988**, *27*, 4241.
(207) Brown, L. D.; Lipscomb, W. N. *Inorg. Chem.* **1977**, *16*, 1.
(208) Dodds, A. R.; Kodama, G. *Inorg. Chem.* **1976**, *15*, 741.
(209) DePoy, R. E.; Kodama, G. *Inorg. Chem.* **1988**, *27*, 4077.
(210) Subotnik, J. E.; Sodt, A.; Head-Gordon, M. *Phys. Chem. Chem. Phys.* **2007**, *9*, 5522.
(211) Lipscomb, W. N. *Acc. Chem. Res.* **1973**, *6*, 257.
(212) Sundberg, M. R.; Sanchez-Gonzalez, A. *Inorg. Chem. Commun.* **2007**, *10*, 1229.
(213) Es-sofi, A.; Serrar, C.; Ouassas, A.; Jarid, A.; Boutalib, A.; Nebot-Gil, I.; Tomás, F. *J. Phys. Chem. A* **2002**, *106*, 9065.
(214) Nguyen, V. S.; Matus, M. H.; Nguyen, M. T.; Dixon, D. A. *J. Phys. Chem. C* **2007**, *111*, 9603.
(215) Gunderloy, F. C., Jr. *Inorg. Chem.* **1963**, *2*, 221.
(216) Gunderloy, F. C., Jr. *Inorg. Synth.* **1967**, *9*, 13.
(217) Goubeau, J. *Adv. Chem. Ser.* **1964**, *42*, 87.
(218) Hanousek, F.; Haruda, F. *Collect. Czech. Chem. Commun.* **1973**, *38*, 2692.
(219) Rasul, G.; Prakash, G. K. S.; Olah, G. A. *Inorg. Chem.* **1999**, *38*, 5876.
(220) Andrianov, V. I.; Atovmyan, L. O.; Golovina, N. I.; Klitskaya, G. A. *Zh. Strukt. Khim.* **1967**, *8*, 303.
(221) Hügle, T.; Kühnel, M. F.; Lentz, D. *J. Am. Chem. Soc.* **2009**, *131*, 7444.
(222) Zhigach, A. F.; Zakharov, V. V.; Manelis, G. B.; Nechiporenko, G. N.; Nikitin, V. S.; Esel'son, B. M. *Zh. Neorg. Khim.* **1973**, *18*, 1762.
(223) Nguyen, V.-S.; Swinnen, S.; Matus, M. H.; Nguyen, M. T.; Dixon, D. A. *Phys. Chem. Chem. Phys.* **2009**, *11*, 6339.
(224) Groshens, T. J.; Hollins, R. A. *Chem. Commun.* **2009**, 3089.
(225) Titov, L. V.; Levicheva, M. D.; Dubikhina, G. N. *Zh. Neorg. Khim.* **1972**, *17*, 1181.
(226) Titov, L. V.; Levicheva, M. D. *Zh. Neorg. Khim.* **1969**, *14*, 2886.
(227) Kirpichev, E. P.; Rubtsov, Y. I.; Titov, L. V.; Levicheva, M. D. *Zh. Neorg. Khim.* **1971**, *16*, 56.
(228) Titov, L. V.; Makarova, M. D.; Rosolovskii, V. Y. *Dokl. Akad. Nauk SSSR* **1968**, *180*, 381.
(229) Parry, R. W.; Schultz, D. R.; Girardot, P. R. *J. Am. Chem. Soc.* **1958**, *80*, 1.
(230) Karkamkar, A.; Kathmann, S. M.; Schenter, G. K.; Heldebrant, D. J.; Hess, N.; Gutowski, M.; Autrey, T. *Chem. Mater.* **2009**, *21*, 4356.
(231) Taylor, R. C.; Schultz, D. R.; Emery, A. R. *J. Am. Chem. Soc.* **1958**, *80*, 27.
(232) (a) Baranov, L. Y.; Charkin, O. P. *Zh. Neorg. Khim.* **1989**, *34*, 1928. (b) Baranov, L. Y.; Charkin, O. P. *Zh. Neorg. Khim.* **1990**, *35*, 2888.
(233) Baranov, L. Y.; Charkin, O. P. *Zh. Strukt. Khim.* **1989**, *30*, 27.
(234) (a) Rozas, I.; Alkorta, I.; Elguero, J. *Chem. Phys. Lett.* **1997**, *275*, 423. (b) Alkorta, I.; Rozas, I.; Elguero, J. *THEOCHEM* **1998**, *452*, 227.
(235) Zuliani, F.; Götz, A. W.; Guerra, C. F.; Baerends, E. J. *Phys. Rev. B: Condens. Matter Mater. Phys.* **2009**, *79*, 165106/1.
(236) Hausdorf, S.; Baitalow, F.; Wolf, G.; Mertens, F. O. R. L. *Int. J. Hydrogen Energy* **2008**, *33*, 608.
(237) Sneddon, L. G. Amineborane-Based Chemical Hydrogen Storage, DoE Hydrogen Program Review, 2007, http://www.hydrogen.energy.gov/pdfs/review07/st_27_sneddon.pdfi.
(238) Davis, B. L.; Dixon, D. A.; Garner, E. B.; Gordon, J. C.; Matus, M. H.; Scott, B.; Stephens, F. H. *Angew. Chem., Int. Ed.* **2009**, *48*, 6812.
(239) Sutton, A. D.; Davis, B. L.; Bhattacharyya, K. X.; Ellis, B. D.; Gordon, J. C.; Power, P. P. *Chem. Commun.* **2010**, *46*, 148.
(240) Klinger, R. J.; Bloom, I.; Rathke, W. J. *Organometallics* **1985**, *4*, 1893.
(241) Basu, S.; Diwan, M.; Abiad, M. G.; Zheng, Y.; Campanella, O. H.; Varma, A. *Int. J. Hydrogen Energy* **2010**, *35*, 2063.
(242) Storozhenko, P. A.; Svitsyn, R. A.; Ketsko, V. A.; Buryak, A. K.; Ul'yanov, A. V. *Zh. Neorg. Khim.* **2005**, *50*, 980.

(243) Weaver, J. R.; Shore, S. G.; Parry, R. W. *J. Chem. Phys.* **1958**, *29*, 1.
(244) Matus, M. H.; Grant, D. J.; Nguyen, M. T.; Dixon, D. A. *J. Phys. Chem. C* **2009**, *113*, 16553.
(245) Couturier, M.; Andresen, B. M.; Tucker, J. L.; Dubé, P.; Brenek, S. J.; Negri, J. T. *Tetrahedron Lett.* **2001**, *42*, 2763.
(246) Couturier, M.; Tucker, J. L.; Andresen, B. M.; Dubé, P.; Negri, J. T. *Org. Lett.* **2001**, *3*, 465.
(247) Couturier, M.; Andresen, B. M.; Jorgensen, J. B.; Tucker, J. L.; Busch, F. R.; Brenek, S. J.; Dubé, P.; am Ende, D. J.; Negri, J. T. *Org. Process Res. Dev.* **2002**, *6*, 42.
(248) Chandra, M.; Xu, Q. *J. Power Sources* **2006**, *159*, 855.
(249) Xu, Q.; Chandra, M. *J. Power Sources* **2006**, *163*, 364.
(250) Clark, T. J.; Whittell, G. R.; Manners, I. *Inorg. Chem.* **2007**, *46*, 7522.
(251) Mohajeri, N.; T-Raissi, A.; Adebiyi, O. *J. Power Sources* **2007**, *167*, 482.
(252) Chandra, M.; Xu, Q. *J. Power Sources* **2007**, *168*, 135.
(253) Yao, C. F.; Zhuang, L.; Cao, Y. L.; Ai, X. P.; Yang, H. X. *Int. J. Hydrogen Energy* **2008**, *33*, 2462.
(254) Babu Kalidindi, S.; Indirani, M.; Jagirdar, B. R. *Inorg. Chem.* **2008**, *47*, 7424.
(255) Kalidindi, S. B.; Sanyal, U.; Jagirdar, B. R. *Phys. Chem. Chem. Phys.* **2008**, *10*, 5870.
(256) Simagina, V. I.; Storozhenko, P. A.; Netskina, O. V.; Komova, O. V.; Odegova, G. V.; Larichev, Y. V.; Ishchenko, A. V.; Ozerova, A. M. *Catal. Today* **2008**, *138*, 253.
(257) Park, J.-H.; Kim, H.-S.; Kim, H.-J.; Han, M.-K.; Shul, Y.-G. *Res. Chem. Intermed.* **2008**, *34*, 709.
(258) Babu Kalidindi, S.; Vernekar, A. A.; Jagirdar, B. R. *Phys. Chem. Chem. Phys.* **2009**, *11*, 770.
(259) Metin, Ö.; Şahin, Ş.; Özkar, S. *Int. J. Hydrogen Energy* **2009**, *34*, 6304.
(260) Yan, J.-M.; Zhang, X.-B.; Han, S.; Shioyama, H.; Xu, Q. *Inorg. Chem.* **2009**, *48*, 7389.
(261) Metin, Ö.; Özkar, S. *Energy Fuels* **2009**, *23*, 3517.
(262) Zahmakıran, M.; Özkar, S. *Appl. Catal., B* **2009**, *89*, 104.
(263) Umegaki, T.; Yan, J.-M.; Zhang, X.-B.; Shioyama, H.; Kuriyama, N.; Xu, Q. *J. Power Sources* **2009**, *191*, 209.
(264) Basu, S.; Brockman, A.; Gagare, P.; Zheng, Y.; Ramachandran, P. V.; Delgass, W. N.; Gore, J. P. *J. Power Sources* **2009**, *188*, 238.
(265) Umegaki, T.; Yan, J.-M.; Zhang, X.-B.; Shioyama, H.; Kuriyama, N.; Xu, Q. *Int. J. Hydrogen Energy* **2009**, *34*, 3816.
(266) Durap, F.; Zahmakıran, M.; Özkar, S. *Int. J. Hydrogen Energy* **2009**, *34*, 7223.
(267) Eom, K.; Kim, M.; Kim, R.; Nam, D.; Kwon, H. *J. Power Sources* **2010**, *195*, 2830.
(268) Zahmakıran, M.; Durap, F.; Özkar, S. *Int. J. Hydrogen Energy* **2010**, *35*, 187.
(269) Çalişkan, S.; Zahmakıran, M.; Özkar, S. *Appl. Catal., B* **2010**, *93*, 387.
(270) Basu, S.; Zheng, Y.; Varma, A.; Delgass, W. N.; Gore, J. P. *J. Power Sources* **2010**, *195*, 1957.
(271) Metin, Ö.; Mazumder, V.; Özkar, S.; Sun, S. *J. Am. Chem. Soc.* **2010**, *132*, 1468.
(272) Erdoğan, H.; Metin, Ö.; Özkar, S. *Phys. Chem. Chem. Phys.* **2009**, *11*, 10519.
(273) Rakap, M.; Özkar, S. *Int. J. Hydrogen Energy* **2010**, *35*, 3341.
(274) Demirci, U. B.; Miele, P. *J. Power Sources* **2010**, *195*, 4030.
(275) Jiang, H.-L.; Umegaki, T.; Akita, T.; Zhang, X.-B.; Haruta, M.; Xu, Q. *Chem.—Eur. J.* **2010**, *16*, 3132.
(276) Tong, D. G.; Zeng, X. L.; Chu, W.; Wang, D.; Wu, P. *J. Mater. Sci.* **2010**, *45*, 2862.
(277) Yan, J.-M.; Zhang, X.-B.; Akita, T.; Haruta, M.; Xu, Q. *J. Am. Chem. Soc.* **2010**, *132*, 5326.
(278) Patel, N.; Fernandes, R.; Guella, G.; Miotello, A. *Appl. Catal., B* **2010**, *95*, 137.
(279) Rakap, M.; Özkar, S. *Int. J. Hydrogen Energy* **2010**, *35*, 1305.

CR100088B